

DISSERTATION

EVOLUTIONARY INCREASE IN GENOME SIZE DRIVES CHANGES IN CELL BIOLOGY
AND ORGAN STRUCTURE

Submitted by

Michael Walter Itgen

Department of Biology

In partial fulfillment of the requirements

For the Degree of Doctor of Philosophy

Colorado State University

Fort Collins, Colorado

Summer 2022

Doctoral Committee:

Advisor: Rachel Lockridge Mueller

Daniel B. Sloan
Kim L. Hoke
Wen Zhou

Copyright by Michael Walter Itgen 2022

All Rights Reserved

ABSTRACT

EVOLUTIONARY INCREASE IN GENOME SIZE DRIVES CHANGES IN CELL BIOLOGY AND ORGAN STRUCTURE

The evolution of large genome size has been associated with patterns of phenotypic change in cell and organismal biology. The most fundamental of these is between genome size and cell size, which share a strong positive and deterministic relationship. As a result, increases in cell size alter the structure and function of the cell. Genome and cell size, together, are hypothesized to produce emergent consequences on development and physiology at the cellular and organismal level. My dissertation aims to better understand these patterns and identify potential mechanisms underlying these phenotypic changes. I test for the effects of genome and cell size on cell function, cellular physiology, and organ morphology by leveraging the natural variation in genome size found in salamanders (Genus: *Plethodon*). First, I show that transcriptomic data supports the predictions that large genome and cell size has functional consequences on cell biology. I also reject the hypothesis that large cell size is functionally linked to lower metabolic rate at the cellular level, but I provide transcriptomic evidence that cell size alters the metabolic state of cells. Finally, I show that genome and cell size drives morphological change in organ-specific ways in the heart and liver. I conclude that large cell size does not lower metabolic rate in salamanders. As an alternative, I propose that the evolution of low metabolic rate lifts the constraint of cell size, thus permitting the evolution of genome gigantism.

ACKNOWLEDGEMENTS

Specimens of *Ambystoma mexicanum* were obtained from the Ambystoma Genetic Stock Center, which is funded through National Institutes of Health grant: P40-OD019794. We thank A. Summers, the Summers lab, and the Karel Liem Bioimaging Facility at the University of Washington's Friday Harbor Laboratories for allowing us access to their CT scanner and for assistance scanning the specimens. I would like to thank Lance Li Puma for assistance and support with the collection of physiological data. For assistance in the field, I thank Amanda Cicchino, Aaron H. Griffing, Jackie Hayes, Marc Hayes, Eileen Itgen, Jackie Itgen, Mike Itgen, Fabiola Rodríguez Vásquez, and Stanley K. Sessions. For discussion of analyses and the manuscript, I would like to thank members of my dissertation committee: K. Hoke, D. Sloan, and W. Zhou.

This research was funded by the National Science Foundation (grant 1911585 awarded to R.L. Mueller), the GREG R.C. Lewontin Early Award from the Society of the Study of Evolution, the Chicago Herpetological Society Grant from the Chicago Herpetological Society, the Stephen and Ruth Wainwright Endowment from Friday Harbor Laboratories, the Helen T. and Frederick M. Gage Award from the American Society of Ichthyologists and Herpetologists, and the Grants-in-Aid of Research award from the Society of Integrative and Comparative Biology.

DEDICATION

This dissertation is dedicated to my family, friends, and mentors for their support and encouragement while I pursued this goal.

TABLE OF CONTENTS

ABSTRACT	ii
ACKNOWLEDGEMENTS	iii
DEDICATION	iv
1. INTRODUCTION	1
2. TRANSCRIPTOMIC ANALYSIS REVEALS CELL-SIZE-RELATED CHANGES IN FUNCTIONS AND PROCESSES	10
3. GENOME AND CELL SIZE INFLUENCE THE METABOLIC STATE, BUT NOT THE METABOLIC COST OF CELLS	39
4. GENOME SIZE DRIVES MORPHOLOGICAL EVOLUTION IN ORGAN-SPECIFIC WAYS	71
5. CONCLUSION	109
SUPPLEMENTAL INFORMATION 2.1	115

1. INTRODUCTION

Genome content and size varies extensively across organisms, driven by levels of repetitive non-coding DNA (Gregory, 2005). Transposable elements (TEs) are a diverse group of mobile sequences that significantly contribute to genomic content (Canapa et al., 2015). TE communities are dynamic, primarily driven by rates of replication and deletion from the genome. The relative diversity and activity of TE types also vary over time and across species (Böhne et al., 2008; Canapa et al., 2015). Although the host genome actively monitors and suppresses TE activity, TE proliferation can occasionally become rampant (Czech and Hannon, 2016; Madison-Villar et al., 2016; Mueller, 2017). Under these conditions, excessive TE proliferation, coupled with low rates of deletion, can dramatically increase genome size (Sun et al., 2008; Sun et al., 2012; Wang et al., 2021). The evolution of large genome size, in turn, impacts several aspects of an organism's biology (Gregory, 2005).

Genome size shows a strong positive correlation with nucleus and cell size (Gregory, 2001, 2005; Beaulieu et al., 2008). In fact, DNA content has been shown to be a direct determinant of cell size via cell cycle-related pathways (D'Ario et al., 2021). Because of this mechanism, the proliferation of TEs and expansion of genome size has a direct consequence on cell structure and function. Genome size has also been shown to correlate with other phenotypic traits, including rate of cell division, developmental rate, tissue and organ morphology, and metabolism (Szarski, 1983; Sessions and Larson, 1987; Roth et al., 1994; Licht and Lowcock, 1991; Gregory, 2005; Šímová and Herben, 2012; Itgen et al., 2022). Despite these broad patterns of phenotypic co-variation, the underlying effects of genome size on cell and organismal biology remain incompletely understood.

One of the main hypothesized mechanisms linking genome size to these correlated traits has been the impact of genome size on cell size. Increases in cell size, driven by increased DNA content, impact the structure and composition of the cell. There is a decrease in the surface area-to-volume (SV) ratio, which causes larger cells to have proportionally more volume (i.e., cytoplasm) relative to surface area (i.e., plasma membrane) (Cavalier-Smith, 1978; Szarski, 1983; Kozłowski et al., 2003). These changes to the SV ratio likely have functional implications on cellular processes, such as diffusion and intracellular transport (Kozłowski et al., 2003; Marshall et al., 2012; Miettinen et al., 2017). The altered physiology of large cells is hypothesized to underlie the broader correlations, such as metabolic rate and development. However, many of the theoretical predictions relating cell function to cell size lack robust empirical evidence.

One of the more significant traits to correlate with genome and cell size is metabolic rate. An association between these traits was first described in vertebrates (Szarski, 1983). Szarski (1983) posited that cell size was an adaptation for different metabolic strategies. For example, endotherms with high metabolic demands evolved small cells with high surface areas that were adaptive for nutrient and gas exchange (Szarski, 1983; Gregory, 2002). Conversely, ectotherms with extremely low metabolic rates had large cells that were thought to be less energetically costly (Szarski, 1983; Kozłowski et al., 2003). These larger cheaper cells would be adaptive for species living in hypoxic environments or those that underwent long periods without food (Szarski, 1983). Theoretical work supported the hypothesis that larger cells were relatively less expensive, which reduced the total metabolic rate of the organism (Kozłowski et al., 2003; Savage et al., 2007; Starostová et al., 2009; Glazier, 2014; Takemoto, 2015). The key mechanism in this model is the cost of maintaining ion gradients. For example, the active transport of sodium

and potassium across the plasma membrane can account for 20–50% of the metabolic expense of a tissue (Milligan and McBride, 1985). Larger cells with relatively less surface area should have slower rates of passive leak of ions across the plasma membrane (Kozłowski et al., 2003; Miettinen et al., 2017). In turn, these larger cells should require less energy to maintain their Na/K ion gradients (Kozłowski et al., 2003; Miettinen et al., 2017). The difference in metabolic cost of this process relative to cell size is thought to drive differences in metabolic rate at the tissue and organismal levels (Szarski, 1983; Kozłowski et al., 2003). Further, comparative studies have found conflicting evidence connecting genome and cell size to metabolic rate (Monnickendam and Balls, 1973; Licht and Lowcock, 1991; Gregory, 2003; Uyeda et al., 2017; Gardner et al., 2020; Johnson et al., 2021). The outstanding question remains: are extreme increases in genome size the product of selection for large cells and decreased metabolism, or are these traits the result of nonadaptive evolution towards genome gigantism?

Genome and cell size also impact development and morphogenesis, and by consequence, the morphology of tissues and organs (Horner and Macgregor, 1983; Sessions and Larson, 1987; Roth et al., 1994; Womack et al., 2019; Itgen et al., 2022). Large genome and cell size affects development through two primary processes: 1) slowing down the rate of development and 2) altering tissue structure and the number of cells comprising a tissue (Horner and Macgregor, 1983; Sessions and Larson, 1987; Hanken and Wake, 1993; Schmidt and Roth, 1993). The universal slowing of development rate is hypothesized to be the cumulative impact of large genome and cell size on cell function and physiology (Sessions and Larson, 1987). Several mechanisms have been identified as mediators of this broader process, such as the slower rates of cell division, cell migration, and cell differentiation (Horner and Macgregor, 1983; Sessions and Larson, 1987; Schmidt and Roth, 1993; Roth et al. 1994; Šímová and Herben, 2012). Large

genome size, and associated long intron lengths, can also slow development by prolonging transcription times and negatively affecting the rate of gene expression (Swinburne and Silver, 2008; Heyn et al., 2014; Sessions and Wake, 2021). These mechanisms have been hypothesized or shown to slow developmental processes that ultimately produce under-developed morphologies (Schmidt and Roth, 1993; Roth et al., 1994; Roth and Walkowiak, 2015; Womack et al., 2019; Itgen et al., 2021, 2022). In other words, genome and cell size can facilitate the evolution of paedomorphic traits. Evolutionary increase in cell size also alters the organization of tissues (Hanken and Wake, 1993; Itgen et al., 2022). Cell number and cell size are important parameters during development. As cell size increases, it will either cause a tissue to become larger (if cell number remains constant) or produce a “pixelated” organ of the same size but comprised of fewer larger cells. Cell size can therefore result in increased organism size or introduce a spatial constraint on organ structure (Hanken and Wake, 1993; Roth and Walkowiak, 2015; Decena-Segarra et al., 2020; Itgen et al., 2022). In the case of the latter, tissues and organs composed of fewer cells show significant changes to the organization of cells and the relative amounts of specialized cells required for specific functions. Extreme examples of this process have resulted in compensatory evolution to prevent loss of function in organs such as the eyes and brain (Linke et al., 1986; Roth et al., 1994; Roth and Walkowiak, 2015). These effects — slower developmental rate and altered tissue geometry — have been associated with morphological change in several organs, but the patterns of change vary across organs (Fankhauser, 1945; Schmidt and Roth, 1993; Roth et al., 1994; Roth and Walkowiak, 2015; Itgen et al., 2021, 2022). An important goal is to better understand whether these patterns of morphological change associated with genome and cell size occur in a universal or predictable way.

The goal of this dissertation is to reveal the effects of genome and cell size on a broad range of phenotypic traits, from the molecular to organismal levels. My research uses the natural variation in genome size found in *Plethodon* salamanders to test the effects of genome and cell size on cell function, cellular physiology, and organ morphology. My study system consists of 9 species of *Plethodon* with a 29.3–67.0 Gb range in genome size, and I tested for genome size correlations in heart and liver tissue. Chapter 2 focuses on correlations among genome and cell size and cellular functions and processes using cross-species transcriptomics. I found that the evolution of large cell size is accompanied by the upregulation of genes associated with intracellular transport and chromatin and the downregulation of genes related to the cell cycle, protein biosynthesis and degradation, and cell-cell communication. Chapter 3 tests if genome and cell size is correlated with cellular metabolic rate and mitochondrial physiology. Specifically, I test if large cell size correlated with lower metabolic rate of tissues and whether differences in cell size alter the relative cost of maintaining ion gradients. I assessed if large genome and cell size is associated with differences in mitochondrial physiology. Finally, I analyzed transcriptomic data to determine if there are expression-related differences in cell size related to physiological processes. I found that genome and cell size is not correlated with differences in tissue metabolic rates, the relative costs of ion gradient maintenance, or mitochondrial physiologies. Chapter 4 investigates the correlations of genome and cell size on heart and liver morphology. Tissue structure in both organs was significantly altered as genome and cell size increase; the heart showed a dramatic reduction of ventricle musculature, and the liver showed a change in the vasculature that resulted in fewer larger vascular structures. These distinct patterns suggest that genome and cell size change morphology in organ-specific ways. These chapters

further our understanding of the complex relationships between genome size and important phenotypic and physiological traits.

REFERENCES

- Beaulieu, J.M., I.J. Leitch, S. Patel, A. Pendharkar, and C.A. Knight. 2008. Genome size is a strong predictor of cell size and stomatal density in angiosperms. *New Phytologist* 179:975–986.
- Böhne, A., F. Brunet, G. Galiana-Arnoux, C. Schultheis, and J.N. Volff. 2008. Transposable elements as drivers of genomic and biological diversity in vertebrates. *Chromosome Research* 16:203–215.
- Capana, A., M. Barucca, M.A. Biscotti, M. Forconi, and E. Olmo. 2015. Transposons, genome size, and evolutionary insight in animals. *Cytogenetic and Genome Research* 147:217–239.
- Cavalier-Smith, T. 1978. Nuclear volume control by nucleoskeletal DNA, selection for cell volume, cell growth rate, and the solution of the DNA C-value paradox. *Journal of Cell Science* 34:247–278.
- Czech, B., and G.J. Hannon. 2016. One loop to rule them all: The ping-pong cycle and piRNA-guided silencing. *Trends in Biochemical Sciences* 41:324–337.
- D’Ario, M., R. Tavares, K. Schiessl, B. Desvoyes, M. Howard, and R. Sablowski. 2021. Cell size controlled in plants using DNA content as an internal scale. *Science* 372:1176–1181.
- Decena-Segarra, L.P., L. Bizjak-Mali, A. Kladnik, S.K. Sessions, and S.M. Rovito. 2020. Miniaturization, genome size, and biological size in a diverse clade of salamanders. *The American Naturalist* 196:634–648.
- Fankhauser, G. 1945. The effects of changes in chromosome number on amphibian development. *The Quarterly Review of Biology* 20:20–78.
- Gardner, J.D., M. Laurin, and C.L. Organ. 2020. The relationship between genome size and metabolic rate in extant vertebrates. *Philosophical Transactions of the Royal Society B* 375:20190146.
- Glazier, D.S. 2014. Metabolic scaling in complex living systems. *Systems* 2:451–540.
- Gregory, T.R. 2001. Coincidence, coevolution, or causation? DNA content, cell size, and the C-value enigma. *Biological Reviews of the Cambridge Philosophical Society* 76:65–101.
- Gregory, T.R. 2002. A bird’s-eye view of the c-value enigma: genome size, cell size, and metabolic rate in class Aves. *Evolution* 56:121–130.
- Gregory, T.R. 2003. Variation across amphibian species in the size of the nuclear genome supports a pluralistic, hierarchical approach to the c-value enigma. *Biological Journal of the Linnean Society* 79:329–339.
- Gregory, T.R. 2005. Genome size evolution in animals. In: Gregory T. R., editor. *The Evolution of the Genome*. New York: Elsevier.
- Hanken, J., and D.B. Wake. 1993. Miniaturization of body size: organismal consequences and evolutionary significance. *Annual Review of Ecology and Systematics* 24:501–519.
- Heyn, P., A.T. Kalinka, P. Tomancak, and K.M. Neugebauer. 2015. Introns and gene expression: cellular constraints, transcriptional regulation, and evolutionary consequences. *Bioessays* 37:148–154.
- Horner, H.A., and H.C. Macgregor. 1983. C value and cell volume: their significance in the evolution and development of amphibians. *Journal of Cell Science* 63:135–146.

- Itgen, M.W., C.M. Crookston, M.G. Carbonell, P.P. Krakker, J.W. Presch, D.S. Siegel, R.L. Mueller, and J.H. Townsend. 2021. Comparative osteology of montane climbing salamanders (Plethodontidae: *Bolitoglossa* subgenus *Magnadigita*) from Nuclear Central America. *Ichthyology & Herpetology* 109:489–500.
- Itgen, M.W., G.R. Natalie, D.S. Siegel, S.K. Sessions, and R.L. Mueller. 2022. Genome size drives morphological evolution in organ-specific ways. *Evolution*.
- Johnson, B.B., J.B. Searle, and J.P. Sparks. 2021. Genome size influences adaptive plasticity of water loss, but not metabolic rate, in lungless salamanders. *Journal of Experimental Biology* 224:jeb242196.
- Kozłowski, J., M. Konarzewski, and A.T. Gawelczyk. 2003. Cell size as a link between noncoding DNA and metabolic rate scaling. *Proceedings of the National Academy of Sciences* 100:14080–14085.
- Licht, L. E., and L. A. Lowcock. 1991. Genome size and metabolic rate in salamanders. *Comparative Biochemistry and Physiology Part B: Comparative Biochemistry* 100:83–92.
- Linke, R., G. Roth, and B. Rottluff. 1986. Comparative studies on the eye morphology of lungless salamanders, family Plethodontidae, and the effect of miniaturization. *Journal of Morphology* 189:131–143.
- Madison-Villar, M. J., C. Sun, N. C. Lau, M. L. Settlers, and R. L. Mueller. 2016. Small RNAs from a big genome: the piRNA pathway and transposable elements in the salamander species *Desmognathus fuscus*. *Journal of Molecular Evolution* 83:126–136.
- Marshall, W.F., K.D. Young, M. Swaffer, E. Wood, P. Nurse, A. Kimura, J. Frankel, J. Wallingford, V. Walbot, X. Qu, and A.H. Roeder. 2012. What determines cell size? *BMC Biology* 10:101.
- Miettinen, T.P., M.J. Caldez, P. Kaldis, and M. Björklund. 2017. Cell size control – a mechanism for maintaining fitness and function. *BioEssays* 39:1700058.
- Milligan, L.P., and B.W. McBride. 1985. Energy costs of ion pumping by animal tissues. *The Journal of Nutrition* 115:1374–1382.
- Monnickendam, M.A., and M. Balls. 1973. The relationship between cell sizes, respiration rates and survival of amphibian tissues in long-term organ cultures. *Comparative Biochemistry and Physiology Part A: Physiology* 44:871–880.
- Mueller, R. L. 2017. piRNAs and evolutionary trajectories in genome size and content. *Journal of Molecular Evolution* 85:169–171.
- Roth, G., J. Blanke, and D. B. Wake. 1994. Cell size predicts morphological complexity in the brains of frogs and salamanders. *Proceedings of the National Academy of Sciences* 91:4796–4800.
- Roth, G., and W. Walkowiak. 2015. The influence of genome and cell size on brain morphology in amphibians. *Cold Spring Harbor Perspectives in Biology* 7:a019075.
- Schmidt, A., and G. Roth. 1993. Patterns of cellular proliferation and migration in the developing tectum mesencephali of the frog *Rana temporaria* and the salamander *Pleurodeles waltl*. *Cell and Tissue Research* 272:273–287.
- Sessions, S.K., and A. Larson. 1987. Developmental correlates of genome size in plethodontid salamanders and their implications for genome evolution. *Evolution* 41:1239–1251.
- Sessions, S.K., and D.B. Wake. 2021. Forever young: linking regeneration and genome size in salamanders. *Developmental Dynamics* 250:768–778.

- Šímová, I., and T. Herben. 2012. Geometrical constraints in the scaling relationships between genome size, cell size and cell cycle length in herbaceous plants. *Proceedings of the Royal Society B: Biological Sciences* 279:867–875.
- Starostová Z, et al. 2009. Cell size but not genome size affects scaling of metabolic rate in eyelid geckos. *American Naturalist* 174:E100–E105.
- Sun, C., D.B. Shepard, R.A. Chong, J.L. Arriaza, K. Hall, T.A. Castoe, C. Feschotte, D.D. Pollock, R.L. Mueller. 2012. LTR retrotransposons contribute to genomic gigantism in plethodontid salamanders. *Genome Biology and Evolution* 4:168–183.
- Sun, C., J.R. López Arriaza, and R.L. Mueller. 2012. Slow DNA loss in the gigantic genomes of salamanders. *Genome Biology and Evolution* 4:1340–1348.
- Swinburne, I.A., D.G. Miguez, D. Landgraf, and P.A. Silver. 2008. Intron length increases oscillatory periods of gene expression in animal cells. *Genes & Development* 22:2342–2346.
- Szarski, H. 1983. Cell size and the concept of wasteful and frugal evolutionary strategies. *Journal of Theoretical Biology* 105:201–209.
- Takemoto, K. 2015. Heterogeneity of cells may explain allometric scaling of metabolic rate. *BioSystems* 130:11–16.
- Uyeda, J.C., M.W. Pennell, E.T. Miller, R. Maia, and C.R. McClain. 2017. The evolution of energetic scaling across the vertebrate tree of life. *The American Naturalist* 190:185–199.
- Wang, J., M.W. Itgen, Y. Gong, H. Wang, Y. Gong, J. Jiang, J. Li, C. Sun, S.K. Sessions, and R.L. Mueller. 2021. Gigantic genomes provide empirical tests of transposable element dynamics models. *Genomics, Proteomics & Bioinformatics* 19:123–139.
- Womack, M.C., M.J. Metz, and K.L. Hoke. 2019. Larger genomes linked to slower development and loss of late-developing traits. *The American Naturalist* 194:854–864.

2. TRANSCRIPTOMIC ANALYSIS REVEALS CELL-SIZE-RELATED CHANGES IN FUNCTIONS AND PROCESSES

Summary

Large genome size is associated with the evolution of low metabolic rate and slower rates of development at broad taxonomic levels. The correlations between genome size and these complex traits are hypothesized to be mediated by cell size. DNA content is a key determinant of cell size and underlies the strong positive correlation between the two traits. As a result, evolutionary increases in genome size cause corresponding increases in cell size. As cells increase in size, there is a shift in the surface-area-to-volume (SV) ratio. This scaling property causes larger cells to have proportionally less plasma membrane and proportionally more cytoplasm. These relative changes are thought to impact surface area- and volume-dependent cellular processes, such as diffusion and intracellular transport, and intracellular concentrations of organelles and proteins. We test the hypothesis that the evolution of large genome and cell size is accompanied by changes in gene expression related to surface area-dependent and volume-dependent processes. We performed comparative transcriptomic analyses of 4 species of *Plethodon* with a 29.3–67.0 Gb range in genome size. We found that large genome and cell size was associated with the upregulation of processes related to intracellular transport and chromatin-modification. We hypothesize these changes are in response to greater intracellular distances in large cells and the increased DNA content. Conversely, small cell size was associated with the upregulation of protein turnover and pathways associated with cell cycle progression. Together, these results support the hypothesis that cell size impacts cellular processes and mediates the correlations between genome size and organismal biology.

Introduction

Cell size is an important functional trait. It can influence the metabolic state, functional capacity, and overall physiology of the cell (Miettinen and Björklund, 2017; Miettinen et al., 2017). Cells have optimal sizes that can maximize diffusion efficiency and maintain ideal protein concentration that influence the rates of biochemical reactions. Cell size can vary by cell type, but can also fluctuate during transient events, such as mitosis, developmental stages, or metabolic states (Miettinen et al., 2017; Nassiri and McCall, 2018). However, each cell type maintains a specific cell size outside of these transient events (Ginzberg et al., 2015). As a result, populations of cells in a tissue or organism do not vary much in size (Milo and Phillips, 2015). Natural variation in cell size is often related to cell-type specific functions that require distinct morphologies (Chan and Marshall, 2010; Ginzberg et al., 2015). DNA content, or genome size, of the organism is a significant determinant of cell size (Gregory, 2001, 2005; Beaulieu et al., 2008). Genome size has been shown to determine nucleus size and total cell size (D'Ario et al., 2021). Because of this relationship, evolutionary changes in genome size result in a corresponding change in cell size within an organism regardless of the cell type (Gregory, 2005). Further, the evolution of large genome size sets a limit on minimum cell size based on the spatial requirements of the genome.

Increases in cell size change cell structures and functions (Chan and Marshall, 2010; Crowder et al., 2015; Heald et al., 2015; Spencer et al., 2017). Most significantly, increased cell size lowers the surface-area-to-volume (SV) ratio, resulting in a cell with proportionally smaller membrane and proportionally larger cytoplasmic volume (Okie et al., 2016). This, in turn, has likely functional consequences for all volume- and surface area-dependent processes. Intracellular organelles are also predicted to scale with cell size depending on their functional

role and structure. Because these processes are predicted to be impacted by the geometric scaling of cell size, we would expect larger cells to exhibit altered functions that counteract any negative consequences on the overall physiology of the cell (Brangwynne, 2013; Marshall, 2011; Miettinen, et al. 2017).

Volume-dependent processes are largely associated with the cytoplasm and cytoskeleton, including intracellular transport processes, cytoskeletal dynamics, and the maintenance of optimal protein concentrations (Kozłowski et al., 2003; Chan and Marshall, 2010; Marshall, 2011; Miettinen et al., 2017). Greater cytoplasmic volume increases intracellular transport distances and renders diffusion-based transport inefficient (Dill et al., 2011; Soh et al., 2013). Large cells are predicted to increase active intracellular transport to accommodate longer intracellular distances (Miettinen et al., 2014). This would include an upscaling of the endomembrane system and transport-related organelles, such as the Golgi apparatus, vesicles, and endoplasmic reticulum. The cytoskeleton would also have to be scaled to volume, not only to support increased intracellular transport, but to maintain structural integrity associated with larger cell size as well. An increase in cell volume could also dilute protein concentrations (Neurohr et al., 2019; Lanz et al., 2021). Protein concentrations are maintained at a specific level to optimize the rate of biochemical reactions (Zhou et al., 2008). The biosynthetic capacity and overall proteome would have to scale with cell volume to avoid cytoplasmic dilution.

A proportional reduction in surface area impacts plasma membrane-related functions and processes, such as the maintenance of ion gradient concentrations, cellular import and export, cell-cell communication, and cell adhesion elements (Kozłowski et al., 2003; Chan and Marshall, 2010; Marshall, 2011). Diffusion rate is limited in larger cells as the relative surface area decreases. This decreased diffusion rate has two important consequences for the cell. First, larger

cells passively lose ions at a slower rate (Jimenez, et al. 2011; Jimenez, et al. 2013; Johnston, et al. 2003). Cells expend a significant amount of energy maintaining ion gradients across the plasma membrane by actively transporting sodium and potassium across the membrane. Since passive diffusion rates are reduced, larger cells should decrease the activity of ion pumps such as the Na⁺/K⁺-ATPase (Kozłowski et al., 2003; Jimenez, et al. 2011). The limited diffusion rate also restricts the rate of nutrient and waste exchange (Marshall et al., 2012). As a result, diffusion rate should restrict the metabolic and biosynthetic capacities of large cells. Finally, relatively less plasma membrane could alter the composition of the plasma membrane itself. The plasma membrane is comprised of several lipid types, transmembrane proteins important for cell-cell communication, and cytoskeletal elements that support cell adhesion (Kusumi et al., 2012). Surface area changes could impact the relative numbers of these plasma membrane elements. The differential upregulation of certain elements compared to others likely becomes a trade-off between structural integrity of the plasma membrane and processes such as signal transduction or cell adhesion.

While the functional consequences of cell size have been thoroughly considered in a theoretical framework, there is a lack of empirical data supporting these predictions (Kozłowski et al., 2003; Chan and Marshall, 2010; Marshall, 2011; Miettinen et al., 2017). Our study investigates the effect of cell size on the expression of several SV-related pathways using transcriptomic analyses. We hypothesize that large cell size necessitates compensatory changes in the allocation of resources to various cellular processes. We predict that larger cells have higher relative expression of pathways associated with intra-cellular processes underlying general cell function (e.g., protein trafficking) and lower relative expression of pathways associated with membrane-associated processes (e.g., the maintenance of ion gradients

underlying membrane potential) and extra-cellular processes (e.g., cell-cell communication) than do smaller cells because of the lower SV ratio. We leveraged the natural variation in genome and cell size within the salamander genus *Plethodon* and selected 4 species that span a 29.3–67.0 gigabase (Gb) range in genome sizes (Itgen et al., 2022). Since these differences in genome and cell size have evolved over long periods of time and do not represent transient events or experimental manipulations, we hypothesize that *Plethodon* species have evolved differences in cell physiology to compensate for large cell sizes. By using these two cell types, we can identify more general changes in cell physiology as well as those specific to a cell type. More broadly, our goal is to better understand how cell-size-dependent changes in cellular functions and processes might be related to broader phenotypic patterns associated with large genome and cell size, such as slower development and lower metabolic rates.

Methods

RNA extraction and transcriptome assembly

We collected heart and liver tissue samples from adult individuals of *Plethodon cinereus*, *P. dunni*, *P. idahoensis*, and *P. glutinosus* between May–July of 2018 (Supplementary Information 2.1). There were three replicates per tissue and species except for liver tissue in *P. cinereus* (n = 2). We chose to analyze the heart and liver tissue because of differences in cell morphology and function. First, the cell types have different morphologies that impact geometric scaling in the two cell types. Liver is primarily comprised of hepatocytes that have a cuboidal morphology – a shape that has a dramatic shift in SV ratio as cells become larger. Conversely, the cardiomyocytes of the heart become highly elongate, which has a less dramatic change in SV ratio as the cells become larger. Second, these two cell types have distinct functional roles.

Hepatocytes primarily perform secretory and metabolic functions whereas cardiomyocytes undergo mechanical contractions. The salamanders were humanely euthanized using neutral-buffered (pH 7) 1% MS-222 and tissues were stored at -80°C in RNAlater. We extracted total RNA from tissues using TRIzol and following the manufacturer's protocol (Invitrogen). We added 4 µl of glycogen to the heart samples to increase RNA yield due to the small size of the heart samples. We quantified RNA concentration using a Qubit 2.0 fluorometer and assessed RNA quality (RQN > 6) with an Agilent 5300 Fragment Analyzer. The extracted RNA samples were sent to Yale Genomics Core for Ribosome reduction library preparation and sequencing. The protocols for animal research, husbandry, and euthanasia were approved by the Institutional Animal Care and Use Committee of Colorado State University and carried out in accordance with protocol 17-7189A.

A total of 23 individual libraries were sequenced on a NovaSeq S4 as paired end 150 base pair (bp) reads with ~45 million paired end reads per library. We trimmed off adapter sequences and removed poor quality reads using Trimmomatic v0.39 using a 4-bp sliding window. We discarded any reads with a Q score less than 5 or less than 25 bp in length. We filtered out contaminants by aligning reads to the viral and bacterial NCBI RefSeq database using Bowtie2 v2.4.5 (Bolger et al., 2014; Langmead and Salzberg, 2012). We assembled a single reference transcriptome for each tissue and biological replicate (i.e., each library) using rnaSPAdes v3.15.4 with default settings (Bushmanova et al., 2019). We chose this approach because tissue-specific assemblies created by assembling all replicates together yielded high amounts of fragmented and redundant contigs.

Ortholog identification, differential expression, and functional enrichment analysis

Our overall goal in our first analysis was to identify differentially expressed genes (DEGs) across all four *Plethodon* species using a set of single copy orthologs. Following assembly, we identified open reading frames (ORFs) in the reference transcriptomes for each species and tissue using TransDecoder and selected the longest ORF for each contig. We increased the sensitivity of our ORF detection using homology-based searches with blastp (e-value $1e-5$) against the SwissProt database and hmmscan v3.3.2 against the Pfam database (Camacho et al., 2008; Eddy, 2011). We then predicted the coding regions of transcripts for each reference transcriptome to use in our ortholog search. We used OrthoFinder v2.5.4 to identify single-copy orthologs across all four species (Emms and Kelly, 2019), and we used these single-copy orthologs for downstream identification of differentially expressed genes (DEGs) across all four species.

We quantified transcript abundance of the ortholog set for each species with RSEM v1.3.3 (Li and Dewey, 2011). We normalized the count data for library size using the trimmed mean of M-values (TMM) and calculated the counts per million (CPM) using edgeR (Robinson et al., 2010; McCarthy et al., 2012). We then used edgeR to identify DEGs across all possible pair-wise comparisons across the four species. We used an FDR of $P < 0.001$ and a log-fold change of 2 in at least one pairwise comparison as our criteria for considering a gene significantly differentially expressed.

In order to identify DEGs associated with evolutionary changes in cell size, we first performed a soft clustering analysis using the R package Mfuzz v2.54.0 (Kumar and Futschik, 2007). We averaged the TMM- and CPM-transformed expression values for all of the DEGs across the replicates for each species. We standardized these expression values by setting the mean = 0 and the standard deviation = 1. We then estimated the optimal fuzzifier for the dataset

and selected 8 soft clusters based on the minimum centroid distance in Mfuzz. We identified the two DEG clusters whose expression levels across our four target species most closely approximate monotonic increase and decrease with increased cell size. We considered these two clusters to be our candidate cell size-associated genes for further analysis.

In order to identify functions enriched in our candidate cell size-associated clusters, we annotated the clusters using blastx (e-value 1e-15) against the SwissProt database. We then mapped the genes to the *Silurana (Xenopus) tropicalis* Ensembl gene ID for gene ontology analysis. We performed a functional enrichment analysis on each of the annotated clusters with g:Profiler against the Gene Ontology (GO) molecular function, GO cellular component, GO biological process, KEGG, and Reactome databases (Raudvere et al., 2019). We used *S. tropicalis* as the reference organism against all known genes, limited maximum term size to 2,500, and used the g:SCS threshold algorithm for multiple test correction with a p-value cutoff of 0.05.

Gene Set Enrichment Analysis

To complement our naïve soft clustering analysis, we also performed hypothesis-driven analyses of sets of genes predicted to be up- or downregulated to maintain cell functionality at large cell sizes. For this approach, we compared gene expression between *P. cinereus* and *P. idahoensis*, the species with the smallest and largest genome/cell sizes, respectively, using Broad Institute's Gene Set Enrichment Analysis (GSEA) v4.2.3. We compiled gene sets from the Molecular Signatures Database (MsigDb v7.5.1 <http://software.broadinstitute.org/gsea/msigdb/index.jsp>) that enabled us to test for expression differences associated with: 1) mitosis, as M-phase duration and frequency vary with cell size; 2)

cytoskeleton, intracellular transport systems, and the plasma membrane, as SV ratio varies with cell size; 3) organelle biogenesis and function, as organelle size, number, and distribution scale variously with cell size; and 4) transcription and translation, as protein concentration and turnover likely scale with cell size. We also included GO terms related to organ-specific functional pathways for heart and liver to test if cell size impacts how organ function is accomplished at the cell physiological level. In total, there were 1,167 gene sets in the heart analysis and 1,662 gene sets in the liver analysis.

We identified single copy orthologs present in both *P. cinereus* and *P. idahoensis* using OrthoFinder v2.5.4 and the predicted ORFs from each of the liver and heart tissue transcriptomes (Emms and Kelly, 2019). We used blastx (e-value 1e-15) against the human UniProt proteome database and retained only the orthologs that had a significant hit. We quantified transcript abundance of the annotated ortholog sets using RSEM and performed a TMM and CPM normalization on the abundance estimates using edgeR (Robinson et al., 2010). The GSEA was conducted using the classic enrichment statistic and ratio of classes metric for ranking genes.

Results

Differential expression and functional enrichment analysis in hepatic tissue

We identified a set of 6,066 single copy orthologs from the liver transcriptomes that were present in all four species. The differential expression analysis found 2,704 DEGs in liver tissue for at least one pairwise comparison (Fig. 1). The soft clustering analysis recognized 8 distinct expression profiles among the 2,704 liver DEGs (Fig. 1). Liver cluster 7 (251 DEGs) and heart cluster 9 (185 DEGs) showed a size-negative expression pattern (Fig. 1, 2). Liver cluster 8 (255 DEGs) and heart cluster 10 (200 DEGs) showed a size-positive expression pattern (Fig. 1, 2).

We successfully annotated and mapped 209 (83.3%) DEGs in the size-positive cluster and 193 (75.7%) DEGs in the size-negative cluster to ENSEMBL gene IDs belonging to *Silurana tropicalis* for the GO enrichment analysis with g:Profiler. In the size-negative cluster, there were a total of 229 significantly enriched terms and pathways. The top 20 enrichment terms were broadly associated with transcription and translation, protein metabolism, and mitosis (Table 1). The size-positive cluster had 16 significantly enriched GO terms and pathways (Table 2). As predicted, most of these enriched terms were associated with intracellular transport and endocytosis, with enrichment of the Golgi apparatus, endoplasmic reticulum, and vesicle-related processes (Table 2).

Differential expression and functional enrichment analysis in cardiac tissue

We identified a set of 5,257 single copy orthologs from the heart transcriptomes in all four species. The differential expression analysis found 2,090 DEGs in the heart tissue for at least one pairwise comparison (Fig. 2). We successfully annotated and mapped 148 (80%) DEGs in the size-negative cluster (cluster 9) and 139 (69.5%) DEGs in the size-positive cluster (cluster 10) to ENSEMBL gene IDs belonging to *Silurana tropicalis* for the GO enrichment analysis with g:Profiler. In the size-negative cluster, there were 13 significantly enriched terms and pathways (Table 3). Several terms were associated with protein metabolism and modification, zinc transport, and intracellular signaling (Table 3). There was also enrichment for positive regulation of stress fiber assembly and glucose metabolism (Table 3). The size-positive cluster had 9 significantly enriched GO terms and pathways (Table 4). The size-positive cluster showed enrichment for amide and peptide metabolic processes, translation, cytoplasm, and the mitochondria (Table 4).

GSEA: comparison between smallest and largest cell size in cardiac and hepatic tissue

We identified 15,194 single copy orthologs in the hepatic tissue and 15,785 single copy orthologs in the cardiac tissue between *P. cinereus* and *P. idahoensis*. We successfully annotated 7,172 and 7,433 orthologs in the liver and heart, respectively, using the human UniProt proteome.

Plethodon cinereus had 69 significantly enriched gene sets in the liver tissue, with 14 of these gene sets significant at FDR < 25%. The top 20 significantly enriched gene sets ($P < 0.05$) in the liver tissue of *P. cinereus* were associated with transcription and translation (6 sets), proteolysis and protein degradation (4 sets), the mitochondria (4 sets), and mitosis (1 set) (Table 5). The GSEA and functional enrichment analysis results are broadly concordant, showing that species with smaller cells have enrichment for pathways associated with protein production and degradation, the progression through the cell cycle, and mitochondrial physiology. There were 53 significantly enriched gene sets in the heart tissue of *P. cinereus*, with 2 of these gene sets significant at FDR < 25% (Table 7). The top 20 significantly enriched gene sets ($P < 0.05$) in the heart tissue of *P. cinereus* were mostly associated with lipid transferring activity (3 sets), protein secretion and localization (5 sets), the mitochondria (2 sets), and signaling pathways (2 sets) (Table 7). In addition, there are singlet terms related to proteasome activity, cell-cell junctions, and the positive regulation of heart rate (Table 7).

Plethodon idahoensis had 51 significantly enriched gene sets in hepatic tissue, with 6 of these gene sets significant at FDR < 25% (Table 6). The top enriched gene sets in the liver tissue of *P. idahoensis* consisted of pathways associated with vesicle-based transport (2 sets), cell growth (2 sets), cell polarity and localization (4 sets), transcriptional regulation and suppression

(4 sets), chromatin modification (2 sets), and cell-cell adhesion and junctions (3 sets) (Table 6). The GSEA and functional enrichment analysis of DEGs in the liver support the enrichment of transport-related processes in species with larger cells. There were 34 significantly enriched gene sets in the heart tissue of *P. idahoensis*, with 7 of these gene sets significant at FDR < 25% (Table 8). The top 20 significantly enriched gene sets ($P < 0.05$) in the heart tissue of *P. idahoensis* were mostly associated with vesicle-based transport and secretion (3 sets), modification of chromatin (2 sets), translation (3 sets), and proteasome-related complexes (4 sets) (Table 8). There is also enrichment of single terms related to cell substrate binding, ankyrin binding, and inward rectifier potassium channel activity.

Discussion

Cell size and the cell cycle

One of the most fundamental and well-documented consequences of large genome and cell size is their effect on slowing the cell cycle (Horner and Macgregory, 1983; Francis et al., 2008; Šímová and Herben, 2011). It is thought that both genome and cell size play a role in this process, with increased DNA content prolonging the S-phase and greater nuclear and cell volumes impacting the concentration-dependent cyclin / CDK pathways (Gregory, 2001). We found size-negative DEGs and significantly enriched gene sets that support these patterns in the liver transcriptome. Specifically, we found that smaller cells had size-negative DEGs and gene sets that were enriched for several cell cycle-related pathways in hepatic tissue. The enrichment for progression through the cell cycle suggests that smaller cells are entering the cell cycle more frequently compared to larger cells. Therefore, it would imply that a population of large cells within a tissue have lower rates of cellular replacement.

Transport

Intracellular transport is one of the key cellular processes that would be negatively impacted by this shift towards more cytoplasm and volume (Marshall, 2011; Brangwynne, 2013; Miettinen, et al. 2017). Proteins, metabolites, or other cellular components and molecules move through the cell via two main processes: diffusion and active transport. Active transport is a time efficient process but introduces an energetic cost to the cell. In contrast, diffusion-based transport is optimal across small distances since it has no energetic cost but becomes extremely limiting across greater distances or for larger molecules or transport vesicles (Soh et al., 2013; Miettinen et al., 2017). Diffusion rates of proteins have been considered a significant limitation to cell size, which can limit the rate of protein interactions and therefore limit the rates of chemical reactions (Dill et al., 2011). Larger cells are predicted to compensate for this biophysical limitation of diffusion by upregulating transport-related processes. We found that large cell size was associated with the enrichment and upregulation of various transport pathways, including intracellular transport and endocytosis, in both cardiac and hepatic cell types. We found the DEGs in hepatic cells were functionally enriched for the endomembrane system, endocytosis pathway, and intracellular transport processes. Large hepatic cells also showed upregulation and functional enrichment of the Golgi apparatus and endoplasmic reticulum – two organelles that serve key roles in transport. In addition, there was significant upregulation and functional enrichment of several processes related to clathrin-coated vesicles in larger hepatic cells relative to smaller ones. The GSEA of the cardiac cells also identified enrichment of gene sets associated with secretory vesicles and granules, as well as gene sets associated with the vesicle lumen. These patterns were much more evident in the hepatic cells compared to cardiomyocytes. This

difference is possibly explained by the elongate morphology of cardiomyocytes, which lessens the scaling changes to the cell's SV ratio. Therefore, cardiomyocytes would be less limited by volume-related processes than more spherical or cuboidal cell types, such as hepatocytes.

Downregulation of protein turnover associated with large cell volumes

How the proteome scales with cell size has significant implications for the physiology and metabolism of a cell. Proteome dynamics are regulated by rates of biosynthesis and degradation (i.e., protein turnover), which can involve changes in transcription, translation, protein maturation, or several protein degradation pathways. First principles propose that the proteome should scale proportionally with volume to allow the cell to maintain protein and RNA concentrations to optimize biochemical reaction rates (Dill et al., 2011). Larger cells would then have a proportionally greater biosynthetic capacity and demand compared to small cells. However, our results do not fit this model and suggest that protein turnover is negatively impacted by increases in volume. We found this pattern most obvious in the hepatocytes, which show a more drastic shift in SV scaling compared to the cardiomyocytes. Both the functional enrichment analysis and GSEA identified a suite of upregulated pathways and functions in small cells associated with ribosome biogenesis, transcription and translation, protein modification, and various protein degradation pathways. Conversely, large hepatocytes were found to have upregulation of gene sets associated with transcriptional repression.

These results suggest that the proteome and biosynthetic capacity of a cell does not adequately scale with cell volume. Experimental manipulation of cell volume has shown suboptimal scaling of RNA and protein concentrations at larger cell volumes, resulting in cytoplasmic dilution (Neurohr et al., 2019; Lanz et al., 2021). As a result, larger cells fail to

generate optimal concentrations for biochemical reactions and likely suffer from physiological and metabolic consequences. Further evidence seems to suggest that these suboptimal concentrations might be caused by a ratio of cytoplasmic volume to ploidy. In other words, transcription is limited by the number of gene copies present in the genome (Neurohr et al., 2019; Lanz et al., 2021). And while polyploid organisms, which also deal with increased cell sizes, can circumvent this problem because of the increased number of gene copies, the *Plethodon* salamanders in this study are diploid and therefore would be restricted by the rate of transcription. These salamanders have also evolved enormous genome sizes through the universal increase of TEs, including intronic regions. Intron length has been found to prolong the time it takes to transcribe and process mRNA (Swinburne and Silver, 2008; Heyn et al., 2014). Together, genome and cell size can have confounding effects on proteome dynamics that can have profound consequences on cell physiology.

One possible solution to cytoplasmic dilution in these salamanders could depend on cellular localization. Recent studies have found that subcellular localization is an important proteomic component and can increase the efficiency and lifespan of proteins (Yousefi et al., 2021). Indeed, we found upregulation of localization processes in large hepatocytes, particularly associated with the polarization of the cytoplasm. It is possible that large cells mitigate the impacts of cytoplasmic dilution by having highly localized functional regions within the cell.

Surface-area related processes altered by cell size

Changes in cell size are predicted to impact the structure, composition, and function of the plasma membrane (Miettinen et al., 2014). The maintenance of ion gradients is an example of a physiologically significant process that is thought to be affected by cell size (Kozłowski et al.,

2003; Miettinen et al., 2014, 2017). The energetic cost of maintaining ion gradients, such as the sodium/potassium one, is predicted to decrease in large cells since diffusion rate is determined by surface area (Kozłowski et al., 2003; Miettinen et al., 2014, 2017). We found no evidence that large cells are differentially expressing genes related to ion transmembrane transport. These results are concordant with Miettinen et al. (2014) and further suggest that large cells are not adjusting for the different diffusion rates. Surface area is also predicted to limit the rate of import and export and, by extension, metabolic rate. We did find small cardiomyocytes upregulated the import of glucose and the export / secretion of proteins. We also found several other plasma membrane-related processes were differentially upregulated in smaller cells. Lipid transfer activities were upregulated in smaller cardiomyocytes, which could be driven by the greater relative plasma membrane compared to larger cells (Miettinen et al., 2014). Smaller cardiomyocytes also showed functional enrichment of processes related to cell-cell communication and signal transduction. One interesting pattern was related to the regulation of membrane-related cytoskeletal elements. Large hepatocytes and small cardiomyocytes both showed enrichment for cell-cell adhesion and junction. We hypothesize that this is related to differences in tissue morphology that are mediated by genome and cell size (Itgen et al., 2022). Large genome and cell size was associated with a dramatic reduction of cardiac tissue in the heart and increased cell packing in hepatic tissue across *Plethodon* species (Itgen et al., 2022). Therefore, cell size-related changes in tissue morphology appears to determine the expression of membrane-related cytoskeletal elements.

Table 2.1 – Functionally enriched terms in the size-negative cluster of DEGs in hepatic cells.

Term name	Source	Term ID	Adjusted <i>P</i>-value
Cellular protein metabolic process	GO:BP	GO:0044267	2.0E-06
Gene expression (Transcription)	REAC	REAC:R-XTR-74160	6.8E-06
Cellular responses to stimuli	REAC	REAC:R-XTR-8953897	7.7E-05
Cellular responses to stress	REAC	REAC:R-XTR-2262752	7.7E-05
M Phase	REAC	REAC:R-XTR-68886	0.0002
Post-translational protein modification	REAC	REAC:R-XTR-597592	0.0003
Separation of Sister Chromatids	REAC	REAC:R-XTR-2467813	0.0003
Anion binding	GO:MF	GO:0043168	0.0005
Metabolism of proteins	REAC	REAC:R-XTR-392499	0.0005
Mitotic Metaphase and Anaphase	REAC	REAC:R-XTR-2555396	0.0005
Mitotic Anaphase	REAC	REAC:R-XTR-68882	0.0005
Transferase complex	GO:CC	GO:1990234	0.0008
Metabolism of RNA	REAC	REAC:R-XTR-8953854	0.0014
Small molecule binding	GO:MF	GO:0036094	0.0021
Cellular Senescence	REAC	REAC:R-XTR-2559583	0.0032
Cell Cycle	REAC	REAC:R-XTR-1640170	0.0033
Nucleotide binding	GO:MF	GO:0000166	0.0038
Nucleoside phosphate binding	GO:MF	GO:1901265	0.0038
Purine ribonucleoside triphosphate binding	GO:MF	GO:0035639	0.0041
ATP binding	GO:MF	GO:0005524	0.0041

Table 2.2 – Functionally enriched terms in the size-positive cluster of DEGs in hepatic cells.

Term name	Source	Term ID	Adjusted <i>P</i>-value
Endomembrane system	GO:CC	GO:0012505	7.0E-05
Endoplasmic reticulum	GO:CC	GO:0005783	0.0003
Cytoplasm	GO:CC	GO:0005737	0.0006
Metabolic pathways	KEGG	KEGG:01100	0.0017
Clathrin-coated vesicle	GO:CC	GO:0030136	0.0149
Golgi apparatus	GO:CC	GO:0005794	0.0149
Clathrin vesicle coat	GO:CC	GO:0030125	0.016
Clathrin-coated vesicle membrane	GO:CC	GO:0030665	0.026
Endocytosis	KEGG	KEGG:04144	0.0278
Phosphatidylinositol binding	GO:MF	GO:0035091	0.034
Clathrin coat	GO:CC	GO:0030118	0.0418
Intracellular transport	GO:BP	GO:0046907	0.0438
Cellular localization	GO:BP	GO:0051641	0.0438
Mediator complex	GO:CC	GO:0016592	0.0478
Clathrin coat of coated pit	GO:CC	GO:0030132	0.0478

Table 2.3 – Functionally enriched terms in the size-negative cluster of DEGs in cardiac cells.

Term name	Source	Term ID	Adjusted <i>P</i>-value
Cytoplasm	GO:CC	GO:0005737	0.0239
Intracellular signal transduction	GO:BP	GO:0035556	0.0299
Cellular protein modification process	GO:BP	GO:0006464	0.0299
Protein modification process	GO:BP	GO:0036211	0.0299
Cellular protein metabolic process	GO:BP	GO:0044267	0.0299
Organonitrogen compound metabolic process	GO:BP	GO:1901564	0.0299
Zinc influx into cells by the SLC39 gene family	REAC	REAC:R-XTR-442380	0.0388
Cell-cell communication	REAC	REAC:R-XTR-1500931	0.0388
Glucose metabolism	REAC	REAC:R-XTR-70326	0.0388
Positive regulation of stress fiber assembly	GO:BP	GO:0051496	0.0432
Macromolecule modification	GO:BP	GO:0043412	0.0432
Protein metabolic process	GO:BP	GO:0019538	0.0448
Zinc transporters	REAC	REAC:R-XTR-435354	0.0499

Table 2.4 – Functionally enriched terms in the size-positive cluster of DEGs in cardiac cells.

Term name	Source	Term ID	Adjusted <i>P</i>-value
Cytoplasm	GO:CC	GO:0005737	5.3E-05
Cellular amide metabolic process	GO:BP	GO:0043603	0.0137
Peptide metabolic process	GO:BP	GO:0006518	0.0175
Mitochondrion	GO:CC	GO:0005739	0.0331
Protein-containing complex	GO:CC	GO:0032991	0.0331
Mediator complex	GO:CC	GO:0016592	0.0337
Amide biosynthetic process	GO:BP	GO:0043604	0.038
Translation	GO:BP	GO:0006412	0.0433
Peptide biosynthetic process	GO:BP	GO:0043043	0.0433

Table 2.5 – Top 20 significantly enriched gene sets in the hepatic tissue of the small genome and cell size species, *P. cinereus*.

Ontology	ID	Term	NES	P-value	FDR q-value
CC	GO:0098798	Mitochondrial protein containing complex	2.52	< 0.001	0.08
CC	GO:0005840	Ribosome	2.44	< 0.001	0.089
CC	GO:0000502	Proteasome complex	2.28	< 0.001	0.188
BP	GO:0042254	Ribosome biogenesis	2.24	0.004	0.189
BP	GO:0043043	Peptide biosynthetic process	2.22	0.002	0.177
CC	GO:1990904	Ribonucleoprotein complex	2.17	< 0.001	0.216
CC	GO:0070069	Cytochrome complex	2.13	< 0.001	0.239
MF	GO:0008138	Protein tyrosine-serine-threonine phosphatase activity	2.12	< 0.001	0.23
CC	GO:0005759	Mitochondrial matrix	2.09	0.002	0.249
MF	GO:0008135	Translation factor activity RNA binding	2.09	0.004	0.225
CC	GO:0098800	Inner mitochondrial membrane protein complex	2.09	0.006	0.205
BP	GO:0033619	Membrane protein proteolysis	2.05	0.006	0.237
CC	GO:0022624	Proteasome accessory complex	2.05	0.004	0.223
BP	GO:0098876	Vesicle-mediated transport to the plasma membrane	2.03	0.006	0.237
BP	GO:0016559	Peroxisome fission	1.97	0.006	0.327
BP	GO:0010458	Exit from mitosis	1.91	0.008	0.451
BP	GO:0017038	Protein import	1.91	0.012	0.428
CC	GO:0005770	Late endosome	1.88	0.016	0.475
MF	GO:0001016	RNA polymerase III transcription regulatory region sequence-specific DNA binding	1.87	0.014	0.48
CC	GO:1905369	Endopeptidase complex	1.85	0.013	0.508

Table 2.6 – Top 20 significantly enriched gene sets in the hepatic tissue of the large genome and cell size species, *P. idahoensis*.

Ontology	ID	Term	NES	P-value	FDR q-value
BP	GO:0071774	Response to fibroblast growth factor	2.85	< 0.001	0.004
MF	GO:0003700	DNA-binding transcription factor activity	2.62	< 0.001	0.019
MF	GO:0000987	cis-regulatory region sequence-specific DNA binding	2.41	< 0.001	0.07
CC	GO:0009986	Cell surface	2.29	< 0.001	0.131
MF	GO:0071889	14-3-3 protein binding	2.24	< 0.001	0.151
BP	GO:1901725	Regulation of histone deacetylase activity	2.18	< 0.001	0.21
BP	GO:0051090	Regulation of DNA-binding transcription factor	2.04	< 0.001	0.452
MF	GO:0019838	Growth factor binding	2.03	0.006	0.411
MF	GO:0005068	Transmembrane receptor protein tyrosine kinase adaptor activity	1.95	0.006	0.602
MF	GO:0030228	Lipoprotein particle receptor activity	1.93	0.006	0.622
CC	GO:0035102	PRC1 complex	1.91	0.016	0.62
CC	GO:0016323	Basolateral plasma membrane	1.86	0.006	0.782
CC	GO:0045178	Basal part of cell	1.86	0.006	0.736
CC	GO:0017053	Transcription repressor complex	1.85	0.01	0.722
MF	GO:0001217	DNA-binding transcription repressor activity	1.85	0.01	0.678
CC	GO:0005911	Cell-cell junction	1.84	0.008	0.676
BP	GO:0016264	GAP junction assembly	1.82	0.018	0.681
BP	GO:0098609	Cell-cell adhesion	1.8	0.022	0.738
MF	GO:0035612	AP-2 adaptor complex binding	1.79	0.015	0.717
CC	GO:0045177	Apical part of cell	1.79	0.02	0.704

Table 2.7 – Top 20 significantly enriched gene sets in the cardiac tissue of the small genome and cell size species, *P. cinereus*.

Ontology	ID	Term	NES	P-value	FDR <i>q</i>-value
MF	GO:0005085	Guanyl nucleotide exchange factor activity	2.36	< 0.001	0.324
BP	GO:0120009	Intermediate lipid transfer	2.32	0.002	0.224
MF	GO:0120013	Lipid transfer activity	2.26	< 0.001	0.216
MF	GO:0120014	Phospholipid transfer activity	2.17	< 0.001	0.295
CC	GO:0031463	CUL3-ring ubiquitin ligase complex	2.16	0.004	0.255
BP	GO:1903829	Positive regulation of protein localization	2.06	0.002	0.388
BP	GO:1904951	Positive regulation of establishment of protein localization	2.03	0.006	0.394
MF	GO:0042887	Amide transmembrane transporter activity	2.02	0.006	0.377
MF	GO:0051721	Protein phosphatase 2A binding	1.96	0.002	0.475
BP	GO:0032446	Protein modification by small protein conjugation	1.94	0.002	0.46
BP	GO:0097320	Plasma membrane tubulation	1.94	0.012	0.428
BP	GO:0017004	Cytochrome complex assembly	1.9	0.006	0.488
BP	GO:2000010	Positive regulation of protein localization to cell membrane	1.9	0.006	0.466
BP	GO:0050714	Positive regulation of protein secretion	1.86	0.014	0.542
CC	GO:0043296	Apical junction complex	1.84	0.012	0.563
MF	GO:0003925	G protein activity	1.82	0.017	0.584
BP	GO:0051882	Mitochondrial depolarization	1.81	0.023	0.581
BP	GO:0010460	Positive regulation of heart rate	1.79	0.008	0.6
BP	GO:0050708	Regulation of protein secretion	1.79	0.021	0.587
BP	GO:0046326	Positive regulation of glucose import	1.77	0.03	0.604

Table 2.8 – Top 20 significantly enriched gene sets in the cardiac tissue of the large genome and cell size species, *P. idahoensis*.

Ontology	ID	Term	NES	<i>P</i> -value	FDR <i>q</i> -value
CC	GO:0099503	Secretory vesicle	2.62	< 0.001	0.028
CC	GO:0030055	Cell substrate junction	2.55	< 0.001	0.03
CC	GO:0030141	Secretory granule	2.53	< 0.001	0.022
BP	GO:0006338	Chromatin remodeling	2.31	< 0.001	0.092
CC	GO:1905368	Peptidase complex	2.28	0.002	0.084
MF	GO:0030506	Ankyrin binding	2.17	< 0.001	0.157
CC	GO:1905369	Endopeptidase complex	2.06	< 0.001	0.275
CC	GO:0042575	DNA polymerase complex	2.03	0.006	0.299
CC	GO:0000228	Nuclear chromosome	2.02	0.002	0.266
BP	GO:0002181	Cytoplasmic translation	2.01	0.002	0.257
BP	GO:0034724	DNA replication-independent chromatin organization	2.0	0.006	0.252
MF	GO:0005242	Inward rectifier potassium channel activity	1.99	< 0.001	0.245
CC	GO:0005840	Ribosome	1.9	0.01	0.381
CC	GO:0032993	Protein DNA complex	1.87	0.006	0.424
CC	GO:0005581	Collagen trimer	1.85	0.03	0.443
BP	GO:0042274	Ribosomal small subunit biogenesis	1.82	0.01	0.481
CC	GO:0043596	Nuclear replication fork	1.76	0.018	0.627
CC	GO:0005839	Proteasome core complex	1.76	0.027	0.603
CC	GO:0031983	Vesicle lumen	1.76	0.019	0.572
CC	GO:0000502	Proteasome complex	1.75	0.029	0.548

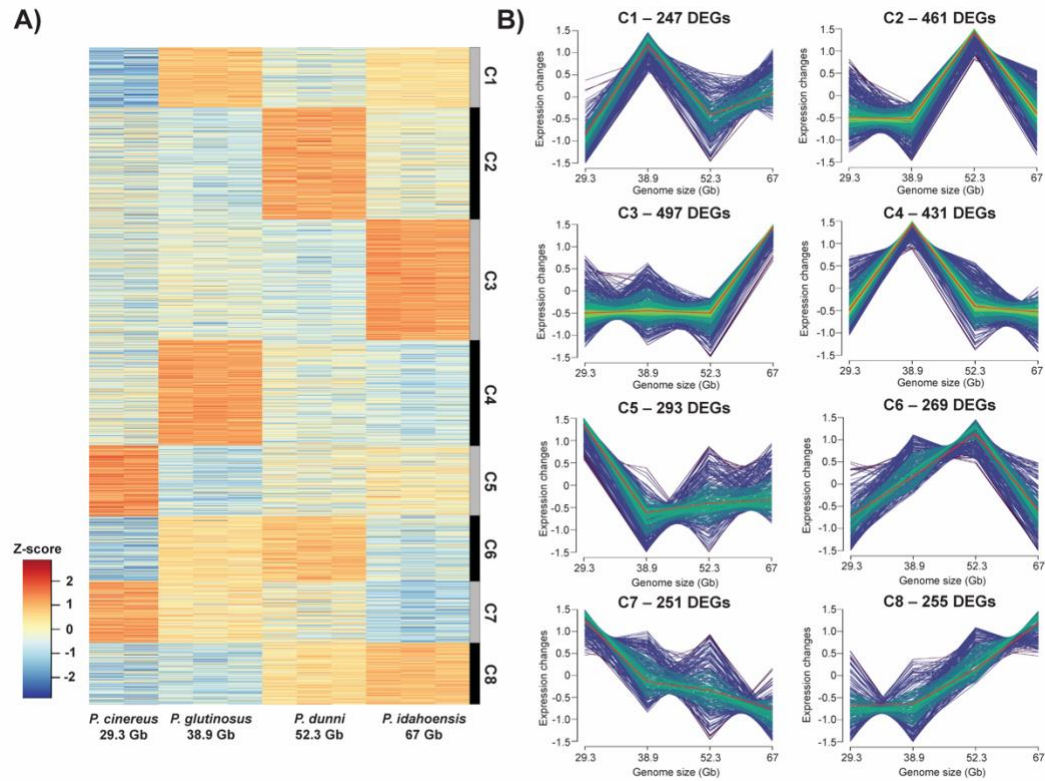


Figure 2.1 – Heatmap visualizing the genes that were differentially expressed in at least one pairwise comparison across the four species of *Plethodon* in the hepatic tissue. A - Genes are grouped into the 8 soft clusters. Gene expression values were normalized using TMM and CPM, and a Z-score normalization was applied for visualization. B - Gene expression patterns in each of the 8 soft clusters of DEGs in the hepatic tissues. Expression data were averaged for each species and plotted against genome size. The number of DEGs assigned to each cluster is denoted above the plot. Each line represents a gene within the cluster and the color of the lines represents membership probability. The red line represents the average across all genes for the species in that specific cluster.

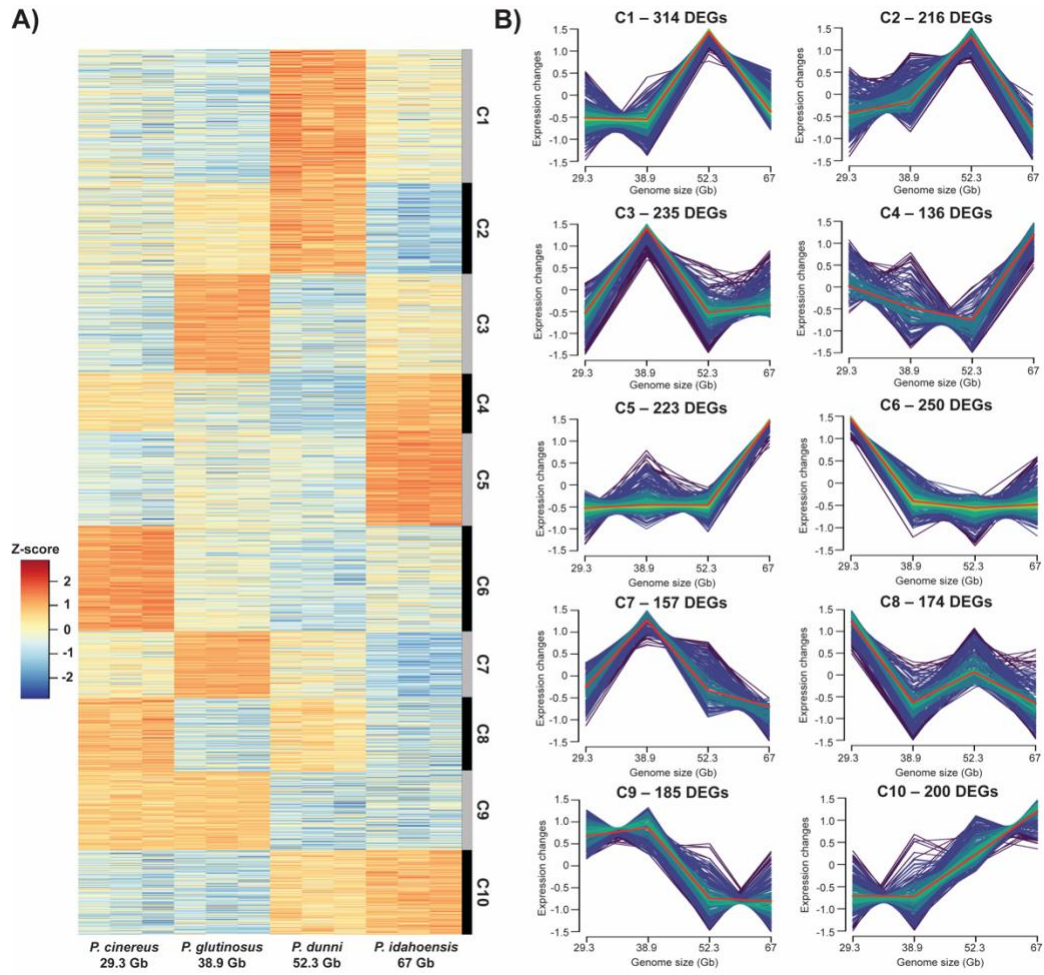


Figure 2.2 – Heatmap visualizing the genes that were differentially expressed in at least one pairwise comparison across the four species of *Plethodon* in the cardiac tissue. A - Genes are grouped into the 10 soft clusters. Gene expression values were normalized using TMM and CPM, and a Z-score normalization was applied for visualization. B - Gene expression patterns in each of the 10 soft clusters of DEGs in the cardiac tissues. Expression data were averaged for each species and plotted against genome size. The number of DEGs assigned to each cluster is denoted above the plot. Each line represents a gene within the cluster and the color of the lines represents membership probability. The red line represents the average across all genes for the species in that specific cluster.

REFERENCES

- Beaulieu, J.M., I.J. Leitch, S. Patel, A. Pendharkar, and C.A. Knight. 2008. Genome size is a strong predictor of cell size and stomatal density in angiosperms. *New Phytologist* 179:975–986.
- Brangwynne, C.P. 2013. Phase transitions and size scaling of membrane-less organelles. *Journal of Cell Biology* 203: 875.
- Bolger, A.M., Lohse, M., and Usadel, B. 2014. Trimmomatic: a flexible trimmer for Illumina sequence data. *Bioinformatics* 30:2114-2120.
- Bushmanova, E., D. Antipov, A. Lapidus, and A.D. Prjibelski. 2019. rnaSPAdes: a de novo transcriptome assembler and its application to RNA-Seq data. *GigaScience* 8:giz100.
- Camacho, C., G. Coulouris, V. Avagyan, N. Ma, J. Papadopoulos, K. Bealer, and T.L. Madden. 2008. BLAST+: architecture and applications. *BMC Bioinformatics* 10:421.
- Chan Y.H.M., and W.F. Marshall. 2010. Scaling properties of cell and organelle size. *Organogenesis* 6: 88-96.
- Crowder Marina E, et al. 2015. A comparative analysis of spindle morphometrics across metazoans. *Current Biology* 25: 1542-1550.
- D’Ario, M., R. Tavares, K. Schiessl, B. Desvoyes, M. Howard, and R. Sablowski. 2021. Cell size controlled in plants using DNA content as an internal scale. *Science* 372:1176–1181.
- Dill, K.A., K. Ghosh, and J.D. Schmit. 2011. Physical limits of cells and proteomes. *Proceedings of the National Academy of Sciences* 108:17876–17882.
- Eddy, S.R. 2011. Accelerated profile HMM searches. *PLOS Computational Biology* 7:e1002195.
- Emms, D.M., and S. Kelly. 2019. OrthoFinder: phylogenetic orthology inference for comparative genomics. *Genome Biology* 20:1–14.
- Francis, D.M., S. Davies, and P.W. Barlow. 2008. A strong nucleotypic effect on the cell cycle regardless of ploidy level. *Annals of Botany* 101:747–757.
- Gregory, T.R. 2001. Coincidence, coevolution, or causation? DNA content, cell size, and the C-value enigma. *Biological Reviews of the Cambridge Philosophical Society* 76: 65-101.
- Gregory TR. 2005. *The Evolution of the Genome*. San Diego, CA: Academic Press.
- Ginzberg, M.B., Kafri, R., and M. Kirschner. 2015. On being the right (cell) size. *Science* 348:1245075.
- Heald R, et al. 2015. *Size Control in Biology: From Organelles to Organisms*. In. Cold Spring Harbor perspectives in biology: Cold Spring Harbor Laboratory Press.
- Heyn, P., A.T. Kalinka, P. Tomancak, and K.M. Neugebauer. 2015. Introns and gene expression: cellular constraints, transcriptional regulation, and evolutionary consequences. *Bioessays* 37:148–154.
- Horner, H.A. and H.C. Macgregor. 1983. C value and cell volume: their significance in the evolution and development of amphibians. *Journal of Cell Science* 63:135–146.
- Itgen, M.W., G.R. Natalie, D.S. Siegel, S.K. Sessions, and R.L. Mueller. 2022. Genome size drives morphological evolution in organ-specific ways. *Evolution*.
- Jimenez, A.G., S.K. Dasika, B.R. Locke, and S.T. Kinsey. 2011. An evaluation of muscle maintenance costs during fiber hypertrophy in the lobster *Homarus americanus*: are larger muscle fibers cheaper to maintain? *Journal of Experimental Biology* 214:3688–2697.

- Jimenez A.G., R.M. Dillaman, and S.T. Kinsey. 2013. Large fiber size in skeletal muscle is metabolically advantageous. *Nature Communications* 4:2150–2150.
- Johnston, I.A., D.A. Fernández, J. Calvo, V.L. Vieira, A.W. North, M. Abercromby, and T. Garland, Jr. 2003. Reduction in muscle fibre number during the adaptive radiation of notothenioid fishes: a phylogenetic perspective. *Journal of Experimental Biology* 206: 2595–2609.
- Kozowski J., M. Konarzewski, and A.T. Gawelczyk. 2003. Cell size as a link between noncoding DNA and metabolic rate scaling. *Proceedings of the National Academy of Sciences, USA* 100:14080.
- Kumar, L., and M.E. Futschik. 2007. Mfuzz: a software package for soft clustering of microarray data. *Bioinformatics* 2:5.
- Kusumi, A., T.K. Fujiwara, R. Chadda, M. Xie, T.A. Tsunoyama, Z. Kalay, R.S. Kasai, and K.G.N. Suzuki. 2012. Dynamic organizing principles of the plasma membrane that regulate signal transduction: commemorating the fortieth anniversary of Singer and Nicolson’s fluid-mosaic model. *Annual Review of Cell and Developmental Biology* 28:215–250.
- Langmead, B., and S. Salzberg. 2012. Fast gapped-read alignment with Bowtie 2. *Nature Methods* 9:357–359.
- Lanz, M.C., E. Zatulovskiy, M.P. Swaffer, L. Zhang, S. Zhang, D.S. You, G. Marinov, P. McAlpine, J.E. Elias, and J.M. Skotheim. 2021. Increasing cell size remodels the proteome and promotes senescence. *BioRxiv* 2021.07.29.454227; doi: <https://doi.org/10.1101/2021.07.29.454227>.
- Li, B., and C.N. Dewey. 2011. RSEM: accurate transcript quantification from RNA-Seq data with or without a reference genome. *BMC Bioinformatics* 12:323.
- Marshall WF 2011. Origins of cellular geometry. *BMC Biology* 9: 57.
- Marshall, W.F., K.D. Young, M. Swaffer, E. Wood, P. Nurse, A. Kimura, J. Frankel, J. Wallingford, V. Walbot, X. Qu, and A.H. Roeder. 2012. What determines cell size? *BMC Biology* 10:101.
- McCarthy, D.J., Y. Chen, and G.K. Smyth. 2012. Differential expression analysis of multifactor RNA-Seq experiments with respect to biological variation. *Nucleic Acids Research* 40:4288–4297.
- Miettinen, T.P., H.K.J. Pessa, M.J. Caldez, T. Fuhrer, M.K. Diril, U. Sauer, P. Kaldis, and M. Björklund. 2014. Identification of transcriptional and metabolic programs related to mammalian cell size. *Current Biology* 24:598–608.
- Miettinen, T.P., and M. Björklund. 2017. Mitochondrial function and cell size: an allometric relationship. *Trends in Cell Biology* 26:393–402.
- Miettinen, T.P., M.J. Caldez, P. Kaldis, and M. Björklund. 2017. Cell size control – a mechanism for maintaining fitness and function. *BioEssays* 39:1700058.
- Milo, R., and R. Phillips. 2015. *Cell biology by the numbers*. New York, NY. Garland Science.
- Nassiri, I., and M.N. McCall. 2018. Systematic exploration of cell morphological phenotypes associated with a transcriptomic query. *Nucleic Acids Research* 46:e116.
- Neurohr, G.E., R.L. Terry, J. Lengefeld, M. Bonney, G.P. Brittingham, F. Moretto, T.P. Miettinen, L.P. Vaites, L.M. Soares, J.A. Paulo, J.W. Harper, J. Buratowski, S. Manalis, F.J. van Werven, L.J. Holt, and A. Amon. 2019. Excessive cell growth causes cytoplasmic dilution and contributes to senescence. *Cell* 176:1083–1097.

- Okie, J.G., V.H. Smith, and M. Martin-Cereceda. 2016. Major evolutionary transitions of life, metabolic scaling and the number and size of mitochondria and chloroplasts. *Proceedings of the Royal Society B: Biological Sciences* 283:20160611.
- Raudvere, U., L. Kolberg, I. Kuzmin, T. Arak, P. Adler, H. Peterson, and J. Vilo. 2019. g: Profiler: a web server for functional enrichment analysis and conversions of gene lists. *Nucleic Acids Research* 47:W191–W198.
- Robinson, M.D., McCrathy, D.J., and Smyth, G.K. 2010. edgeR: a Bioconductor package for differential expression analysis of digital gene expression data. *Bioinformatics* 26:139–140.
- Šímová, I., and T. Herben. 2012. Geometrical constraints in the scaling relationships between genome size, cell size and cell cycle length in herbaceous plants. *Proceedings of the Royal Society B: Biological Sciences* 279:867–875.
- Spencer AK, et al. 2017. Scaling of cytoskeletal organization with cell size in *Drosophila*. *Molecular Biology of the Cell* 28:1519–1529.
- Soh, S., M. Banaszak, K. Kandere-Grzybowska, and B.A. Gryzbowski. 2013. Why are cells microscopic: a transport-time perspective. *The Journal of Physical Chemistry Letters* 4:861–865.
- Yousefi, R., K. Jevdokimenko, V. Kluever, D. Pacheu-Grau, and E.F. Fornasiero. 2021. Influence of subcellular localization and functional state on protein turnover. *Cell* 10:1747.
- Zhou, H.X., G. Rivas, and A.P. Minton. 2008. Macromolecular crowding and confinement: biochemical, biophysical, and potential physiological consequences. *Annual Review of Biophysics* 37:375–397.

3. GENOME AND CELL SIZE INFLUENCE THE METABOLIC STATE, BUT NOT THE METABOLIC COST OF CELLS

Summary

Metabolic rate is a diverse trait that significantly impacts the ecology and physiology of an organism. Because of this, a central goal in evolutionary biology is understanding the determinants that underlie variation in metabolic rate. Genome size has been hypothesized to influence metabolic rate, and large genome size has been associated with the evolution of extremely low metabolic rate in vertebrates. Genome size is hypothesized to lower metabolic rate through its impact on cell size: DNA content is a determinant of cell size. As a result, evolutionary increase in genome size is accompanied by a universal increase in cell size. Cell size is proportional to surface area and, by extension, diffusion rate. Because of this, it is hypothesized that larger cells spend less energy regulating the passive loss of ions across the plasma membrane, which is a metabolically expensive process. This, in turn, has been proposed to lower the metabolic cost at the tissue and organismal level. We tested if cell size is a determinant of cellular and mitochondrial physiology in the liver and heart tissues of 9 species of salamanders (genus *Plethodon*) with a 29.3–67.0 gigabase range in genome size. We found that cell size is not correlated with the metabolic rate of tissues or the relative respiratory cost of maintaining the Na⁺/K⁺-ATPase. We also found no pattern in the evolution of mitochondrial efficiency or capacity that would reflect different metabolic demands related to cell size. However, our transcriptomic analyses suggest that size does alter the metabolic state of cells. We conclude that there is no functional relationship between large cell size and metabolic rate, but that cell size does influence the metabolic state of cells.

Introduction

Metabolism has a central role in the evolution of diverse life histories, physiologies, and morphologies across vertebrates (Glazier, 2004, 2010, 2014; Uyeda et al., 2017; Gardner et al., 2020). Variation in metabolic rate is driven by difference in the energetic needs of an organism. The energy required to maintain an organism, known as the basal metabolic rate, is determined by several phenotypic traits. The strongest predictor of basal metabolism is body size and these two traits scale allometrically with each other (Glazier, 2005, 2010, 2014; Demetrius, 2006). As a result, organisms require relatively less energy per unit of mass as they become larger. Beyond this relationship, there is still substantial variation in basal metabolic rate associated with differences in life history strategies, physiological adaptations, and environment (Uyeda et al., 2017; Gardner et al., 2020).

Genome size has been hypothesized to influence the metabolic rate of an organism. Szarski (1983) was among the first to make a connection between genome size, life history strategies, and metabolic rate in vertebrates. Szarski (1983) described variation in basal metabolic rates among vertebrates as a continuum that exists between two extremes: a wasteful and frugal strategy. Mammals and birds represented the wasteful end of the range due to their high basal metabolic rate required to sustain endothermy, high cognitive function, and powered flight in bats and most birds. Salamanders and lungfish exist on the other end and were described as having a 'frugal' metabolic strategy. Salamanders and lungfish represent two lineages that have extremely low basal metabolic rates, are capable of years-long aestivations, and often exist in hypoxic habitats (Szarski, 1983). Genome size covaries with these dramatic differences in metabolic strategies. Mammals and birds exhibit relatively small genome sizes with low

variation, spanning <1.0–6.5 gigabases (Gb) between both clades (Gregory, 2022). On the other end, salamanders and lungfish have enormous genomes that are also highly variable, which span 9–130 Gb between the two clades. This pattern of covariation led Szarski (1983) to propose that variation in genome size played an underlying role in the variation of metabolic rate. More specifically, large genome and cell size lowers the metabolic demands of an organism.

The connection between increased DNA content and lower metabolic rate is hypothetically mediated by the impact of genome size on cells (Kozłowski et al., 2003; Savage et al., 2007; Starostová et al., 2009; Glazier, 2014; Takemoto, 2015). Genome size determines the size of the nucleus and, in turn, the size of the cell (Gregory, 2001, 2005). As a result, genome and cell size share a strong positive relationship regardless of cell type – as genome size increases, so does the minimum cell size (Gregory, 2001, 2005). Increases in cell size has been shown to dramatically impact the function of cellular processes (Miettinen et al., 2014, 2017; Ginzberg et al., 2015). As cells become larger, their surface area and volume scale to the power of 2 and 3, respectively. Because larger cells have less surface area (i.e., plasma membrane) relative to volume (i.e., cytoplasm). These changes in the surface area-to-volume (SV) ratio have been shown to impact various cellular processes, such as intracellular transport and biosynthetic capacity (Miettinen et al., 2014; Neurohr et al., 2019; Lanz et al., 2021). Further, it has been inferred that the physiological changes in cell biology driven by large cell size underlie the broader patterns of phenotypic change in organisms, such as low metabolic rate (Szaraski, 1983; Licht and Lowcock, 1991; Kozłowski et al., 2003; Gregory, 2005).

The proposed model explaining the evolution of genome size and metabolic rate postulates that the metabolic cost of a tissue or organism decreases as it is comprised of fewer larger cells (Kozłowski et al., 2003). The key mechanism in this model focuses on the

maintenance of ion gradients. The maintenance of ion gradients across the plasma membrane is an energy-expensive process. It is estimated that ~20% of an organism's metabolic rate consists of the active transport of sodium and potassium across the plasma membrane (Milligan and McBride, 1985). Larger cells have lower SV ratios and therefore slower rates of passive diffusion, it is predicted that large cells spend lower proportion of energy maintaining this Na^+/K^+ ion gradient (Kozłowski et al., 2003; Miettinen et al., 2017). The relative decrease in metabolic expense in larger cells is hypothesized to scale levels of complexity, resulting in a decrease in basal metabolic rate at the tissue- and organismal-level (Kozłowski et al., 2003).

The association between genome size and metabolic rate has been an outstanding question in the genome size and physiology fields for decades (Szarski, 1983; Licht and Lowcock, 1991; Vinogradov, 1995, 1997; Kozłowski et al., 2003; Wright et al., 2014; Johnson et al., 2021). Despite strong support from theoretical modeling, comparative studies investigating the correlation between genome and cell size and metabolic rate have been conflicting. Several studies have found a negative effect of genome size on metabolic rate, particularly in mammals and birds (Vinogradov, 1995, 1997; Gregory, 2002; Waltari and Edwards, 2002; Smith et al., 2013; Wright et al., 2014). Yet even among mammals and birds, some of these studies and others have found no significant relationship in either group (Vinogradov, 1995; Ji and DeWoody, 2017). Evidence for a genome size and metabolic relationship is just as complicated when considering groups with enormous genome sizes, especially amphibians. Early work found that dry cell area was negatively correlated with the amount of CO_2 produced by the whole organism in frogs and salamanders (Smith, 1925). Cellular metabolic rates were also found to be correlated with cell size across amphibian taxa (Goniakowska, 1970, 1973; Monnickendam and Balls, 1973). Then, Licht and Lowcock (1991) were the first to robustly test for a genome size effect on

whole organism metabolic rate in salamanders, but only found a slight negative correlation at some temperatures but not others. Gregory (2003) reanalyzed the relationship between genome size and metabolic rate in amphibians and found an overall negative pattern across all amphibians, but not within frogs or salamanders. Johnson et al. (2021) also tested for a genome size effect on organismal respiration rates in two lungless salamander genera, *Plethodon* and *Eurycea*, and found no evidence that genome size influences the metabolic rate of salamanders despite enormous ranges in genome size. More broadly, phylogenetic models found that genome size did not explain variation in metabolic rate across the vertebrate clade (Uyeda et al., 2017; Gardner et al., 2020). The conflicting support across taxonomic groups leaves the effect of genome and cell size on metabolic rate an open-ended question.

Whole organism metabolic rate is determined by several complex interactions across biological levels, and the relative amount of specific cell types can determine metabolic rate (Savage et al., 2007; Glazier, 2014; Takemoto, 2015). Therefore, even if there is an effect of genome and cell size, it can be obscured by other, more powerful, predictors of metabolic rate (Glazier, 2004, 2010, 2015). One critical missing component to understanding this potential correlation is a robust study on the impact of genome and cell size on cellular physiology. Our goal is to test if genome and cell size impacts the respiratory rate of tissues in the salamander genus *Plethodon*. A clear prediction from the Kozłowski et al. (2003) model is that tissues comprised of larger cells should have lower metabolic rates compared to similar tissue comprised of smaller cells. Further, the underlying mechanism for this model suggests that tissues formed from larger cells are cheaper because it is less expensive to maintain ion gradients, such as Na^+/K^+ (Szarski, 1983; Milligan and McBride, 1985; Kozłowski et al., 2003). We test these hypotheses by measuring the respiration rates of hepatic tissue in 9 species of

Plethodon salamanders with genome sizes ranging 29.3–67.0 gigabases (Gb) (Itgen et al., 2022). We then test whether maintaining ion gradients is relatively cheaper in large cells by inhibiting Na^+/K^+ -ATPase activity and calculating the relative decrease in respiration rates of the hepatic tissues. Next, we also measured several functional aspects of mitochondrial physiology, such as oxidative phosphorylation (OXPHOS) efficiency, to determine if there are patterns of evolution that suggest differential metabolic demands associated with changes in cell size. Lastly, we used RNA-Seq data to perform a gene set enrichment analysis (GSEA) comparing the two species with the smallest and largest genome sizes and determine if cell size alters the metabolic state of the cell.

Methods

Animal and tissue collection

We collected 5 adult individuals of *P. cinereus*, *P. cylindraceus*, *P. dumni*, *P. glutinosus*, *P. idahoensis*, *P. metcalfi*, *P. montanus*, *P. vandykei*, and *P. vehiculum* (Supplemental Information 2.1). Salamanders were kept on wet paper towels in containers at 15°C and were fed fruit flies weekly. The protocols for animal research, husbandry, and euthanasia were approved by the Institutional Animal Care and Use Committee of Colorado State University and carried out in accordance with protocol 17–7189A.

Salamanders were euthanized in buffered 1% MS-222 3 days after feeding. The liver and hearts were dissected out and transferred into Biops solution and kept on ice. Liver tissue was further dissected to a wet weight ranging from 15-25 mg and the ventricle was dissected out entirely, rinsed of blood, and weighed. Tissues were then transferred to MiR05 and kept on ice prior to experimentation.

Basal cellular respiration rate

Our first goal was to test whether respiration rates differ across cells of different sizes. To this end, basal cellular respiration rates were measured as the rate of oxygen consumption of intact hepatocyte cells from liver tissue. Respiration rates were measured using the Oxygraph-2k (O2K) high-resolution respirometer system (Oroboros Instruments GmbH, Innsbruck, Austria) at 25°C using 2 mL of MiR05 as the substrate. We selected 25°C based on preliminary experiments and because it was one of the temperatures at which Licht and Lowcock (1991) found a significant genome size effect in salamanders. Experiments were done in a hyper-oxygenated environment by injecting oxygen into the chamber until oxygen concentrations reached 440 μM . All measurements of oxygen consumption rate were standardized by the wet mass of the tissue sample.

Na/K pump respiratory cost

Our second goal was to test whether cells of different sizes expend different relative amounts of their total energy budget on Na^+/K^+ -ATPase activity, given their differences in SV ratio. After obtaining measurements of basal cellular respiration rate (above), the respiratory cost of Na^+/K^+ -ATPase activity was measured by inhibiting the transmembrane pump proteins with a high concentration (60 μM) of ouabain and measuring the associated decrease in oxygen consumption, holding all other conditions unchanged. We then calculated the proportional change from basal cellular respiration to respiration with inhibited Na^+/K^+ -ATPase.

Mitochondrial LEAK, oxidative respiration, and ATP synthesis

Our third goal was to test whether the mitochondria from cells of different sizes differ in functional output. We used both liver and heart cells for this experiment; the liver cells were first assessed for basal respiration and Na^+/K^+ -ATPase cost (above). Cell membranes were permeabilized using 25 $\mu\text{g}/\text{mL}$ of digitonin to expose the mitochondria. We also added 60 μM of blebistatin to the heart tissue to inhibit myosin heavy chain activity. Mitochondrial respiration and ATP synthesis rates were then assessed using a multi-substrate titration protocol. Experiments were conducted using the O2K with 2 mL of MiRO5 substrate in a hyper-oxygenated environment at 25°C, as above.

We first measured leak respiration, which reflects an uncoupling or dyscoupling of the electron transport chain from ATP synthesis; leak respiration (i.e. LEAK) is a compensatory mechanism in response to protons that leak back through the inner mitochondrial membrane in the absence of ADP phosphorylation. We induced LEAK by providing mitochondria with reducing substrates (1mM of malate, 10 mM of pyruvate) in the absence of ADP and measuring oxygen consumption. Next, we measured maximal oxidative respiration capacity during oxidative phosphorylation (OXPHOS) by adding 2.5 mM of ADP, 10 mM of glutamate, and 10 mM of succinate — thereby reconstituting the TCA cycle — and measuring oxygen consumption. Finally, with the TCA cycle fully reconstituted, we measured maximal ATP synthesis rates by adding 5.5 μM of the Magnesium Green fluorophore (MgG) and attaching a 503 nm LED and a 530 nm filter, enabling us to visualize newly synthesized ATP molecules in real time. We calculated OXPHOS efficiency for each species/tissue type as the ratio of maximal rate of ATP synthesis to maximal oxidative respiration.

Testing for differences in respiratory phenotypes across genome sizes

We first tested for among-species differences in all respiratory variables using a MANOVA on log-transformed data: basal cellular respiration rates in hepatocytes; Na/K pump respiratory cost in hepatocytes; and LEAK, maximum oxidative respiratory capacity, maximum ATP synthesis rates, and OXPHOS efficiency in mitochondria from both hepatocytes and cardiomyocytes. We performed a post-hoc test on significantly different variables using a one-way ANOVA and a least significant difference test with a Hommel p-value adjustment on the same log-transformed data. Statistical analyses were performed in R v 4.1.3 (R core team, 2022).

We then tested for an effect of genome size on these same log-transformed respiratory variables using phylogenetic generalized least squares (PGLS) models. The phylogeny and genome sizes for our nine focal species of *Plethodon* were taken from Itgen et al. (2022). We applied a Brownian motion model of trait evolution to all variables and included a simultaneous estimation of Pagel's lambda for each trait (Revell, 2010). Individual models were created for each respiratory variable, with genome size as the independent variable in all analyses and the mean species value for the respiratory trait as the dependent variable. A Benjamini-Hochberg false discovery rate correction was applied to adjust for multiple testing (Benjamini and Hochberg, 2000). The PGLS analyses were conducted using R v 4.1.3 and the packages *caper* and *nlme* (Orne et al., 2013; R core team, 2016; Pinheiro et al., 2021). Prior to both the MANOVA and PGLS analyses, extreme outliers for all respiratory variables were excluded; however, inclusion of these presumably erroneous measurement values did not affect our conclusions.

Testing for differences in respiratory gene expression between small and large genome/cell sizes

Our final goal was to complement our cellular and mitochondrial assays with analyses of respiratory gene expression in cells of different sizes. We ran a GSEA in both heart and liver tissue between *Plethodon cinereus* and *P. idahoensis*, the species in our dataset with the smallest and largest genome sizes, using Broad Institute's Gene Set Enrichment Analysis (GSEA) v4.2.3. Transcriptome assemblies and raw reads for both species were obtained from Chapter 2. We identified putative protein coding genes in the heart and liver transcriptomes of *P. cinereus* and *P. idahoensis* using TransDecoder. We only retained the longest ORF per contig and filtered out ORFs using homology-based searches with blastp (e-value 1e-5) against the SwissProt database and hmmscan against the Pfam database. We used OrthoFinder v 2.5.4 to identify single copy orthologs in both species (Emms and Kelly, 2019). We annotated the ortholog sets from the heart and liver transcriptomes against the UniProt human proteome using blastx (e-value 1e-5) and retained orthologs with significant hits. We identified 15,785 single copy orthologs in the heart transcriptomes and 15,194 single copy orthologs in the liver transcriptomes between *P. cinereus* and *P. idahoensis*. We annotated 7,433 of the heart orthologs and 7,171 of the liver orthologs using the UniProt human proteome. We quantified the annotated ortholog sets for each species with RSEM and normalized count data for library size using trimmed mean of M-values (TMM) and calculated the counts per million (CPM) with edgeR (Li and Dewey, 2011; Robinson et al., 2010).

We compiled relevant Gene Ontology (GO) gene sets based on molecular functions and biological processes related to cellular respiration, ATP metabolism, dehydrogenase activity, mitochondrial physiology, and ion transport from the Molecular Signatures Database (MsigDb v7.5.1 <http://software.broadinstitute.org/gsea/msigdb/index.jsp>). In total, our analyses included

86 gene sets. We ran the GSEA with a ratio of classes gene ranking metric and the classic enrichment statistic.

Results

Cellular respiration rate and Na/K pump respiratory cost are similar across salamanders

Mean basal respiration rates of hepatic tissue encompassed a 1.8-fold range of values, from 1.3 JO_2 in *P. cinereus* to 2.4 JO_2 in *P. dunni* (Table 1). Both *P. cinereus* and *P. dunni* were also significantly different from all other species (Fig. 1; Table 3). The mean relative respiratory cost of the Na^+/K^+ -ATPase in hepatic tissue showed a 1.6-fold range, from 14.9% of total respiration in *P. glutinosus* to 24% in *P. montanus*. There were no significant differences in the relative respiratory cost of the Na^+/K^+ -ATPase among species (Table 3).

Mitochondrial respiratory physiology is similar across salamanders

Mean hepatic mitochondrial LEAK respiration rates showed a 2.2-fold range, from 4.6 JO_2 in *P. vandykei* to 10.1 JO_2 in *P. glutinosus*. Mean cardiac mitochondrial LEAK respiration rates showed a 4.8-fold range, from 2.9 JO_2 in *P. cinereus* to 14.0 JO_2 in *P. montanus* (Table 2). There were no significant differences in LEAK respiration rates among species in either tissue (Table 3).

The mean maximal respiration rate of hepatic mitochondria ranged from 2.3 JO_2 in *P. vehiculum* to 4.9 JO_2 in *P. vandykei*, with no significant differences among species (Table 2, Table 3). In contrast to LEAK, which showed no difference between tissues, mean maximal respiration rates of cardiac mitochondria were considerably higher than those of hepatic mitochondria, ranging from 17.7 JO_2 in *P. cylindraceus* and *P. metcalfi* to 55.4 JO_2 in *P.*

montanus (Table 2). There were significant differences in the maximal respiration rate of cardiac mitochondria, with most species separating into two groups and *P. montanus* having significantly higher cardiac mitochondrial respiration rates than all other species (Fig. 1; Table 3).

Interestingly, *P. montanus* also had the highest cardiac mitochondrial LEAK rates. In contrast, *P. vandykei* hepatocytes had the highest respiration rates, but the lowest LEAK rates.

Mean ATP synthesis rates in hepatic tissues showed a ~2.75-fold range, from 0.0004 JATP in *P. glutinosus* to 0.0011 in *P. cinereus* (Table 2). There were no significant differences in maximal ATP synthesis rate in hepatic mitochondria across species (Table 3). Similar to the pattern seen in maximal respiration, mean ATP synthesis rates in cardiac mitochondria were considerably higher than those in hepatic mitochondria (Table 2). There was a ~7.2-fold range in mean ATP synthesis rates in cardiac mitochondria, from 0.0022 JATP in *P. metcalfi* to 0.0159 JATP in *P. cinereus* (Table 2). There were significant differences in ATP synthesis rates of cardiac mitochondria across species, with *P. cinereus* having a significantly higher rate than all species and *P. montanus* and *P. idahoensis* having the second-highest rate, significantly different from the remaining species (Fig. 1; Table 3).

Mean OXPHOS efficiency (P / O ratio) of hepatic tissue showed a 2.8-fold range, from 0.012 in *P. montanus* to 0.034 in *P. vehiculum* (Table 2). The mean OXPHOS efficiency of cardiac mitochondria showed a 5.5-fold range, from 0.012 in *P. glutinosus* to 0.066 in *P. cinereus*. There were no significant differences in OXPHOS efficiencies in either tissue among species (Table 3), and the range of efficiencies in the two tissues overlapped, although the cardiac range was roughly twice as broad.

The maximal respiration rates and ATP synthesis rates were much higher in cardiac mitochondria compared to hepatic mitochondria (Table 2). Since both measurements were mass-

corrected, this result suggests a higher density of mitochondria in cardiac tissue. The OXPHOS coupling efficiencies of mitochondria in the two tissue types were also comparable, further suggesting differences in absolute respiration and ATP synthesis are related to the mitochondrial densities.

Genome size is not correlated with functional measures of cellular or mitochondrial respiratory phenotype

We found no significant correlation between genome size and basal cellular respiration rate ($P = 0.577$) or the relative cost of Na^+/K^+ -ATPase activity ($P = 0.856$) in hepatic tissue (Table 4; Fig. 2). Therefore, our results do not support the hypotheses that 1) larger cell size lowers basal respiration rate of tissues, or 2) lower SA:V ratio decreases the relative cost of maintaining ion gradients across the plasma membrane in larger cells.

We also found no significant relationships between genome size and any of the other mitochondrial respiratory phenotypes we assayed in either hepatic or cardiac mitochondria: LEAK, maximum oxidative respiratory capacity, maximum ATP synthesis rates, or OXPHOS efficiency (Table 4; Fig. 3,4). There were non-significant trends towards negative correlation between genome size and 1) maximal ATP synthesis rate, and 2) OXPHOS coupling efficiency (Fig. 4). Together, these results suggest that genome/cell size is not a strong predictor of mitochondrial respiratory phenotype.

Comparative transcriptomics suggest cell size-related differences in physiology depending on cell type

In the liver tissue, *P. cinereus*, the species with the smaller genome size, had enrichment for 9 gene sets that included aerobic respiration and cellular respiration, oxidative phosphorylation, the respiratory electron transport chain, and inorganic ion transmembrane transport (Table 5). In *P. idahoensis*, the species with the larger genome size, we found enrichment for 8 gene sets that were broadly associated with various redox pathways and cellular responses to reactive oxygen species (Table 6). We found concordant, but weaker ($P < 0.05$; FDR $> 25\%$), support for this pattern in the heart tissue (Table 7,8). We found two significantly enriched terms in the heart tissue of *P. cinereus* including cytochrome complex assembly and positive regulation of potassium ion transport (Table 7). *Plethodon idahoensis* had enrichment for 4 terms including potassium channel activity, voltage-gated potassium channel activity, ligand-gated ion channel activity, and NAD⁺ binding (Table 8). There is overlap between both species in regard to potassium channel-related activity. However, the enrichment for the cytochrome complex assembly gene set in *P. cinereus* and NAD⁺ binding gene set in *P. idahoensis* is concordant with the pattern seen in the liver: upregulation of respiration and OXPHOS in smaller cells and oxygenase activity in larger cells. The overall pattern we found supports the working hypotheses and models stating that cell size impacts cell physiology. Our analyses suggest that cell size might impact the regulation of metabolic pathways, or the metabolic state, of cells.

Discussion

Genome and cell size influence metabolic state but not metabolic rate

Our results do not support the model explaining a potential link between genome and cell size and metabolic rate. Basal respiration rate of hepatic tissues did vary among species, but

there was no significant effect of genome size across the 29.3–67.0 Gb range. While these results do not support the hypothesis that genome and cell size is a significant determinant of metabolic rate, these are concordant with other recent studies (Uyeda et al., 2017; Gardner et al., 2020; Johnson et al., 2021). Therefore, the enormous cell sizes do not impact metabolic rate at the cellular or organismal level in *Plethodon* (Johnson et al., 2021).

We also found no evidence that large cell size reduces the metabolic cost of maintaining the Na⁺/K⁺ ion gradient, which has been the theoretical mechanism underlying this potential correlation. In fact, the relative cost of the Na⁺/K⁺-ATPase in the salamander hepatic tissue is comparable to other vertebrates, including mammals (Milligan and McBride, 1985). These results are interesting, since cell size has been shown to impact the respiratory cost of the Na⁺/K⁺-ATPase activity in other, albeit limited, empirical studies. For example, the Na⁺/K⁺-ATPase metabolic cost was 2-fold higher in smaller skeletal muscle cells compared to larger ones in lobsters (Jimenez et al., 2011, 2013). It is possible that the effects of cell size are dependent on cell type. However, we predicted that hepatocytes were more likely to show a cell size-related pattern due to the cuboidal morphology being more severely impacted by the SV scaling as they become larger (Miettinen et al., 2017).

Although we found no correlation between metabolic rate and genome / cell size, our transcriptomic analyses suggest that cell size alters the metabolic pathways (i.e., metabolic state) of cells. Cells can alter their metabolic state depending on nutrient availability, transient states, cell type, or cell size, often over short time scales (Sieber and Spradling, 2017). Since cell size has been shown to alter functional pathways effected by differences in surface area and volume, it is likely cells must alter their metabolic pathways as well (Ginzberg et al., 2015; Miettinen et al., 2017; Sieber and Spradling, 2017). Smaller hepatocytes appear to undergo more OXPHOS

and ion transmembrane transport relative to larger cells. Interestingly, this provides support that smaller cells with greater SV ratios must increase the Na^+/K^+ -ATPase to maintain ion gradients, but our functional data shows that this difference doesn't translate into differences in metabolic rate. Conversely, larger cells are upregulating oxidoreductase activity and cellular responses to reactive oxygen species. These patterns suggest that the metabolic demands do change relative to cell size, but this change does not result in larger cells being cheaper.

Mitochondrial physiology matches low metabolic rate of salamanders but not genome size

There were no significant patterns in the evolution of mitochondrial function and efficiency that suggests increased genome / cell size alters the metabolic demands of the cell. Instead, it appears that mitochondria are evolving under relaxed functional selection due to the low metabolic demands of salamanders (Chong and Mueller, 2013). We found that cardiac and hepatic mitochondria have exceptionally low respiration and ATP synthesis rates compared to other vertebrates. Further, OXPHOS is incredibly inefficient in salamanders despite low LEAK respiration rates. These results are concordant with other related studies. First, our results match the findings of Chicco et al. (unpublished) that salamanders have distinct mitochondrial phenotype that reflect the low metabolic demands of these organisms. Second, we provide functional support to the results of Chong and Mueller (2013), who showed that the protein coding sequences of OXPHOS-related genes were evolving under relaxed selection relative to frogs. There is a clear relationship between cellular and mitochondrial physiology and organismal metabolic rates in salamanders and other vertebrates (Chicco et al., unpublished). We hypothesize that the low metabolic rates are a unique and functionally unrelated trait to genome

and cell size in salamanders. Further comparative work is necessary to understand the drivers of the extraordinarily low metabolic rates of salamanders and the cellular and organismal level.

Table 3.1 – Mean and standard deviation for cellular physiological measurements in hepatic tissues. n = 5 individuals unless otherwise noted.

Species	Genome size (Gb)	Basal respiration rate J_{O_2} (pmol O ₂ s ⁻¹ mg ⁻¹)	Percent of basal respiration rate related to Na ⁺ /K ⁺ -ATPase
<i>P. cinereus</i>	29.3	1.3 ± 0.7 (n=4)	23.4 ± 6.7 (n=4)
<i>P. montanus</i>	36.0	2.1 ± 0.6	24.0 ± 5.6 (n=4)
<i>P. cylindraceus</i>	37.1	1.7 ± 0.4	16.6 ± 7.0
<i>P. metcalfi</i>	38.3	1.6 ± 0.4	19.8 ± 9.6
<i>P. glutinosus</i>	38.9	2.0 ± 0.3	14.9 ± 4.3
<i>P. vehiculum</i>	46.4	2.2 ± 0.2 (n=6)	21.5 ± 7.8 (n=6)
<i>P. dunni</i>	52.3	2.4 ± 0.6 (n=4)	18.7 ± 5.1
<i>P. vandykei</i>	54.6	1.4 ± 0.1 (n=3)	16.5 ± 4.1 (n=3)
<i>P. idahoensis</i>	67.0	1.6 ± 0.6 n=6)	23.8 ± 12.3 (n=6)

Table 3.2 – Mean and standard deviation for mitochondrial physiological measurements in hepatic and cardiac tissues. n = 5 individuals unless otherwise noted.

Species	Genome size (Gb)	Hepatic mitochondria				Cardiac mitochondria			
		LEAK respiration rate JO_2 (pmol O_2 s ⁻¹ mg ⁻¹)	Maximal respiration rate JO_2 (pmol O_2 s ⁻¹ mg ⁻¹)	Maximal ATP synthesis rate $JATP$	OXPHOS coupling efficiency	LEAK respiration rate JO_2 (pmol O_2 s ⁻¹ mg ⁻¹)	Maximal respiration rate JO_2 (pmol O_2 s ⁻¹ mg ⁻¹)	Maximal ATP synthesis rate $JATP$	OXPHOS coupling efficiency
<i>P. cinereus</i>	29.3	9.0 ± 3.9 (n=4)	4.0 ± 0.9 (n=4)	0.0011 ± 0.0005 (n=4)	0.027 ± 0.008 (n = 4)	2.9 ± 1.0 (n = 8)	24.5 ± 11.0 (n=7)	0.0159 ± 0.007 (n=7)	0.066 ± 0.03 (n=6)
<i>P. montanus</i>	36.0	6.4 ± 3.6	3.4 ± 0.7 (n=4)	0.0005 ± 0.0003	0.012 ± 0.008	14.0 ± 9.3	55.4 ± 13.4 (n=4)	0.0095 ± 0.006	0.016 ± 0.01 (n=4)
<i>P. cylindraceus</i>	37.1	7.4 ± 3.7	3.2 ± 0.6	0.0005 ± 0.0003	0.016 ± 0.009	8.6 ± 3.3	17.7 ± 7.5	0.0028 ± 0.001	0.019 ± 0.01
<i>P. metcalfi</i>	38.3	4.5 ± 1.8	2.7 ± 1.0	0.0009 ± 0.0006 (n=4)	0.033 ± 0.016	11.8 ± 4.1	17.7 ± 3.9	0.0022 ± 0.001	0.013 ± 0.01
<i>P. glutinosus</i>	38.9	10.1 ± 6.3	3.4 ± 1.4	0.0004 ± 0.0002	0.016 ± 0.008	7.5 ± 3.0	21.0 ± 10.2	0.0023 ± 0.002	0.012 ± 0.01
<i>P. vehiculum</i>	46.4	4.9 ± 2.7	2.3 ± 0.7	0.0007 ± 0.0006 (n=6)	0.034 ± 0.027 (n = 6)	8.7 ± 5.1 (n = 6)	33.3 ± 11.3 (n=6)	0.0048 ± 0.005 (n = 6)	0.013 ± 0.01 (n=6)
<i>P. dunni</i>	52.3	7.2 ± 3.6 (n=4)	2.4 ± 0.8	0.0004 ± 0.0003 (n=4)	0.015 ± 0.012 (n = 4)	9 ± 3.1 (n = 4)	23.7 ± 3.6	0.0031 ± 0.002 (n = 4)	0.013 ± 0.01 (n=4)
<i>P. vandykei</i>	54.6	4.6 ± 1.6	4.9 ± 1.9	0.001 ± 0.0005	0.026 ± 0.023	8.8 ± 3.7 (n = 4)	21.3 ± 10.2	0.0057 ± 0.004	0.028 ± 0.02
<i>P. idahoensis</i>	67.0	7.6 ± 3.0 (n=6)	3.9 ± 1.1 (n=6)	0.0008 ± 0.0009	0.017 ± 0.015	8.5 ± 6.5 (n=6)	30.0 ± 12.5 (n=6)	0.0079 ± 0.004	0.027 ± 0.02

Table 3.3 – Summary of MANOVA testing for species-specific differences in cellular and mitochondrial physiological measurements. Significant p-values are bolded.

		df	Mean Squares	F-statistic	<i>P</i>
Hepatic tissue	Basal cellular respiration	8,22	0.09	6.5	< 0.001
	NaK-related metabolic cost in hepatocytes	8,22	0.1	0.5	0.838
Hepatic mitochondria	Maximal O2 consumption rate	8,22	0.15	1.6	0.189
	Maximal ATP Synthesis rate	8,22	2.76E-07	0.8	0.64
	OXPHOS Coupling	8,22	0.0003	0.9	0.551
	LEAK Respiration	8,22	0.29	0.93	0.513
Cardiac mitochondria	Maximal O2 consumption rate	8,22	0.62	2.9	0.005
	Maximal ATP Synthesis rate	8,22	3.70E-05	2.9	0.023
	OXPHOS Coupling	8,22	0.001	2.1	0.075
	LEAK Respiration	8,22	0.675	2.2	0.071

Table 3.4 – Summary of the PGLS linear regressions showing the individual interactions between the predictor and response variables.

		t-value	<i>P</i>
Hepatic tissue	Basal cellular respiration	0.58	0.577
	NaK-related metabolic cost in hepatocytes	-0.19	0.856
Hepatic mitochondria	Maximal O ₂ consumption rate	-0.54	0.605
	Maximal ATP Synthesis rate	-0.43	0.68
Hepatic mitochondria	O ₂ PHOS Coupling	-0.3	0.777
	LEAK Respiration	-0.83	0.432
Cardiac mitochondria	Maximal O ₂ consumption rate	0.12	0.908
	Maximal ATP Synthesis rate	-1.31	0.232
	O ₂ PHOS Coupling	-1.9	0.1
	LEAK Respiration	1.12	0.298

Table 3.5 – Significantly enriched gene sets in the hepatic tissue of *P. cinereus*, the small genome and cell size species.

Ontology	ID	Term	Enrichment Score	Nominal <i>P</i> -value	FDR <i>q</i> -value
CC	GO:0098800	Inner mitochondrial membrane protein complex	0.2	0.002	0.203
BP	GO:0098660	Inorganic ion transmembrane transport	0.11	0.01	0.178
BP	GO:0006119	Oxidative phosphorylation	0.18	0.012	0.249
BP	GO:0009060	Aerobic respiration	0.15	0.011	0.248
MF	GO:0016887	ATP hydrolysis activity	0.11	0.018	0.217
CC	GO:0031304	Intrinsic component of mitochondrial inner membrane	0.25	0.019	0.191
BP	GO:0045333	Cellular respiration	0.14	0.04	0.199
BP	GO:2000379	Positive regulation of reactive oxygen species metabolic process	0.23	0.033	0.248
MP	GO:0022904	Respiratory electron transport chain	0.19	0.06	0.228

Table 3.6 – Significantly enriched gene sets in the hepatic tissue of *P. idahoensis*, the large genome and cell size species.

Ontology	ID	Term	Enrichment Score	Nominal <i>P</i> -value	FDR <i>q</i> -value
MF	GO:0016709	Oxidoreductase activity acting on paired donors with incorporation or reduction of molecular oxygen NADPH as one donor and incorporation of one atom of oxygen	0.36	0.002	0.075
MF	GO:0016706	2-oxoglutarate dependent dioxygenase activity	0.3	0.002	0.041
MF	GO:0016705	Oxidoreductase activity acting on paired donors with incorporation or reduction of molecular oxygen	0.18	0.002	0.065
MF	GO:0051213	Dioxygenase activity	0.22	< 0.001	0.07
MF	GO:0004497	Monooxygenase activity	0.22	0.022	0.159
BP	GO:0000302	Response to reactive oxygen species	0.14	0.032	0.2
BP	GO:1902108	Regulation of mitochondrial membrane permeability involved in apoptotic process	0.31	0.037	0.212
BP	GO:0034614	Cellular response to reactive oxygen species	0.15	0.029	0.186

Table 3.7 – Significantly enriched gene sets in the cardiac tissue of *P. cinereus*, the small genome and cell size species.

Ontology	ID	Term	Enrichment Score	Nominal <i>P</i> -value	FDR <i>q</i> -value
BP	GO:0017004	Cytochrome complex assembly	1.84	0.01	0.54
BP	GO:0043268	Positive regulation of potassium ion transport	1.83	0.022	0.296

Table 3.8 – Significantly enriched gene sets in the cardiac tissue of *P. idahoensis*, the large genome and cell size species.

Ontology	ID	Term	Enrichment Score	Nominal <i>P</i> -value	FDR <i>q</i> -value
MF	GO:0005267	Potassium channel activity	1.79	0.014	0.753
MF	GO:0005249	Voltage-gated potassium channel activity	1.71	0.026	0.592
MF	GO:0015276	Ligand-gated ion channel activity	1.65	0.031	0.523
MF	GO:0051287	NAD ⁺ binding	1.63	0.044	0.44

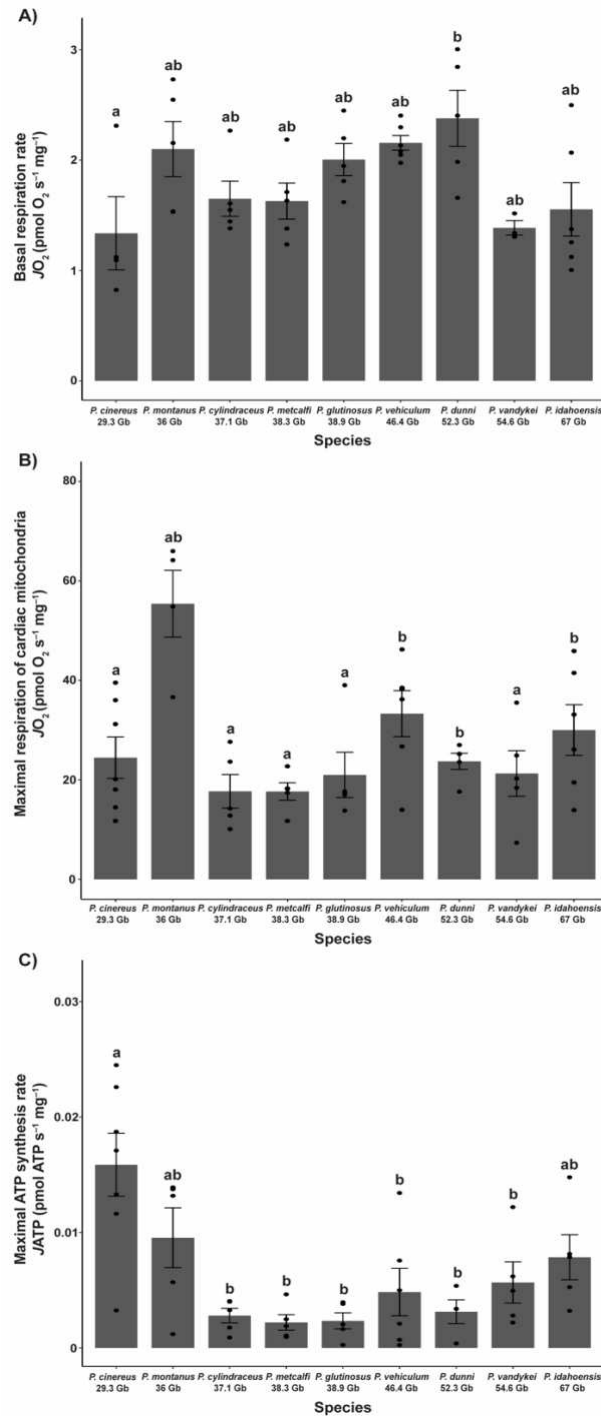


Figure 3.1 – Interspecific variation of significantly different physiological traits among species. A - Basal respiration rate of hepatic tissue. B - Maximal respiration rate of cardiac mitochondria. C - Maximal ATP synthesis rate in cardiac mitochondria. Letters denote statistically significant differences. Error bars represent standard deviation.

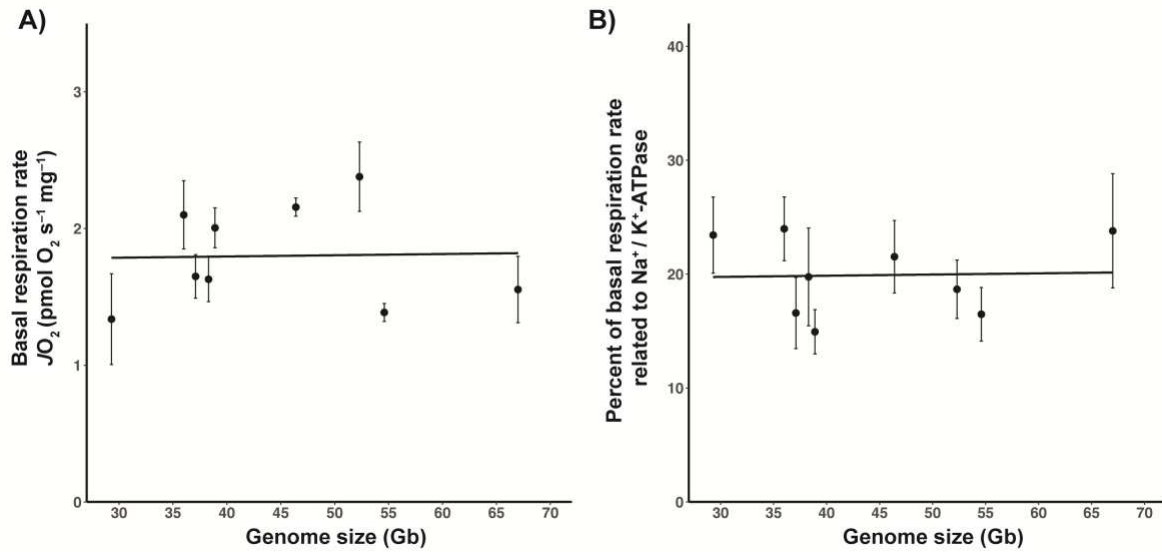


Figure 3.2 – Relationship between genome size and hepatic tissue metabolic traits. A - Basal respiration rate of hepatic tissue of each species plotted against genome size. **B** - The relative respiratory cost of the Na^+/K^+ -ATPase of each species plotted against genome size. Trend lines shown for visualization. Error bars represent standard error.

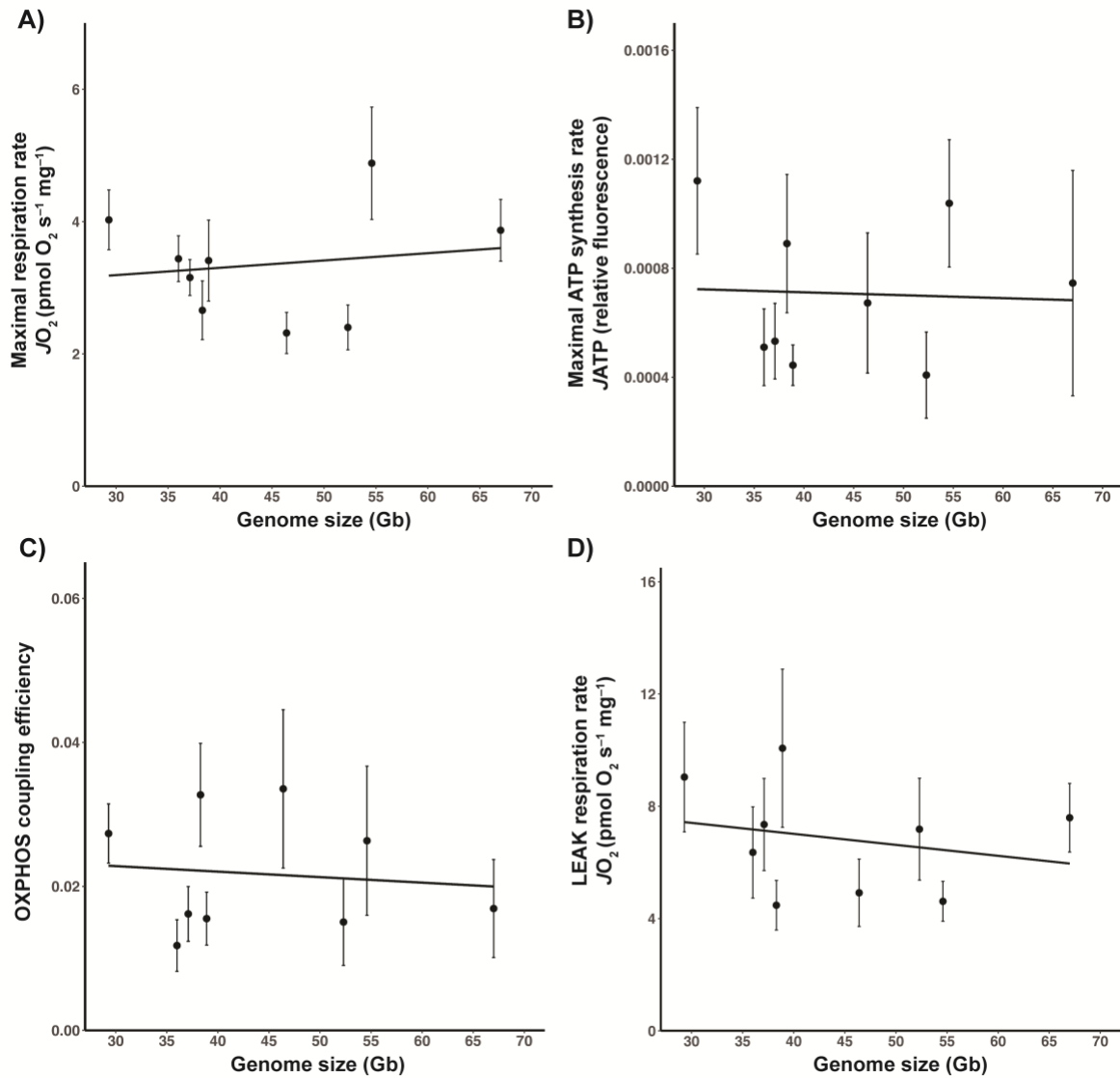


Figure 3.3 – Relationship between genome size and hepatic mitochondrial efficiency and capacity. **A** - Maximal respiration rate of hepatic mitochondria of each species plotted against genome size. **B** - Maximal ATP synthesis rate of hepatic mitochondria of each species plotted against genome size. **C** - OXPHOS coupling efficiency of hepatic mitochondria of each species plotted against genome size. **D** - LEAK respiration rate of hepatic mitochondria of each species plotted against genome size. Trend lines shown for visualization. Error bars represent standard error.

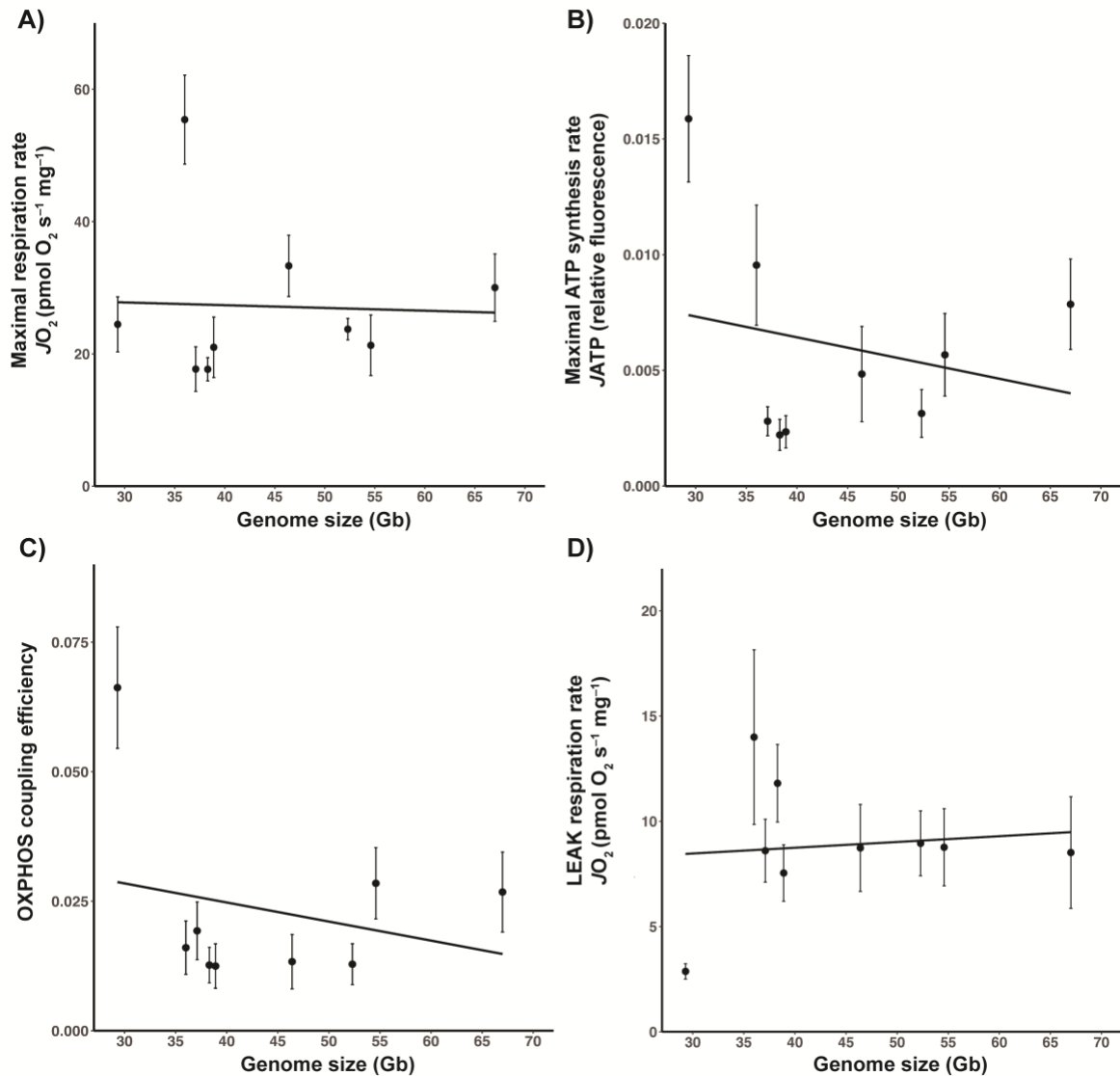


Figure 3.4 – Relationship between genome size and cardiac mitochondrial efficiency and capacity. **A** - Maximal respiration rate of cardiac mitochondria of each species plotted against genome size. **B** - Maximal ATP synthesis rate of cardiac mitochondria of each species plotted against genome size. **C** - OXPHOS coupling efficiency of cardiac mitochondria of each species plotted against genome size. **D** - LEAK respiration rate of cardiac mitochondria of each species plotted against genome size. Trend lines shown for visualization. Error bars represent standard error.

REFERENCES

- Benjamini, Y., and Y. Hochberg. 2000. On the adaptive control of the false discovery rate in multiple testing with independent statistics. *Journal of Educational and Behavioral Statistics* 25:60–83.
- Chong, R.A., and R.L. Mueller. 2013. Low metabolic rates in salamanders are correlated with weak selective constraints on mitochondrial genes. *Evolution* 67:894–899.
- Demetrius, L. 2006. The origin of allometric scaling laws in biology. *Journal of Theoretical Biology* 243:455–467.
- Gardner, J.D., M. Laurin, and C.L. Organ. 2020. The relationship between genome size and metabolic rate in extant vertebrates. *Philosophical Transactions of the Royal Society B* 375:20190146.
- Ginzberg, M.B., R. Kafri, and M. Kirschner. 2015. On being the right (cell) size. *Science* 348:1245075.
- Glazier, D.S. 2005. Beyond the ‘3/4-power law’: variation in the intra- and interspecific scaling of metabolic rate in animals. *Biological Reviews* 80:611–662.
- Glazier, D.S. 2010. A unifying explanation for diverse metabolic scaling in animals and plants. *Biological Reviews* 85:111–138.
- Glazier, D.S. 2014. Metabolic scaling in complex living systems. *Systems* 2:451–540.
- Gregory, T.R. 2002. A bird’s-eye view of the c-value enigma: genome size, cell size, and metabolic rate in class Aves. *Evolution* 56:121–130.
- Gregory, T.R. 2003. Variation across amphibian species in the size of the nuclear genome supports a pluralistic, hierarchical approach to the c-value enigma. *Biological Journal of the Linnean Society* 79:329–339.
- Gregory T. R. 2022. Animal Genome Size Database. <http://www.genomesize.com>. (Accessed 10 June 2022).
- Goniakowska, L. 1970. The respiration of erythrocytes of some amphibians in vitro. *Bulletin de L’academie Polonaise des Sciences Biologiques* 18:793–797.
- Goniakowska, K. 1973. Metabolism, resistance to hypotonic solutions, and ultrastructure of erythrocytes of five amphibian species. *Acta Biologica Cracoviensia Series Zoologia* 16:113–134.
- Itgen, M.W., G.R. Natalie, D.S. Siegel, S.K. Sessions, and R.L. Mueller. 2022. Genome size drives morphological evolution in organ-specific ways. *Evolution* 76:1–16.
- Ji, Y., and J.A. DeWoody. 2017. Relationships among powered flight, metabolic rate, body mass, genome size, and the retrotransposon complement of volant birds. *Evolutionary Biology* 44:261–272.
- Jimenez, A.G., S.K. Dasika, B.R. Locke, and S.T. Kinsey. 2011. An evaluation of muscle maintenance costs during fiber hypertrophy in the lobster *Homarus americanus*: are larger muscle fibers cheaper to maintain? *Journal of Experimental Biology* 214:3688–2697.
- Jimenez A.G., R.M. Dillaman, and S.T. Kinsey. 2013. Large fiber size in skeletal muscle is metabolically advantageous. *Nature Communications* 4:2150–2150.
- Johnston, I.A., D.A. Fernández, J. Calvo, V.L. Vieira, A.W. North, M. Abercromby, and T. Garland, Jr. 2003. Reduction in muscle fibre number during the adaptive radiation of

- notothenioid fishes: a phylogenetic perspective. *Journal of Experimental Biology* 206: 2595–2609.
- Johnson, B.B., J.B. Searle, and J.P. Sparks. 2021. Genome size influences adaptive plasticity of water loss, but not metabolic rate, in lungless salamanders. *Journal of Experimental Biology* 224, jeb242196.
- Kozowski J., M. Konarzewski, and A.T. Gawelczyk. 2003. Cell size as a link between noncoding DNA and metabolic rate scaling. *Proceedings of the National Academy of Sciences, USA* 100:14080.
- Lanz, M.C., E. Zatulovskiy, M.P. Swaffer, L. Zhang, S. Zhang, D.S. You, G. Marinov, P. McAlpine, J.E. Elias, and J.M. Skotheim. 2021. Increasing cell size remodels the proteome and promotes senescence. *BioRxiv* 2021.07.29.454227; doi: <https://doi.org/10.1101/2021.07.29.454227>.
- Li, B., and Dewey, C.N. 2011. RSEM: accurate transcript quantification from RNA-Seq data with or without a reference genome. *BMC Bioinformatics* 12:323.
- Licht, L.E., and L.A. Lowcock. 1991. Genome size and metabolic rate in salamanders. *Comparative Biochemistry and Physiology Part B: Comparative Biochemistry* 100:83–92.
- Miettinen, T.P., H.K.J. Pessa, M.J. Caldez, T. Fuhrer, M.K. Diril, U. Sauer, P. Kaldis, and M. Björklund. 2014. Identification of transcriptional and metabolic programs related to mammalian cell size. *Current Biology* 24:598–608.
- Miettinen, T.P., M.J. Caldez, P. Kaldis, and M. Björklund. 2017. Cell size control – a mechanism for maintaining fitness and function. *BioEssays* 39:1700058.
- Milligan, L.P., and B.W. McBride. 1985. Energy costs of ion pumping by animal tissues. *The Journal of Nutrition* 115:1374–1382.
- Monnickendam, M.A., and M. Balls. 1973. The relationship between cell sizes, respiration rates and survival of amphibian tissues in long-term organ cultures. *Comparative Biochemistry and Physiology Part A: Physiology* 44:871–880.
- Neurohr, G.E., R.L. Terry, J. Lengefeld, M. Bonney, G.P. Brittingham, F. Moretto, T.P. Miettinen, L.P. Vaites, L.M. Soares, J.A. Paulo, J.W. Harper, J. Buratowski, S. Manalis, F.J. van Werven, L.J. Holt, and A. Amon. 2019 Excessive cell growth causes cytoplasmic dilution and contributes to senescence. *Cell* 176:1083–1097.
- Orne, D., R. Freckleton, G. Thomas, T. Petzoldt, S. Fritz, N. Isaac, and W. Pearse. 2013. caper: comparative analyses of phylogenetics and evolution in R. R package, version 0.5.2.
- Pinheiro, J., D. Bates, S. DebRoy, D. Sarkar, and the R Development Core Team. 2021. nlme: linear and nonlinear mixed effects models. R package, version 3.1.
- R Core Team. 2016. R: a language and environment for statistical computing. R Foundation for Statistical Computing, Vienna, Austria. <http://www.R-project.org/>.
- Revell, L.J. 2010. Phylogenetic signal and linear regression on species data. *Methods in Ecology and Evolution* 1:319–329.
- Robinson, M.D., D.J. McCrathy, and G.K. Smyth. 2010. edgeR: a Bioconductor package for differential expression analysis of digital gene expression data. *Bioinformatics* 26:139–140.
- Savage, V.M., A.P. Allen, J.H. Brown, J.F. Gillooly, A.B. Herman, W.H. Woodruff, and G.B. West. 2007. Scaling of number, size, and metabolic rate of cells with body size in mammals. *Proceedings of the National Academy of Sciences* 104:4718–4723.

- Sieber, M.H., and A.C. Spradling. 2017. The role of metabolic states in development and disease. *Current Opinion in Genetics & Development* 45:58–68.
- Smith, H.M. 1925. Cell size and metabolic activity in amphibia. *The Biological Bulletin* 48:347–378.
- Smith, J.D.L., J.W. Bickman, and T.R. Gregory. 2013. Patterns of genome size diversity in bats (order Chiroptera). *Genome* 56:457–572.
- Starostová Z, et al. 2009. Cell size but not genome size affects scaling of metabolic rate in eyelid geckos. *American Naturalist* 174:E100–E105.
- Szarski, H. 1983. Cell size and the concept of wasteful and frugal evolutionary strategies. *Journal of Theoretical Biology* 105:201–209.
- Takemoto, K. 2015. Heterogeneity of cells may explain allometric scaling of metabolic rate. *BioSystems* 130:11–16.
- Uyeda, J.C., M.W. Pennell, E.T. Miller, R. Maia, and C.R. McClain. 2017. The evolution of energetic scaling across the vertebrate tree of life. *The American Naturalist* 190:185–199.
- Vinogradov, A.E. 1995. Nucleotypic effect in homeotherms: Body-mass-corrected basal metabolic rate of mammals is related to genome size. *Evolution* 49:1249–1259.
- Vinogradov, A.E. 1997. Nucleotypic effect in homeotherms: Body-mass-corrected basal metabolic rate of passerine birds is related to genome size. *Evolution* 51:220–225.
- Waltari, E., and S.V. Edwards. 2002. Evolutionary dynamics of intron size, genome size, and physiological correlations in archosaurs. *The American Naturalist* 160:539–552.
- Wright, N.A., T.R. Gregory, and C.C. Witt. 2014. Metabolic ‘engines’ of flight drive genome size reduction in birds. *Proceedings of the Royal Society B: Biological Sciences* 281:20132780.

4. GENOME SIZE DRIVES MORPHOLOGICAL EVOLUTION IN ORGAN-SPECIFIC WAYS

Summary

Morphogenesis is an emergent property of biochemical and cellular interactions during development. Genome size and the correlated trait of cell size can influence these interactions through effects on developmental rate and tissue geometry, ultimately driving the evolution of morphology. We tested whether variation in genome and body size is related to morphological variation in the heart and liver using nine species of the salamander genus *Plethodon* (genome sizes 29.3–67.0 gigabases). Our results show that overall organ size is a function of body size, whereas tissue structure changes dramatically with evolutionary increases in genome size. In the heart, increased genome size is correlated with a reduction of myocardia in the ventricle, yielding proportionally less force-producing mass and greater intertrabecular space. In the liver, increased genome size is correlated with fewer and larger vascular structures, positioning hepatocytes farther from the circulatory vessels that transport key metabolites. Although these structural changes should have obvious impacts on organ function, their effects on organismal performance and fitness may be negligible because low metabolic rates in salamanders relax selective pressure on function of key metabolic organs. Overall, this study suggests large genome and cell size influence the developmental systems involved in heart and liver morphogenesis.

Introduction

The evolutionary trajectories of morphological traits reflect lineages' intrinsic capacities to generate novel phenotypes and selection to match these phenotypes to the environment. While optimal trait values theoretically exist for any organism in any environment, in reality, the number of possible phenotypes is biased by limitations introduced at all levels of biology (Maynard Smith et al., 1985; Arnold, 1992; Brakefield, 2006; Gerber, 2014). Possible phenotypes can be delineated in morphospace from merely theoretical ones by whether or not the phenotypes can be produced by a species' developmental system (Alberch, 1982; Salazar-Ciudad, 2006). The process of development is an emergent property of biochemical and cellular interactions that direct morphogenesis. Morphogenesis as a process involves dynamic changes in gene expression and signal transduction networks that instruct populations of cells to divide, differentiate, migrate, and coalesce (Alberch, 1982; Oster et al., 1988; Chan et al., 2017; Maroudas-Sacks and Keren, 2021). In addition, cells influence their neighbors, relaying positional and deterministic information to one another that results in the induction of tissue formation and organogenesis. When genes, proteins, or cells evolve within this system, any new variant can potentially alter these collective interactions and change the outcome of development.

Alberch (1982) proposed that the primary forces underlying the evolution of morphology are changes to the biochemical and cellular interactions involved in development. Overall, development is robust to change, and variation — both mutational and epigenetic — can often have no impact on the resulting phenotype (Lewontin, 1972; Oster and Alberch, 1982; Wagner, 2011; Uller et al., 2018). However, some changes will result in the developmental system producing a different phenotype (Oster and Alberch, 1982; Uller et al., 2018). These changes

cross a theoretical threshold called a bifurcation boundary, which bounds the amount of variation permissible within a developmental system that still produces the same outcome (Oster and Alberch, 1982). This variation can exist in many parameters, including: sequence, structure, function, and interaction of genes and proteins; rates of diffusion and biochemical reactions; morphology and motility of cells; rates of cellular division and differentiation; and the size and organization of tissues and structures (Alberch, 1983; Brakefield et al., 2003; Mallarino et al., 2011; Keyte and Smith, 2014; Powder et al., 2015). Variation in these parameters can alter morphogenesis and result in larger-scale changes that impact the rate of development, the sequential timing of developmental events, or pattern formation, ultimately producing novel phenotypes (Oster and Alberch, 1982).

Genome size is a trait that can directly impact developmental systems through its effects on cell biology (Gregory, 2005). There is a strong positive correlation between genome size and cell size, resulting in cells becoming larger as DNA accumulates (Gregory, 2005; D'Ario et al., 2021). Large cell size has clear impacts on cell morphology, shifting the ratio between surface area and volume and causing the scaling of intracellular organelles (Marshall et al., 2012). Genome and cell size together have been shown to impact developmental systems through two mechanisms (Gregory, 2005). First, large genome and cell sizes slow developmental rate by causing longer cell cycles and slower rates of cell migration and differentiation (Sessions and Larson, 1987; Schmidt and Roth, 1993; Vinogradov, 1999). This slowing can ultimately shift the timing of developmental events (i.e., lead to heterochrony) and impact the dynamics of morphogenesis (Alberch et al., 1979; Gould, 1985). Changes in cell size also impact the final outcomes of development: the structures of tissues and organs (Alberch and Alberch, 1981; Hanken and Wake, 1993; Roth et al., 1993). Evolutionary increases in genome and cell size can

result in organs and organisms that are composed of fewer, larger cells, assuming body size and organ size remain constant (Hanken and Wake, 1993). Morphogenesis must then emerge from interactions among fewer, larger cells. Extensive work in *Drosophila*, as well as mammalian model systems, has shown the Hippo pathway to be the master regulator of organ size, serving as a hub to integrate information from numerous signaling pathways that are active during development. This network produces morphogen gradients that define organ size, with cells within the field specified by the gradient growing, proliferating, and undergoing apoptosis in response to genetic and mechanical cues to achieve the target size (Gokhale and Shingleton, 2015; Kim and Jho, 2018). Thus, increasing cell size must be accommodated by this conserved network to achieve final organ sizes proportionate to body size. Additionally, the final tissue or organ must maintain structure and function with fewer, larger cells. To highlight the importance of this interaction between cell size and body size, Hanken and Wake (1993) introduced the concept of biological size — a proxy for the number of cells comprising an organism — rooted in empirical observations of how morphology changes when organisms evolve to be composed of few, large cells (Hanken, 1982, 1983; Linke et al., 1986; Roth et al., 1988, 1990, 1993, 1994).

Empirical studies of morphological evolution have suggested that the impacts of increased genome and cell size — mediated through alterations to the developmental system — can vary extensively across different tissues, organs, and species (Fankhauser, 1945; Hanken and Wake, 1993; Roth et al., 1993; Snyder and Sheafor, 1999; Womack et al., 2019). Amphibians, particularly salamanders, have provided a powerful system for studying these patterns and processes due to their enormous range in genome (9.3–120 gigabases (Gb)) and cell size (Horner and Macgregor, 1983; Gregory, 2005; Sessions, 2008; Decena-Segarra et al., 2020; Sessions and Wake, 2021). Much of this work has focused on the brain and nervous system, the skeletal

system, and the circulatory system. For example, within the salamander brain, dramatic changes in gross morphology and tissue organization are connected to larger genome and cell sizes as well as reductions in cell numbers (Roth et al., 1993; Roth and Walkowiak, 2015). Similarly, repeated loss and reduction of skeletal elements have been observed across amphibians resulting from reductions in cell number or slower developmental rates associated with large genome and cell sizes (Alberch and Alberch, 1981; Hanken and Wake, 1993; Womack et al., 2019). In tropical lungless salamanders with exceptionally large genomes, the associated slower development rates appear to be connected to paedomorphic morphologies including fenestrated skulls, highly reduced or even absent phalangeal elements in the digits, and extensively webbed feet (Wake, 1966; Alberch and Alberch, 1981; Alberch, 1983; Jaekel and Wake, 2007; Decena-Segarra et al., 2020).

The diversity of morphological outcomes in the studies carried out to date suggests that the fundamental rules governing the effects of genome and cell size on morphological evolution will be revealed through the analysis of additional organs and the synthesis of results across species and organ systems. As a step towards this goal, our study investigates how increases in genome and cell size impact the morphology of the heart and liver. These two previously unexplored organs differ in morphogenesis and function; the heart has a kinetic biomechanical function and the liver has a biochemical and secretory function. However, the organs are similar in that both serve key functional metabolic roles for the organism. Salamanders have incredibly low metabolic rates that appear unrelated to genome and cell size (Gatten et al., 1992; Uyeda et al., 2017; Gardner et al., 2020; Johnson et al., 2021). Thus, the salamander heart is circulating blood in an organism with the lowest O₂ requirements among terrestrial vertebrates. Low metabolic rates also decrease the demand for the liver to metabolize macromolecules (i.e.

carbohydrates, lipids, proteins) needed for oxidative phosphorylation and glycolysis. We hypothesize that the extremely low metabolic rates of salamanders relax selection on heart and liver function. This relaxed selection, in turn, allows for a larger number of functionally adequate morphologies — a relatively flat adaptive landscape — with organ phenotype free to evolve driven by changes in genome size.

Our study system is the lungless salamander genus *Plethodon*, which includes species with a broad range of genome sizes (23.3–67.0 Gb) and cell sizes shaped by stochastic evolutionary processes, but uniformity or lower diversity in potentially confounding variables (e.g., life history, body size) that could also impact organ structure and function (Highton, 1995; Newman et al., 2016; Mueller et al., 2021). Using diffusible iodine-based contrast-enhanced computed tomography (diceCT) and histology applied to nine focal *Plethodon* species, we quantified metric body size, organ size, and several measures of tissue composition and geometry: 1) proportion of the heart wall comprised of cardiomyocytes versus intertrabecular space (i.e., lacunae), 2) proportion of the liver comprised of hepatocytes versus vascular openings, and 3) the numbers and sizes of distinct vascular structures (sinusoids, veins, arteries) in the liver. We used phylogenetic comparative methods to test whether these variables correlate with evolutionary changes in genome and cell size. Based on our findings, we propose hypotheses connecting cell size, developmental system perturbation, and morphology. More generally, we discuss how relaxed demands on organ function can allow the evolution of a range of structurally different morphologies.

Methods

Animal collection

We collected five adult individuals of *P. cinereus*, *P. cylindraceus*, *P. dunni*, *P. glutinosus*, *P. idahoensis*, *P. metcalfi*, *P. montanus*, *P. vandykei*, and *P. vehiculum* (Supplementary Information 2.1). Salamanders were collected and euthanized in neutral buffered (pH 7) 1% MS-222, fixed in buffered formalin, and transferred through a graded series of ethanol (10%, 30%, 50%, 70%) before storage in 70% ethanol. Due to the rarity of some species included in this study, we used the same specimens for the diceCT and histological analyses. The protocols for animal research, husbandry, and euthanasia were approved by the Institutional Animal Care and Use Committee of Colorado State University and carried out in accordance with protocol 17-7189A.

diceCT data generation and processing

We used diceCT to measure liver and heart volumes (Gignac et al., 2016). I₂KI staining can cause varying degrees of tissue shrinkage, but these artifacts can be minimized by using low concentrations of I₂KI and shorter staining periods (Vickerton et al., 2013; Baverstock et al., 2013; Hedrick et al., 2018). To minimize such shrinkage, we used a 1% I₂KI solution and incubated the specimens for 2 days, which was shown to produce the smallest degree of tissue shrinkage (Vickerton et al., 2013). After scanning, the I₂KI was rinsed out using several changes of 70% ethanol and specimens were stored in 70% ethanol. In addition, all specimens were treated uniformly to minimize the risk of any potential I₂KI-related artifacts or shrinkage introducing noise or bias into subsequent histological analyses. Following these precautions, we did not observe any significant signs of tissue shrinkage across organs and specimens.

Specimens were scanned twice using a Bruker SkyScan 1173 at the Karel F. Liem Bioimaging Center, Friday Harbor Laboratories, University of Washington. Scans were set to 85

kV and 90 μ A with a 1 mm aluminum filter to reduce beam hardening. We first produced full body scans to measure liver volumes at a resolution ranging from 14.9–17 μ m, depending on the size of the specimens. We then produced higher resolution scans for the heart, which were scanned at a resolution ranging from 7.1 to 9.9 μ m. diceCT scans were reconstructed using NRecon (Bruker, 2005–2011) following standard operating procedures including optimal x/y alignment, ring artifact reduction, beam hardening correction, and a post-alignment. Data visualization and analysis were accomplished using 3DSlicer (Fedorov et al., 2012). Liver and heart ventricle volumes were calculated through segmentation of the liver and heart from each specimen.

Organ measurement

Snout–vent lengths were measured to the nearest 0.01 mm for each individual using digital calipers. The hearts and livers were then excised from specimens and were embedded in plastic following standard protocols (Humason, 1962). Tissues were sectioned at 4 μ m and stained with hematoxylin for 4 minutes and toluidine for 3 minutes. Sections were mounted and then visualized using a compound microscope. Images used in the analysis were minimally edited to remove blood cells that obstructed vascular structures or the intertrabecular space of the ventricular myocardium. Five images were taken (one each from 5 different histological sections) at 20x magnification for each individual and a mean value was calculated for each morphological trait per individual. We decided to collect morphological data from 5 images after finding no significant differences when the data were collected from 3, 5, or 10 images. Each image was converted to greyscale and a thresholding method was used to collect the

morphometric data. ImageJ was used for all image processing and analysis (Schneider et al., 2012).

Amphibian livers are primarily comprised of hepatic tissue that is permeated by the vasculature (Akiyoshi and Inoue, 2012). Liver vascular structures consist of hepatic arteries that provide oxygen, portal veins that bring nutrients and toxins to the liver, and sinusoids, which are specialized capillaries where oxygen-rich blood from hepatic arteries and nutrient-rich blood from portal veins mix (Elias and Bengelsdorf, 1952). Liver tissue is generally arranged into many hepatic lobules that are centered by portal triads – an arrangement of hepatic arteries, portal veins, and bile ducts (Elias and Bengelsdorf, 1952). The network of sinusoids gives the hepatic tissue a cord-like appearance in most vertebrate taxa, with hepatocytes forming cords that are 1–2 cells thick; this morphology increases the surface area of each hepatocyte that is in contact with circulating blood (Elias and Bengelsdorf, 1952). However, some species of salamanders have a many-cell thick arrangement of hepatic cords (Akiyoshi and Inoue, 2012). For the liver, we measured the total area of each histological section that was comprised of tissue (primarily hepatocytes) versus vascular openings and the number and size of distinct vasculature (sinusoids, veins, arteries). Twenty nuclei and cells were also measured for each individual to collect data on hepatocyte nuclear and cell area.

Amphibians have a single, thin-walled ventricle that has a central chamber surrounded by a highly trabeculated network of myocardium, which is a characteristic of ectotherms (Stephenson et al., 2017). Heart morphology in *Plethodon* also reflects the lack of lungs in the family Plethodontidae, which has been accompanied by a loss of complete atrial septation (Lewis and Hanken, 2017). For the heart ventricles, we measured the myocardial area in the ventricle walls versus intertrabecular space in each histological section. We focused on this because the

trabeculated myocardium makes it difficult to define the edges of the ventricle chamber. We did not measure any characteristics of the atria because they lack distinct internal structure and their elastic nature made accurate volumetric measurements impossible.

Genome size measurement

Genome size was measured using the Feulgen-staining method on fixed erythrocytes following the protocol of Sessions and Larson (1987). *Ambystoma mexicanum* (32 Gb) was used as a standard to calculate the genome sizes of the other species. The *A. mexicanum* were acquired from the *Ambystoma* Genetic Stock Center at the University of Kentucky. Erythrocytes were extracted from the *Plethodon* and *Ambystoma* specimens fixed in neutral-buffered (pH 7) formalin, and transferred to microscope slides to produce blood smears. We collected blood smears from 3–5 individuals per species. The cells were hydrated for 3 minutes in distilled water, permeabilized in 5 N HCl for 20 minutes at 20°C, and then rinsed three times in distilled water. Nuclei were stained with Schiff's reagent for 90 minutes at 20°C, destained in 0.5% sodium metabisulfite three times for 5 minutes each, and then rinsed in distilled water three times. The stained cells were dehydrated in a graded series of 70%, 95%, and 100% ethanol, dried, and mounted. Each staining run included a slide of *Ambystoma* cells as the standard. We photographed 2–12 ($\bar{x} = 5.5$) nuclei per individual under 100x, and the integrated optical densities (IOD) were measured using IMAGE PRO software (Media Cybernetics, Rockville, Maryland, USA). Genome sizes were calculated by comparing the average IODs of the experimental species to the IOD of the standard. Nuclear areas were measured for each erythrocyte using IMAGE PRO software, and hepatocyte nuclear and cell areas were also calculated for 20 cells from each of 4–5 individuals using IMAGE PRO. We tested for the

predicted correlations between genome size and nuclear area and cell area using linear regression.

Phylogeny

We estimated the phylogenetic relationships among the 9 species of *Plethodon* used in this study to account for phylogenetic non-independence in our analyses. DNA sequences for the mtDNA gene *cytb* and the nuclear gene *Rag1* were obtained from NCBI (<https://www.ncbi.nlm.nih.gov/genbank>; Table S1). The *cytb* and *Rag1* sequences were aligned independently using MUSCLE in MEGA v7 with default parameters and trimmed to 629 and 1,467 basepairs, respectively (Edgar, 2004; Kumar et al., 2016). We applied a codon-specific nucleotide substitution model determined by the best-fit models using AICc with PartitionFinder 2 using the “greedy” search algorithm (Lanfear et al., 2017). We applied the following model scheme: *Rag1* codon position 1, F81; *Rag1* codon position 2, HKY + I; *Rag1* codon position 3, HKY; *cytb* codon positions 1–2, GTR + G; *cytb* codon position 3, HKY + G. The phylogeny was estimated using Bayesian inference with MrBayes v3.2.5 (Ronquist et al., 2012). The analysis ran with four chains (3 heated, 1 cold) for 10 million generations with sampling occurring every 1,000 and the first 10% of the sampled trees discarded as burnin.

Data analysis

We log-transformed all variables to account for non-normal distributions and created phylogenetic generalized least squares (PGLS) models that simultaneously estimated Pagel’s lambda (λ), a measure of phylogenetic signal (Revell, 2010). Each PGLS model included one of the morphological traits as a response and genome size and SVL as the predictor variables to test

if organ morphology is correlated with genome size and/or SVL while accounting for phylogeny. For each species, we also calculated the biological size index (BSI) — a relative measure of the total number of cells comprising an organism that is based on organism size and cell size — by dividing the mean SVL by the square-root of genome size (Hanken and Wake, 1993; Decena-Segarra et al., 2020). Our response variables were liver size, ventricle size, total area comprised of muscle in the ventricle, number of vascular structures in the liver, average size of the vascular structures in the liver, and the total area comprised of hepatic tissues in the liver. The PGLS analyses were conducted using R v 3.4.2 and the packages *caper* and *nlme* (Orne et al., 2013; R core team, 2016; Pinheiro et al., 2021). We applied a Brownian motion model of evolution to all variables, and we applied a Benjamini–Hochberg false discovery rate correction to account for multiple testing (Benjamini and Hochberg, 2000). We visualized the magnitude and direction of changes in genome size across the 9 species of *Plethodon* in the study using the `contMap` function in the R package *phytools* on the estimated topology (Revell, 2012).

Results

The genome size measurements for the 9 *Plethodon* species ranged from 29.3 to 67.0 Gb (Figure 1; Table 1). The genome sizes measured in this study were generally larger than those previously published or fell within the higher range of published measurements (Gregory, 2021). We measured larger genome sizes for *P. cinereus* (29.3 Gb vs. 25.6 Gb, the mean of previously published measurements), *P. dunni* (52.3 Gb vs. previously published mean = 46.5 Gb), and *P. vehiculum* (46.4 Gb vs. previously published mean = 39.1 Gb). Our genome size measurement for *P. glutinosus* was comparable to the higher published measurement for the species (38.9 Gb vs. 42.1 Gb; Bachmann, 1970), but is much larger than the average published value for this

species (mean = 28.0 Gb). We also found that *P. idahoensis* has the largest genome size in the genus at 67.0 Gb (Gregory, 2021). Conversely, we measured a significantly smaller genome size for *P. vandykei* (54.6 Gb vs. 67.8 Gb; Mizuno and Macgregor, 1974), which was previously considered to have the largest genome size in the genus. Intraspecific variation in genome size measurements could, in principle, reflect true variation within and among populations, changes in taxonomic assignments (i.e., *P. glutinosus* complex; Highton, 1989), and/or technical discrepancies across studies (Hardie et al., 2002). We circumvented these sources of uncertainty by collecting our own genome size data on the same organisms we used for morphological analysis. The areas of nuclei from both hepatocytes ($R^2 = 0.955$; $P < 0.001$) and erythrocytes ($R^2 = 0.935$; $P < 0.001$), as well as hepatocyte cell area ($R^2 = 0.915$; $P < 0.001$), all have a significant positive correlation with these genome size measurements (Fig. 4; Table 1). Although these correlations do not verify the accuracy of our measurements of absolute genome sizes, they do provide confidence in the accuracy of their relative sizes, which is the most important feature of the dataset for our downstream analyses.

Morphological and histological trait data are summarized in Table 2. Mean SVL ranged from 40.1 mm in *P. cinereus* to 68.7 mm in *P. dumni*. Mean ventricle volume spanned an order of magnitude across this range of body sizes — from 0.52 mm³ in *P. cinereus* to 5.72 mm³ in *P. dumni*. Mean liver volume showed a ~7-fold range across these body sizes, from 15.9 mm³ in *P. cinereus* to 112.1 mm³ in *P. dumni*. Mean myocardial density showed a ~3-fold range across species, from 0.04 mm² / section in *P. idahoensis* to 0.118 mm² / section in *P. cinereus*. The mean number of vascular structures in the liver showed a ~2.5-fold range, from 23.5 / section in *P. idahoensis* to 60.0 in *P. cinereus*. Mean size of vascular structures showed a ~3-fold range, from 0.0021 mm² in *P. cylindraceus* and *P. glutinosus* to 0.0061 mm² in *P. idahoensis*. Mean

hepatic tissue area showed the smallest range across species, from 0.127 mm² in *P. glutinosus* to 0.143 mm² in *P. idahoensis*.

The results from the PGLS analyses are presented in Table 3. In the heart, genome size was negatively correlated with myocardial area in the ventricle ($P = 0.001$; Fig. 2,6). In the liver, genome size showed both positive and negative correlations with different traits: genome size was positively correlated with the average size of the vascular structures ($P < 0.001$; Fig. 3,6) but negatively correlated with the number of vascular structures ($P < 0.001$; Fig. 3,6). In addition, genome size was positively correlated with the total hepatic tissue area ($P = 0.005$; Fig. 3,6).

Body size (SVL) was positively correlated with ventricle size ($P < 0.001$) and liver size ($P < 0.001$; Fig. 5). There were also significant positive correlations between body size (SVL) and the total hepatic tissue area ($P = 0.004$), the average vascular structure size in the liver ($P = 0.004$), and the number of vascular structures in the liver ($P = 0.012$). Thus, these three liver traits — hepatic tissue area, average size of the vascular structures, and the number of vascular structures — were significantly correlated with both genome size and SVL. We also plotted the biological size index (BSI) and each of these traits to allow visualization of the relationships among them (Fig. 7).

Discussion

Body size, biological size, and heart and liver morphology

The size of an organism or organ is a function of cell size and cell number. We found that ventricle and liver sizes were positively correlated with body size but not genome size in *Plethodon* salamanders, indicating that the size of these organs is a function of body size (Fig. 5). Overall, we found no relationship between genome size and body size in *Plethodon*, indicating

that increases in cell size do not produce larger body sizes. Thus, the evolution of larger genome and cell size in *Plethodon* is accompanied by a reduction in total cell numbers (i.e., reduced biological size) for both the ventricle and liver. Three variables — hepatic area, and number and size of vascular structures in the liver — were correlated with both body size and genome size. For the number and size of liver vascular structures, genome size appeared to be a stronger predictor than BSI, suggesting that it is cell size itself — more so than cell size relative to organ size — that underlies changes in morphology (compare Fig. 6c, d with Fig. 7b, c). Similarly, myocardial area was correlated only with genome size, again suggesting that it is cell size itself that underlies changes in morphology. Only hepatic tissue area was better explained by BSI than cell size.

Organ morphology correlates with genome and cell size in the heart and liver, as well as in other body systems

The heart and liver each showed a distinct pattern of phenotypic change accompanying evolutionary increases in genome and cell size in *Plethodon*. In the heart, large genome and cell size were accompanied by a dramatic reduction in the amount of trabeculated myocardia relative to the intertrabecular space. Because ventricle size was not correlated with genome and cell size, the reduced myocardial density in species with large genome sizes resulted in hearts with relatively fewer myocardial cells overall.

In the liver, the vascular structures were most significantly impacted by genome and cell size, which resulted in distinct changes to tissue geometry. The average area of the vascular structures, which included hepatic arteries, portal veins, and sinusoids, was positively correlated with genome size. Conversely, the total number of these vascular structures was negatively

correlated with genome size. Thus, livers in species with the largest genome sizes had significantly fewer, but larger, vascular structures. These results suggest that arteries, veins, and liver sinusoids increase in size to accommodate larger blood cells, which in turn changes the geometry and composition of liver tissue (Snyder and Sheafor, 1999). The changes in tissue geometry and composition resulted in two dramatic alterations to overall hepatic morphology. First, the arrangement of vascular structures into a portal triad-like organization was uncommon and became increasingly rare as genome and cell size increased. Although the hepatic arteries, portal veins, and bile ducts were present, they were rarely arranged together in a canonical portal triad. Second, the hepatocytes lacked the 1–2 cell-thick, cord-like morphology, which resulted in numerous hepatocytes having no direct contact with circulating blood. Akiyoshi and Inoue (2012) and others described this same several-cell-thick plate morphology in salamanders (Akat and Göçmen, 2014; Akat and Arkan, 2017; Vaissi et al., 2017). Our results show that this morphology is a result of increased genome and cell size.

Previous work on the brain and nervous system, the skeletal system, and the circulatory and excretory systems in salamanders also revealed distinct patterns of phenotypic change accompanying evolutionary increases in genome and cell size. In the brain, larger and fewer cells impact tissue organization, leading to an increase in gray matter relative to white matter as well as increased cell density (Roth et al., 1990). In addition, slower rates of cell proliferation and migration caused by large genome and cell size result in a decrease in lamination within the tectum mesencephali (Schmidt and Roth, 1993). In the skeletal system, increased genome and cell size (in combination with decreased body size) appears to disrupt skeletal development because the prerequisite tissues that form bones are reduced to significantly fewer cells (Hanken, 1982, 1984; Wake, 1991). In some cases, the carpal and tarsal elements of the feet remain

cartilaginous and also fused due to a failure to separate during development (Wake, 1966; Alberch and Alberch, 1981). In the circulatory system, increased genome size is correlated with increased red blood cell size (Villalobos et al., 1988; Mueller et al., 2008) as well as increased capillary diameters (Fig. 6) (Snyder and Sheafor, 1999). In the excretory system, experimental increase in cell size (through induction of polyploidy) altered the morphology and number of cells comprising the pronephric tubules, which are excretory structures similar in morphology to capillaries; however, tubule diameter remained unchanged (Fankhauser, 1945).

Overall, the patterns of phenotypic change that we report in the heart and liver, combined with previous work documenting patterns from the brain, skeleton, circulatory, and excretory systems, suggest that the impact of genome and cell size increase on phenotype is organ-specific. This lack of similarity suggests that, for each developing organ, unique relationships exist between genome- and cell-level parameters and the morphological outcome of the developmental system. Because large genome and cell size decreases the rate of development, reduces the number of cells involved in morphogenesis, and/or alters the composition and geometry of tissues, a full understanding of the link between cell size and morphology requires understanding which of these effects is relevant for each organ. More generally, organs that share structural properties (e.g. tubes vs. solid masses of tissue vs. tissue with lacunae) may respond similarly to increases in genome and cell size, allowing predictions from our work to as-yet-unstudied organs (e.g. our results in the liver predict similar effects on sinusoids in the spleen).

Proposed genome and cell size effects on heart development

We propose three developmental hypotheses explaining the decrease in ventricular musculature associated with increases in genome and cell size. First, blood flow plays a

significant epigenetic role in vertebrate heart development by creating pressure gradients in the developing heart (Santhanakrishnan and Miller, 2011; Johnson et al., 2015). Altering erythrocyte size and morphology can potentially change the fluid dynamics of blood, which in turn would change the degree of pressure in the heart during development (Dupin et al., 2008; AlMomani et al., 2012). Testing this hypothesis would require measuring blood flow, its effects on gene expression, and the morphogenetic outcomes in the developing hearts of salamanders with different genome sizes.

Second, the reduction of ventricle muscle might be the result of slower rates of development and truncation of heart organogenesis at an earlier ontogenetic stage because of large genome and cell size, producing a paedomorphic heart. An ontogenetic study comparing heart morphology in the model salamander *Ambystoma mexicanum* (the axolotl) found that the larval (pre-metamorphic) heart had significantly less trabeculated myocardia and a lack of internal ridges in the ventricle compared to the post-metamorphic heart (Olejnickova et al., 2021). These results are consistent with the hypothesis that paedomorphosis underlies the negative correlation between trabeculated myocardia and genome size in *Plethodon*. *Plethodon* and *A. mexicanum* do have significant differences in life history and morphology. *Ambystoma mexicanum* typically remain in the aquatic form as sexually mature adults that rely on gills for respiration, but under rare circumstances, they can metamorphose into a terrestrial form that relies on lungs and skin for breathing (Olejnickova et al., 2021). In contrast, *Plethodon* salamanders all undergo direct development (i.e., they lack an aquatic larval stage and metamorphosis, and instead hatch from a terrestrial egg in the form of a tiny adult). In addition, *Plethodon* salamanders are lungless, which was demonstrated to impact heart morphology (Lewis and Hanken, 2017). However, direct development in *Plethodon* recapitulates many of the

developmental stages of larval and metamorphic ontogeny inside the egg, and the impacts of lunglessness on heart morphology are largely atrial (Kerney et al., 2011; Lewis and Hanken, 2017). Thus, despite these differences, the *A. mexicanum* results do lend support to the hypothesis of a paedomorphic heart in *Plethodon*.

Third, morphogenesis and pattern formation can be fundamentally changed when cell size and cell number change (Alberch and Gale, 1985). Because ventricle size was not correlated with cell size, increased cell size must be accompanied by decreased cell numbers. The implications of undergoing heart development with fewer, larger cells are not understood. Testing these latter two hypotheses would require comparative developmental analyses across taxa with different genome and cell sizes to reveal how heart morphogenesis is impacted by changes in developmental rate and in the size and number of cells.

Proposed genome and cell size effects on liver structure

The most prominent change in liver phenotype as genome and cell size increases is related to tissue geometry and vasculature, which includes arteries, veins, and sinusoids. As genome and cell sizes increase, the sizes of the vascular structures also increase — likely to accommodate larger blood cells — while the number of vascular structures decreases. Thus, large genome and cell sizes are associated with fewer, larger vascular structures. Liver size is determined by body size in *Plethodon* (Fig. 5), which means that increases in cell size are accompanied by decreases in cell number. We hypothesize that if the number of vascular structures were unchanged, their increased size would likely cause the tissue to become structurally and/or functionally compromised because they would occupy too much space, at the

expense of hepatocytes. Therefore, we hypothesize that the number of vascular structures is constrained to maintain organ structural integrity and functionality.

Implications of morphological evolution on performance and fitness

The morphological changes that result from increased genome and cell size can have functional consequences. In some cases, functional consequences have been inferred from organs showing patterns of compensatory evolution to offset the negative effects of genome and cell size increase. For example, species with extremely low biological size indices have proportionally larger eyes and regions of the brain — thalamus, praetectum, and midbrain — responsible for visual and visuomotor functions (Roth et al., 1990), as well as a proportional shift in the retina to increase the number of small cones relative to the large rods (Roth et al., 1988, 1990). These changes in brain and eye morphology offset the low number of large neurons, maintaining the acuity required for visual predation (Roth et al., 1990). Similarly, the evolution of wider capillary diameters and enucleated erythrocytes in miniaturized lineages are hypothesized to be compensatory responses that facilitate blood flow with larger erythrocytes (Villalobos et al., 1988; Snyder and Sheafor, 1999; Mueller et al., 2008; Itgen et al., 2019; Decena-Segarra et al., 2020).

We hypothesize that heart and liver function are affected by the evolutionary changes we report in *Plethodon* as genome and cell size increase. In the heart, the decreased myocardial volume and increased intertrabecular space in the ventricle likely reduce the ventricle's capacity to produce force. Conversely, this reduction in myocardium allows the ventricle to hold greater blood volume. A reduction of force production and increased volume capacity would alter the stroke volume and ejection fraction of the heart. Overall functional measures such as heart rate

and cardiac output could be affected as well, although Olejnickova et al. (2021) found no differences in heart rate between larval-stage and post-metamorphic individuals of *A. mexicanum*, despite morphological differences in trabeculated myocardia similar to those we report across *Plethodon*. Trabeculated myocardia also serve a critical role in the electrophysiology of amphibian hearts, and tissue geometry has been linked to signal propagation speed of cultured cardiomyocytes (Kucera et al., 1998; Sedmera et al., 2003). Olejnickova et al. (2021) found that the rate of signal transduction was significantly slower in larval-stage hearts than in post-metamorphic hearts in *A. mexicanum*, but that there were no differences in the activation pattern in the ventricle. These findings suggest that changes in trabeculae morphology associated with genome size could also affect *Plethodon* heart electrophysiology.

In the liver, changes in hepatic tissue organization likely affect function as well. Large genome and cell size impacted the organization of portal triads and the cord-like morphology of hepatocytes, as well as reducing the number of vascular structures. As a result, many hepatocytes do not come into direct contact with any vascular structures, limiting their access to oxygen and nutrient supply and thus impacting their metabolic contribution to overall organ function. Testing this hypothesis would require comparative analyses of liver function across taxa with different genome and cell sizes.

It is important to consider, however, whether these hypothesized cell- and organ-level changes in function, associated with a more-than-doubling of genome size, would have any effect on fitness in salamanders. Variation in morphology is connected to fitness through its effects on organismal performance (Arnold, 1983). Morphology can vary without impacting performance, and performance, in turn, can vary without impacting fitness (Bock, 1980). Are the

evolutionary changes that we report here in organ structure, and the accompanying changes we hypothesize in organ function, likely to have impacted organismal performance and fitness? We suggest that the answer is no, as a consequence of salamanders' incredibly low metabolic rates (Gatten et al., 1992; Uyeda et al., 2017; Gardner et al., 2020; Johnson et al., 2021). More generally, we suggest that low metabolic rates relaxed selective pressure on metabolic organ function, allowing for greater variation in morphology without negatively impacting organismal performance or fitness (and without leading to compensatory evolution). This, in turn, allowed cell size to evolve driven largely by genome-level processes (e.g. transposable element proliferation and deletion; Sun et al., 2012). The range of genome and cell sizes produced throughout the clade's evolutionary history has been funneled through a conserved developmental system, producing a range of morphologies during organogenesis. The "permissive" organismal phenotype of salamanders is thus a powerful tool for examining how the output of developmental systems responds to changes in the fundamental parameter of cell size.

Table 4.1 – Mean and standard deviation for measurements of genome size, nuclear areas of erythrocytes and hepatocytes, and cell areas of hepatocytes. n = 5 individuals unless otherwise noted; 3–5 erythrocyte nuclei and 20 hepatic nuclei and cells were measured per individual.

Species	Genome size (Gb)	Nuclear area of erythrocytes (μm^2)	Nuclear area of hepatocytes (μm^2)	Cell area of hepatocytes (μm^2)
	29.3 ±			
<i>Plethodon cinereus</i>	1.34 (n = 4)	54.5 ± 3.6	84.2 ± 3.7	373.8 ± 59.5
<i>P. montanus</i>	36.0 ± 3.4	58.7 ± 5.1	92.5 ± 4.6	515.3 ± 34.8
<i>P. cylindraceus</i>	37.1 ± 5.4	66.9 ± 10.4	92.2 ± 3.9	550.4 ± 27.2
<i>P. metcalfi</i>	38.3 ± 1.04	58.5 ± 2	87.7 ± 3.8	492.7 ± 90.3
<i>P. glutinosus</i>	38.9 ± 3.94	62.5 ± 6.2	97.8 ± 6.4	498.6 ± 42.9
<i>P. vehiculum</i>	46.4 ± 7.08 (n = 3)	86.4 ± 17.6	128.8 ± 5.6	740.1 ± 71.4
<i>P. dunni</i>	52.3 ± 4.06	88.2 ± 5.7	137.1 ± 6.2	755.2 ± 108.6
<i>P. vandykei</i>	54.6 ± 2.2 (n = 4)	104.3 ± 20.4	158.4 ± 9.8	943 ± 227.5
<i>P. idahoensis</i>	67.0 ± 2.31	116.9 ± 2.9	181.7 ± 8	984.5 ± 371

Table 4.2 – Mean and standard deviation for genome size and morphological traits. n = 5 individuals unless otherwise noted; 5 slides were measured per individual.

Species	Heart			Liver		Mean size of vascular structures (mm ²)	
	Snout-vent length (mm)	Ventricle volume (mm ³)	Myocardial area (mm ²)	Liver volume (mm ³)	Hepatic tissue area (mm ²)		Number of sinusoids
<i>Plethodon cinereus</i>	40.1 ± 0.7	0.52 ± 0.06	0.118 ± 0.01	15.9 ± 3.8	0.136 ± 0.01	60 ± 7.1	0.0023 ± 0.0002
<i>P. montanus</i>	49.7 ± 1.1	1.44 ± 0.35	0.101 ± 0.004	33.1 ± 15.9	0.14 ± 0.01	57.1 ± 4.7	0.0024 ± 0.0005
<i>P. cylindraceus</i>	70.4 ± 1.6	3.77 ± 1.24	0.107 ± 0.01	120 ± 72.5	0.123 ± 0.01	58.4 ± 8.8	0.0021 ± 0.0002
<i>P. metcalfi</i>	61.9 ± 4.2	3.74 ± 1.63	0.106 ± 0.004	70.6 ± 41.3	0.136 ± 0.01	54.7 ± 6.6	0.0025 ± 0.0002
<i>P. glutinosus</i>	66.9 ± 2.4	3.71 ± 1.63	0.101 ± 0.002 (n = 4)	77.9 ± 40.3	0.127 ± 0.01	59.6 ± 3.5	0.0021 ± 0.0002
<i>P. vehiculum</i>	50.5 ± 0.7	0.9 ± 0.1	0.09 ± 0.004	40 ± 5.6	0.141 ± 0.003	34.4 ± 3.0	0.0041 ± 0.0005
<i>P. dunni</i>	68.7 ± 1.2	5.72 ± 1.59	0.065 ± 0.01	112.1 ± 63.1 (n = 3)	0.136 ± 0.004	32.4 ± 4.9	0.0042 ± 0.0002
<i>P. vandykei</i>	54.2 ± 2.0	1.51 ± 0.42	0.073 ± 0.01	62.2 ± 17.9 (n = 4)	0.142 ± 0.002	26.3 ± 4.8	0.0054 ± 0.0006
<i>P. idahoensis</i>	58.1 ± 2.1	2.63 ± 0.78	0.043 ± 0.01	40.1 ± 14.7 (n = 4)	0.143 ± 0.004	23.5 ± 3.0	0.0061 ± 0.0002

Table 4.3 – Results from the PGLS linear regressions showing the individual interactions between the predictor and response variables. Significant p-values are bolded.

Response variable	Predictor variable	t	<i>P</i>
Liver volume (mm ³)	Genome size (Gb)	-0.1	0.959
	Snout-vent length (mm)	7.7	< 0.001
Hepatic tissue area (mm ²)	Genome size (Gb)	4.8	0.005
	Snout-vent length (mm)	-5.1	0.004
Average vascular structure size (mm ²)	Genome size (Gb)	14.1	< 0.001
	Snout-vent length (mm)	-5.2	0.004
Number of vascular structures	Genome size (Gb)	-12.8	< 0.001
	Snout-vent length (mm)	3.8	0.012
Ventricle volume (mm ³)	Genome size (Gb)	0.1	0.959
	Snout-vent length (mm)	8.0	< 0.001
Myocardial area (mm ²)	Genome size (Gb)	-6.9	0.001
	Snout-vent length (mm)	0.7	0.612

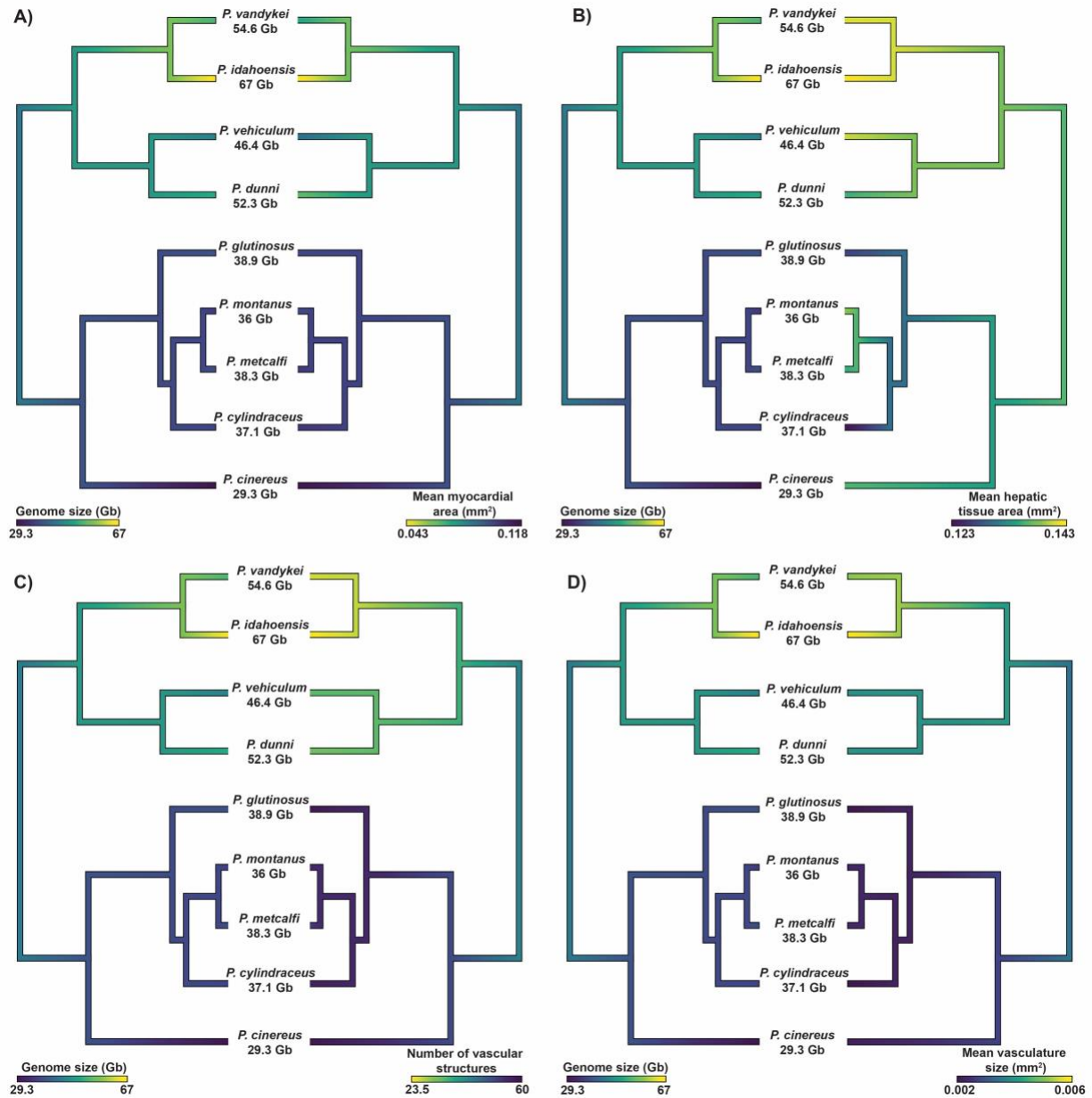


Figure 4.1 – Trait-mapped phylogenies to visualize the coevolution of genome size and organ morphological traits for the 9 species of *Plethodon*. **A** – Continuous trait mapping of genome size and mean myocardial area in the ventricle. **B** - Continuous trait mapping of genome size and mean hepatic tissue area. **C** - Continuous trait mapping of genome size and number of vascular structures in hepatic tissue sections. **D** - Continuous trait mapping of genome size and the mean size of vascular structures in hepatic tissues.

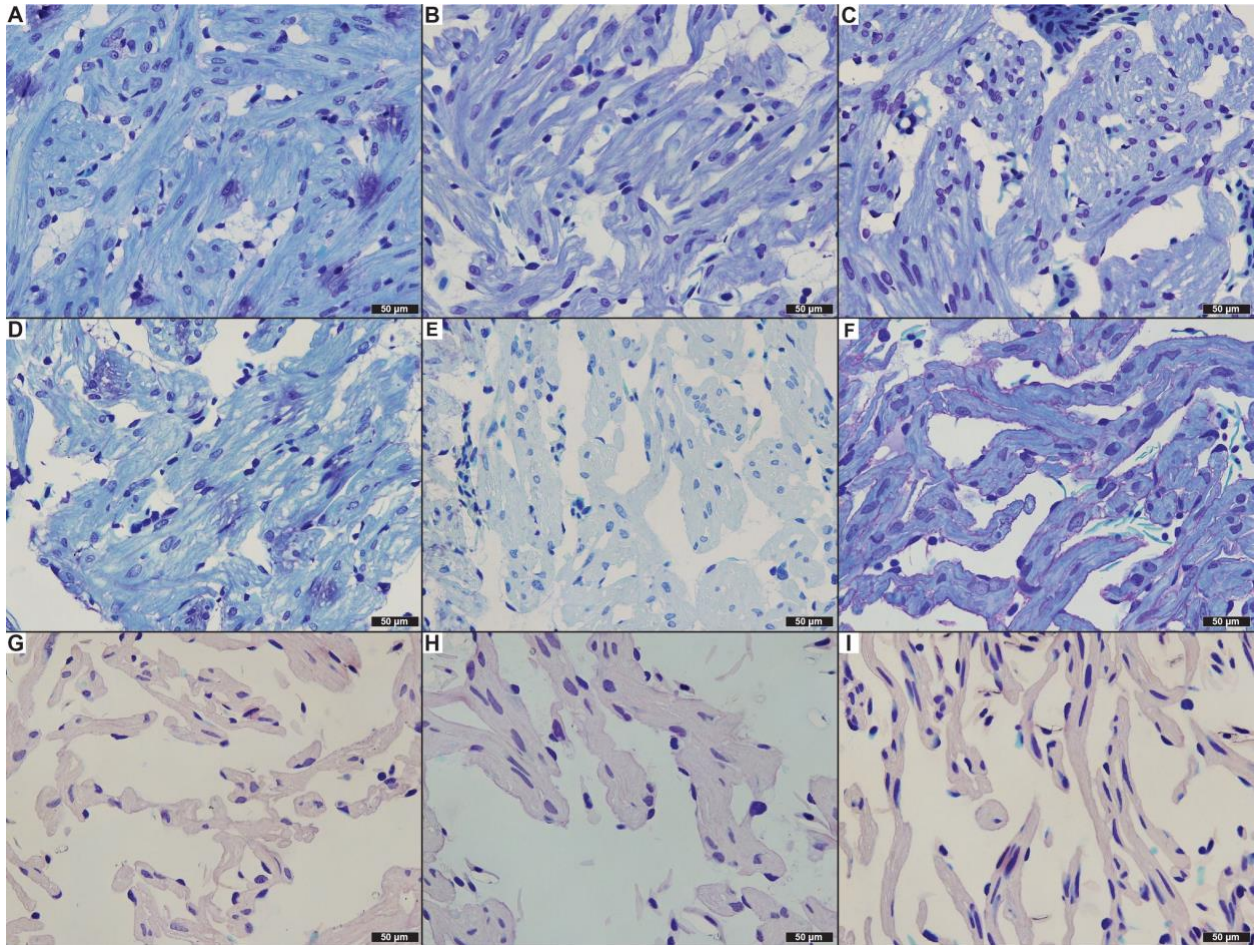


Figure 4.2 – Histological sections of the ventricle at 20x magnification for each species arranged by increasing genome size. A - Ventricle tissue structure of *Plethodon cinereus*, 29.3 Gb. B - Ventricle tissue structure of *P. montanus*, 36.0 Gb. C - Ventricle tissue structure of *P. cylindraceus*, 37.1 Gb. D - Ventricle tissue structure of *P. metcalfi*, 38.3 Gb. E - Ventricle tissue structure of *P. glutinosus*, 38.9 Gb. F - Ventricle tissue structure of *P. vehiculum*, 46.4 Gb. G - Ventricle tissue structure of *P. dunni*, 52.3 Gb. H - Ventricle tissue structure of *P. vandykei*, 54.6 Gb. I - Ventricle tissue structure of *P. idahoensis*, 67.0 Gb.

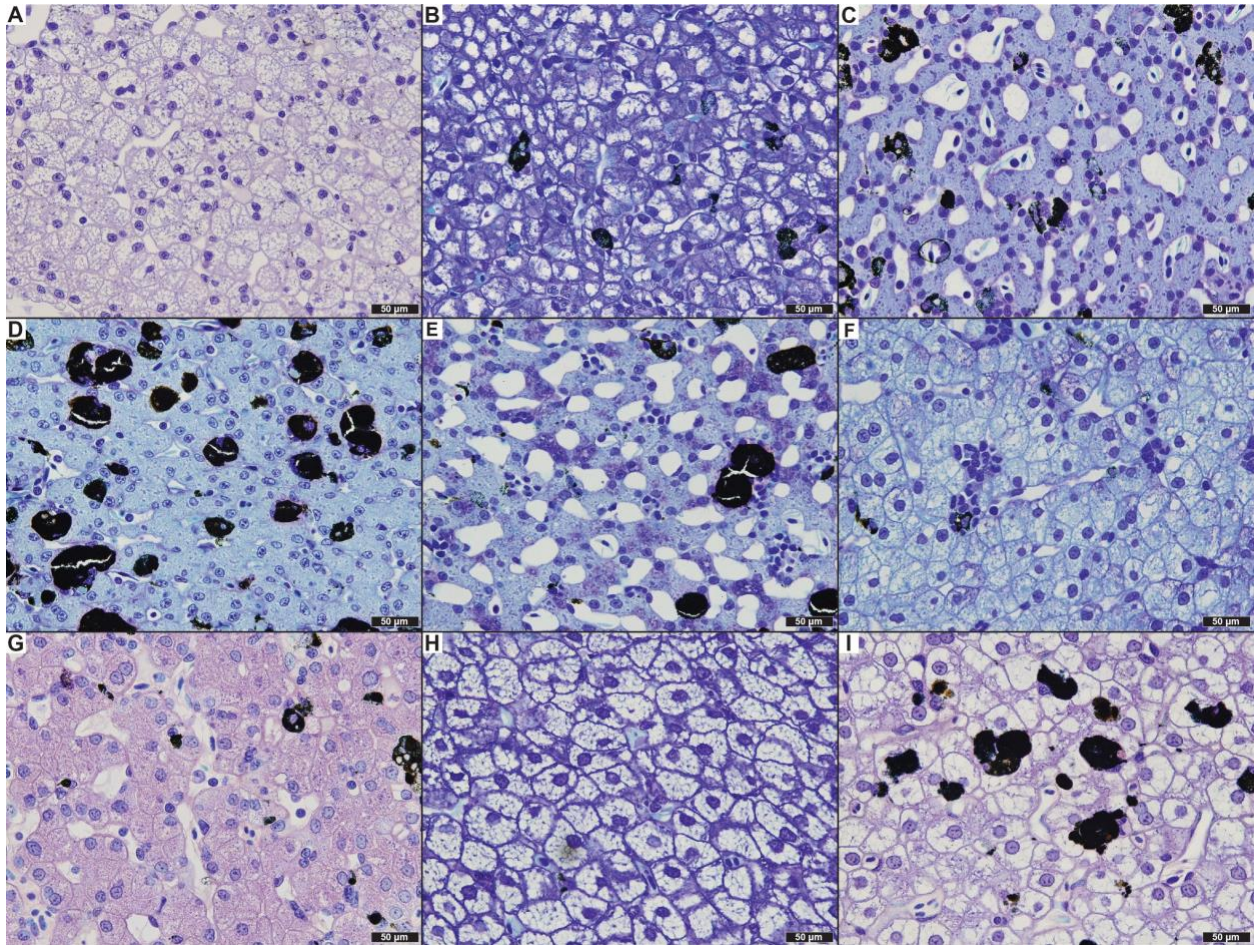


Figure 4.3 – Histological sections of the liver at 20x magnification for each species arranged by increasing genome size. A - Hepatic tissue structure of *Plethodon cinereus*, 29.3 Gb. B - Hepatic tissue structure of *P. montanus*, 36.0 Gb. C - Hepatic tissue structure of *P. cylindraceus*, 37.1 Gb. D - Hepatic tissue structure of *P. metcalfi*, 38.3 Gb. E - Hepatic tissue structure of *P. glutinosus*, 38.9 Gb. F - Hepatic tissue structure of *P. vehiculum*, 46.4 Gb. G - Hepatic tissue structure of *P. dunni*, 52.3 Gb. H - Hepatic tissue structure of *P. vandykei*, 54.6 Gb. I - Hepatic tissue structure of *P. idahoensis*, 67.0 Gb.

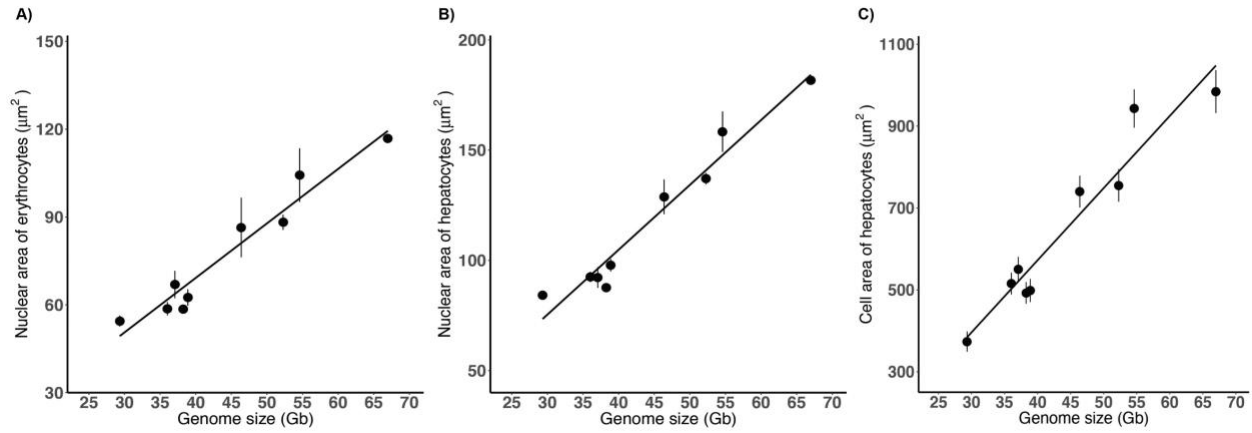


Figure 4.4 – Relationships between genome size and cell morphology. A - Correlation between genome size and nuclear area of erythrocytes. B - Correlation between genome size and nuclear area of hepatocytes. C - Correlation between genome size and cell area of hepatocytes. Trend lines shown for visualization. Error bars represent standard error.

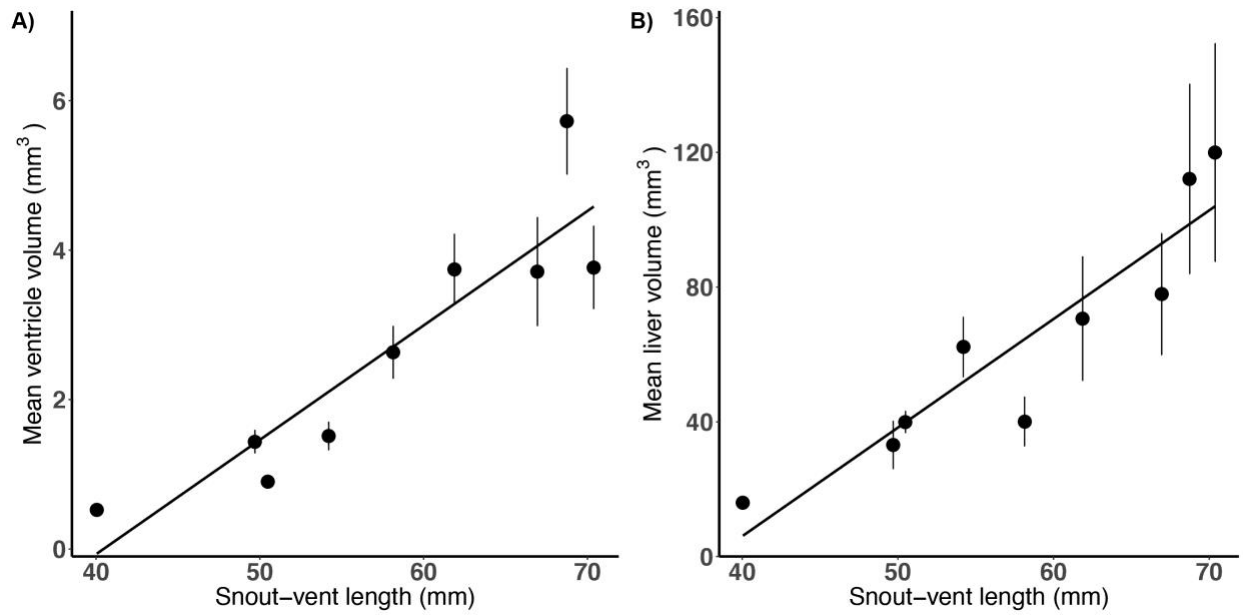


Figure 4.5 – Relationship between body size (snout-vent length) and organ volume. A - relationship between body size and ventricle volume. B - relationship between body size and liver volume. Trend lines shown for visualization. Error bars represent standard error.

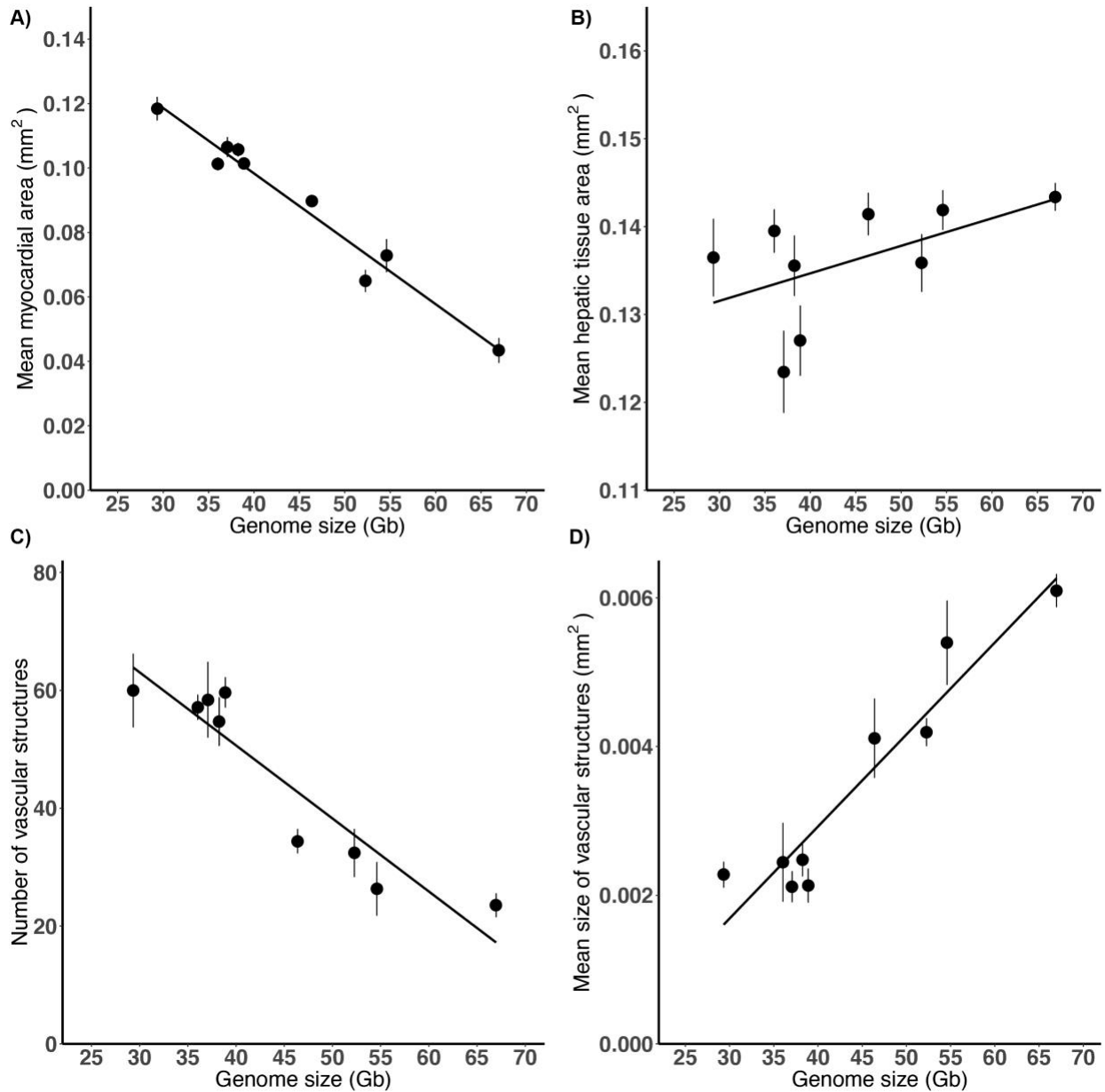


Figure 4.6 – Relationship between genome size and organ morphological traits for the 9 species of *Plethodon*. **A** - Relationship between genome size and mean myocardial area in the ventricle. **B** - Relationship between genome size and hepatic tissue area. **C** - Relationship between genome size and the number of vascular structures in hepatic tissue. **D** - Relationship between genome size and the average size of vascular structures. Trend lines shown for visualization. Error bars represent standard error.

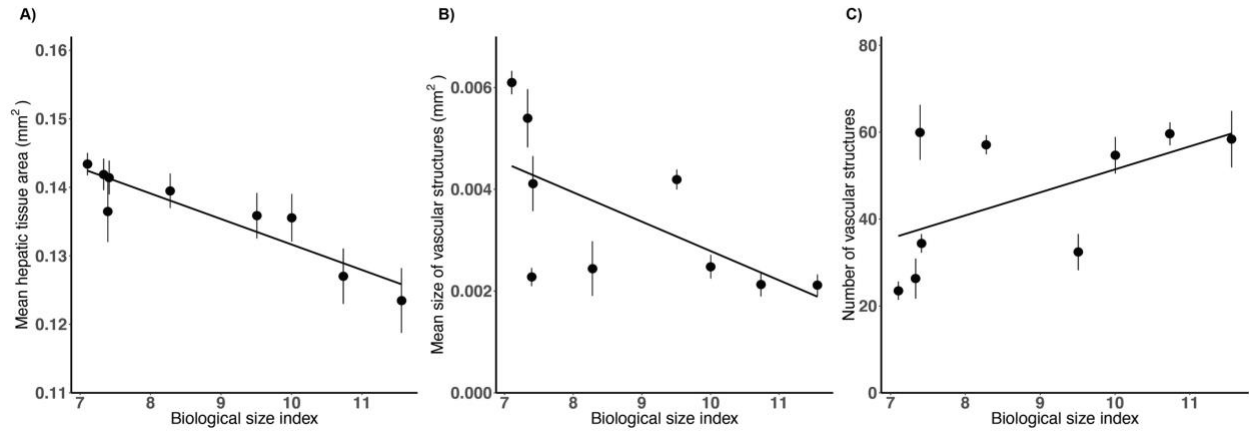


Figure 4.7 – Relationship between biological size index ($SVL / \sqrt{\text{genome size}}$) and hepatic tissue morphology for the 9 species of *Plethodon*. **A - Relationship between biological size index and hepatic tissue area. **B** - Relationship between biological size index and the average size of vascular structures. **C** - Relationship between biological size index and the number of vascular structures in hepatic tissue. Trend lines shown for visualization. Error bars represent standard error.**

REFERENCES

- Akat, E., and B. Göçmen. 2014. A histological study of hepatic structure of *Lyciasalamandra arikani* (Urodela: Salamandridae). *Russian Journal of Herpetology* 21:201–204.
- Akat, E. and H. Arkan. 2017. A histological study on liver of near eastern fire salamander, *Salamandra infraimmaculata martens*, 1885 (Urodela: Salamandridae). *Acta Zoologica Bulgarica* 69:317–321.
- Akiyoshi, H., and A.M. Inoue. 2012. Comparative histological study of hepatic architecture in the three orders of amphibian livers. *Comparative Hepatology* 11:1–8.
- Alberch, P., S.J. Gould, G.F. Oster, and D.B. Wake. 1979. Size and shape in ontogeny and phylogeny. *Paleobiology* 5:296–317.
- Alberch P., and J. Alberch. 1981. Heterochronic mechanisms of morphological diversification and evolutionary change in the neotropical salamander, *Bolitoglossa occidentalis* (Amphibia: Plethodontidae). *Journal of Morphology* 167:249–264.
- Alberch, P. 1982. Developmental constraints in evolutionary processes. Pp. 313–332 in J.T. Bonner, ed. *Evolution and Development*. Dahlen Konferenzen. Springer-Verlag, New York.
- Alberch P. 1983. Morphological variation in the neotropical salamander genus *Bolitoglossa*. *Evolution* 37:906–919.
- Alberch, P., and E. Gale. 1985. A developmental analysis of an evolutionary trend: Digital reduction in amphibians. *Evolution* 39:8–23.
- AlMomani, T.D., S.C. Vigmostad, V. Keshav Chivukula, L. Al-zube, O. Smadi, and S. BaniHani. 2012. Red blood cell flow in the cardiovascular system: a fluid dynamics perspective. *Critical Reviews in Biomedical Engineering* 40:427–440.
- Arnold, S.J. 1983. Morphology, performance, and fitness. *American Zoologist* 23:347–361.
- Arnold, S.J. 1992. Constraints on phenotypic evolution. *The American Naturalist* 140:S85–S107.
- Bachmann, K. 1970. Feulgen slope determinations of urodele nuclear DNA amounts. *Histochemie* 22:289–293.
- Baverstock, H., N.S. Jeffery, and S.N. Cobb. 2013. The morphology of the mouse masticatory musculature. *Journal of Anatomy* 223:46–60.
- Benjamini, Y., and Y. Hochberg. 2000. On the adaptive control of the false discovery rate in multiple testing with independent statistics. *Journal of Educational and Behavioral Statistics* 25:60–83.
- Bock, W.J. 1980. The definition and recognition of biological adaptation. *American Zoologist* 20:217–227.
- Brakefield, P.M., V. French, and B.J. Zwaan. 2003. Development and the genetics of evolutionary change within insect species. *Annual Review of Ecology, Evolution, and Systematics* 34:633–660.
- Brakefield, P.M. 2006. Evo-devo and constraints on selection. *Trends in Ecology & Evolution* 21:362–368.
- Chan, C.J., C.P. Heisenberg, and T. Hiiragi. 2017. Coordination of morphogenesis and cell-fate specification in development. *Current Biology* 27:R1024–R1035.

- D'Ario, M., R. Tavares, K. Schiessl, B. Desvoyes, C. Gutierrez, M. Howard, and R. Sablowski. 2021. Cell size controlled in plants using DNA content as an internal scale. *Science* 372:1176–1181.
- Decena-Segarra, L.P., L. Bizjak-Mali, A. Kladnik, S.K. Sessions, and S.M. Rovito. 2020. Miniaturization, genome size, and biological size in a diverse clade of salamanders. *The American Naturalist* 196:634–648.
- Dupin, M.M., I. Halliday, C.M. Care, and L.L. Munn. 2008. Lattice Boltzmann modelling of blood cell dynamics. *International Journal of Computational Fluid Dynamics* 22:481–492.
- Edgar, R.C. 2004. MUSCLE: multiple sequence alignment with high accuracy and high throughput. *Nucleic Acids Research* 32:1792–1797.
- Elias H., and H. Bengelsdorf. 1952. The structure of the liver of vertebrates. *Acta Anatomica* 14: 297–337.
- Fankhauser, G. 1945. The effects of changes in chromosome number on amphibian development. *The Quarterly Review of Biology* 20:20–78.
- Fedorov, A., R. Beichel, J. Kalpathy-Cramer, J. Finet, J.C. Fillion-Robin, S. Pujol, C. Bauer, D. Jennings, F. Fennessy, M. Sonka, J. Buatti, S. Aylward, J.V. Miller, S. Pieper, and R. Kikinis. 2012. 3D Slicer as an image computing platform for the Quantitative Imaging Network. *Magnetic Resonance Imaging* 30:1323–1341.
- Gardner, J.D., M. Laurin, and C.L. Organ. 2020. The relationship between genome size and metabolic rate in extant vertebrates. *Philosophical Transactions of the Royal Society B* 375, 20190146.
- Gatten, R.E.J., K. Miller, and R.J. Full. 1992. Energetics at rest and during locomotion. Pp. 314–377 in M.E. Feder, ed. *Environmental physiology of the amphibians*. University of Chicago Press, Chicago.
- Gerber, S. 2014. Not all roads can be taken: development induces anisotropic accessibility in morphospace. *Evolution and Development* 16:373–381.
- Gignac, P.M., N.J. Kley, J.A. Clarke, M.W. Colbert, A.C. Morhardt, D. Cerio, I.N. Cost, P.G. Cox, J.D. Daza, C.M. Early, M.S. Echols, R.M. Henkelman, A.N. Herdina, C.M. Holliday, Z. Li, K. Mahlow, S. Merchant, J. Müller, C.P. Orsbon, D.J. Paluh, M.L. Thies, H.P. Tsai, and L.M. Witmer. 2016. Diffusible iodine-based contrast-enhanced computer tomography (diceCT): an emerging tool for rapid, high-resolution, 3-D imaging of metazoan soft tissues. *Journal of Anatomy* 228:889–909.
- Gokhale, R.H., and A.W. Shingleton. 2015. Size control: the developmental physiology of body and organ size regulation. *WIREs Developmental Biology* 4:335–356.
- Gould, S.J. 1985. *Ontogeny and phylogeny*. Harvard University Press, Cambridge, MA.
- Gregory, T.R. 2001. The bigger the C-value, the larger the cell: genome size and red blood cell size in vertebrates. *Blood Cells, Molecules, and Diseases* 27:830–843.
- Gregory, T.R. 2005. Genome size evolution in animals. Pp. 314–377 in T.R. Gregory, ed. *The Evolution of the Genome*. Elsevier, San Diego, CA.
- Gregory, T.R. 2021. Animal Genome Size Database. Available online: <http://www.genomesize.com> (accessed 11 July 2021).
- Hanken, J. 1982. Appendicular skeletal morphology in minute salamanders, genus *Thorius* (Amphibia: Plethodontidae): growth regulation, adult size determination, and natural variation. *Journal of Morphology* 174:57–77.

- Hanken, J. 1983. Miniaturization and its effects on cranial morphology in plethodontid salamanders, genus *Thorius* (Amphibia: Plethodontidae): II. The fate of the brain and sense organs and their role in skull morphogenesis and evolution. *Journal of Morphology* 177:255–268.
- Hanken, J. 1984. Miniaturization and its effects on cranial morphology in plethodontid salamanders, genus *Thorius* (Amphibia: Plethodontidae). I. Osteological variation. *Biological Journal of the Linnean Society* 23:55–75.
- Hanken, J., and D.B. Wake. 1993. Miniaturization of body size: organismal consequences and evolutionary significance. *Annual Review of Ecology and Systematics* 24:501–519.
- Hardie, D.C., T.R. Gregory, and P.D.N. Herbert. 2002. From pixels to picograms: a beginners' guide to genome quantification by Feulgen image analysis densitometry. *Journal of Histochemistry and Cytochemistry* 50:735–749.
- Hedrick, B.P., L. Yohe, A. Vander Linden, L.M. Dávalos, K. Sears, A. Sadier, S.J. Rossiter, K.T.J. Davies, and E. Dumont. 2018. Assessing soft-tissue estimates in museum specimens imaged with diffusible iodine-based contrast-enhanced computed tomography (diceCT). *Microscopy and Microanalysis* 24:284–291.
- Highton, R. 1989. Biochemical evolution in the slimy salamanders of the *Plethodon glutinosus* complex in the eastern United States. Part I. Geographical protein variation. *Illinois Biological Monographs* 57:1–78.
- Highton, R. 1995. Speciation in eastern North American salamanders of the genus *Plethodon*. *Annual Review of Ecology and Systematics* 26:579–600.
- Horner, H.A., and H.C. Macgregor. 1983. C value and cell volume: their significance in the evolution and development of amphibians. *Journal of Cell Science* 63:135–146.
- Humason, G.L. 1962. *Animal Tissue Techniques*. W. H. Freeman and Company, San Francisco, CA.
- Itgen, M.W., P. Prša, R. Janža, L. Skubic, J.H. Townsend, A. Kladnik, L. Bizjak-Mali, and S.K. Sessions. 2019. Genome size diversification in Central American bolitoglossine salamanders (Caudata; Plethodontidae). *Copeia* 107:560–566.
- Jaekel, M., and D.B. Wake. 2007. Developmental processes underlying the evolution of a derived foot morphology in salamanders. *Proceedings of the National Academy of Sciences* 104:20437–20442.
- Johnson, B., D. Bark Jr., I. Van Herck, D. Garrity, and L. Prasad Dasi. 2015. Altered mechanical state in the embryonic heart results in time-dependent decreases in cardiac function. *Biomechanics and Modeling in Mechanobiology* 14:1379–1389.
- Johnson, B.B., J.B. Searle, and J.P. Sparks. 2021. Genome size influences adaptive plasticity of water loss, but not metabolic rate, in lungless salamanders. *Journal of Experimental Biology* 224, jeb242196.
- Kerney, R.R., D.C. Blackburn, H. Müller, and J. Hanken. 2011. Do larval traits re-evolve? Evidence from the embryogenesis of a direct-developing salamander, *Plethodon cinereus*. *Evolution* 66:252–262.
- Keyte, A.L., and K.K. Smith. 2014. Heterochrony and developmental timing mechanisms: changing ontogenies in evolution. *Seminars in Cell and Developmental Biology* 34:99–107.
- Kim, W., and E.H. Jho. 2018. The history and regulatory mechanism of the Hippo pathway. *BMB Reports* 51:106–118.

- Kucera, J.P., A.G. Kléber, and S. Rohr. 1998. Slow conduction in cardiac tissue, II: effects of branching tissue geometry. *Circulation Research* 83:795–805.
- Kumar, S., G. Stecher, and K. Tamura. 2016. MEGA7: Molecular evolutionary genetics analysis version 7.0 for bigger datasets. *Molecular Biology and Evolution* 33:1870–1874.
- Lanfear, R., P.B. Frandsen, A.M. Wright, T. Senfeld, and B. Calcott. 2017. Partitionfinder 2: new methods for selecting partitioned models of evolution for molecular and morphological phylogenetic analyses. *Molecular Biology and Evolution* 34:772–773.
- Lewis, Z.R., and J. Hanken. 2017. Convergent evolutionary reduction of atrial septation in lungless salamanders. *Journal of Anatomy* 230:16–29.
- Lewontin, R.C. 1972. *The Genetic Basis of Evolutionary Change*. Columbia University Press, New York.
- Linke, R., G. Roth, and B. Rottluff. 1986. Comparative studies on the eye morphology of lungless salamanders, family Plethodontidae, and the effect of miniaturization. *Journal of Morphology* 189:131–143.
- Mallarino, R., P.R. Grant, B.R. Grant, A. Herrel, W.P. Kuo, and A. Abzhanov. 2011. Two developmental modules establish 3D beak-shape variation in Darwin’s finches. *Proceedings of the National Academy of Sciences* 108:4057–4062.
- Maroudas-Sacks, Y., and K. Keren. 2021. Mechanical patterning in animal morphogenesis. *Annual Review of Cell and Developmental Biology* 37:469–493.
- Marshall, W.F., K.D. Young, M. Swaffer, E. Wood, P. Nurse, A. Kimura, J. Frankel, J. Wallingford, V. Walbot, X. Qu, and A.H. Roeder. 2012. What determines cell size? *BMC Biology* 10:1–22.
- Maynard Smith, J., R. Burian, S. Kauffman, P. Alberch, J. Campbell, B. Goodwin, R. Lande, D. Raup, and L. Wolpert. 1985. Developmental constraints and evolution. *Quarterly Review of Biology* 60:265–287.
- Mizuno, S., and H.C. Macgregor. 1974. Chromosomes, DNA sequences, and evolution in salamanders of the genus *Plethodon*. *Chromosoma* 48:239–296.
- Mueller, R.L., T.R. Gregory, S.M. Gregory, A. Hsieh, J.L. Boore. 2008. Genome size, cell size, and the evolution of enucleated erythrocytes in attenuate salamanders. *Zoology* 111:218–230.
- Mueller, R.L., C.E. Cressler, R.S. Schwarz, R.A. Chong, and M.A. Butler. 2021. Metamorphosis imposes variable constraints on genome expansion. *bioRxiv* 2021.05.05.442795; doi: <https://doi.org/10.1101/2021.05.05.442795>.
- Newman, C.E., T.R. Gregory, and C.C. Austin. 2016. The dynamic evolutionary history of genome size in North American woodland salamanders. *Genome* 60:285–292.
- Olejnickova, V., H. Kolesova, M. Bartos, D. Sedmera, and M. Gregorovicova. 2021. The tale-tell heart: evolutionary tetrapod shift from aquatic to terrestrial life-style reflected in heart changes in axolotl (*Ambystoma mexicanum*). *Developmental Dynamics* 250:1–11.
- Orne, D., R. Freckleton, G. Thomas, T. Petzoldt, S. Fritz, N. Isaac, and W. Pearse. 2013. caper: comparative analyses of phylogenetics and evolution in R. R package, version 0.5.2.
- Oster, G.F., and P. Alberch. 1982. Evolution and bifurcation of developmental programs. *Evolution* 36:444–462.
- Oster, G., N. Shubin, J.D. Murray, and P. Alberch. 1988. Evolution and morphogenetic rules: The shape of the vertebrate limb in ontogeny and phylogeny. *Evolution* 42:862–884.
- Pinheiro, J., D. Bates, S. DebRoy, D. Sarkar, and the R Development Core Team. 2021. nlme: linear and nonlinear mixed effects models. R package, version 3.1.

- Powder, K.E., K. Milch, G. Asselin, and R.C. Albertson. 2015. Constraint and diversification of developmental trajectories in cichlid facial morphologies. *EvoDevo* 6: <https://doi.org/10.1186/s13227-015-0020-8>.
- R Core Team. 2016. R: a language and environment for statistical computing. R Foundation for Statistical Computing, Vienna, Austria. <http://www.R-project.org/>.
- Revell, L.J. 2010. Phylogenetic signal and linear regression on species data. *Methods in Ecology and Evolution* 1:319–329.
- Revell, L.J. 2012. Phytools: an R package for phylogenetic comparative biology (and other things). *Methods in Ecology and Evolution* 3:217–223.
- Ronquist, F., M. Teslenko, P. van der Mark, D.L. Ayres, A. Darling, S. Höhna, B. Larget, L. Liu, M.A. Suchard, and J.P. Huelsenbeck. (2012). MrBayes 3.2: efficient Bayesian phylogenetic inference and model choice across a large model space. *Systematic Biology*. 61:539–542.
- Roth, G., B. Rottluff, and R. Linke. 1988. Miniaturization, genome size and the origin of functional constraints in the visual system of salamanders. *Naturwissenschaften* 75:297–304.
- Roth, G., B. Rottluff, W. Grunwald, J. Hanken, and R. Linke. 1990. Miniaturization in plethodontid salamanders (Caudata: Plethodontidae) and its consequences for the brain and visual system. *Biological Journal of the Linnean Society* 40:165–190.
- Roth, G., K.C. Nishikawa, C. Naujoks-Manteuffel, A. Schmidt, and D.B. Wake. 1993. Paedomorphosis and simplification in the nervous system of salamanders. *Brain, Behavior, and Evolution* 42:137–170.
- Roth, G., J. Blanke, and D. B. Wake. 1994. Cell size predicts morphological complexity in the brains of frogs and salamanders. *Proceedings of the National Academy of Sciences* 91:4796–4800.
- Roth, G., and W. Walkowiak. 2015. The influence of genome and cell size on brain morphology in amphibians. *Cold Spring Harbor Perspectives in Biology* 7:a019075.
- Salazar-Ciudad, I. 2006. Developmental constraints vs. variation properties: how pattern formation can help to understand evolution and development. *Journal of Experimental Zoology Part B: Molecular and Developmental Evolution* 306:107–125.
- Santhanakrishnan, A., and L.A. Miller. 2011. Fluid dynamics of heart development. *Cell Biochemistry and Biophysics* 61:1–22.
- Schmidt, A., and G. Roth. 1993. Patterns of cellular proliferation and migration in the developing tectum mesencephali of the frog *Rana temporaria* and the salamander *Pleurodeles waltl*. *Cell and Tissue Research* 272:273–287.
- Schneider, C.A., W.S. Rasband, and K.W. Eliceiri. 2012. NIH Image to ImageJ: 25 years of image analysis. *Nature Methods* 9:671–675.
- Sedmera, D., M. Reckova, A. deAlmeida, M. Sedmerova, M. Biermann, J. Volejnik, A. Sarre, E. Raddatz, R.A. McCarthy, R.G. Gourdie, and R.P. Thompson. 2003. Functional and morphological evidence for a ventricular conduction system in zebrafish and *Xenopus* hearts. *American Journal of Physiology – Heart and Circulatory Physiology* 284:H1152–H1160.
- Sessions, S.K. 2008. Evolutionary cytogenetics in salamanders. *Chromosome Research* 16:183–201.
- Sessions, S.K., and A. Larson. 1987. Developmental correlates of genome size in plethodontid salamanders and their implications for genome evolution. *Evolution* 41:1239–1251.

- Sessions, S.K., and D.B. Wake. 2021. Forever young: linking regeneration and genome size in salamanders. *Developmental Dynamics* 250:768–778.
- Snyder, G.K., and B.A. Sheafor. 1999. Red blood cells: centerpiece in the evolution of vertebrate circulatory system. *American Zoologist* 39:189–198.
- Stephenson, A., J.W. Adams, and M. Vaccarezza. 2017. The vertebrate heart: an evolutionary perspective. *Journal of Anatomy* 231:787–797.
- Sun, C., D.B. Shepard, R.A. Chong, J.L. Arriaza, K. Hall, T.A. Castoe, C. Feschotte, D.D. Pollock, and R.L. Mueller. 2012. LTR retrotransposons contribute to genomic gigantism in plethodontid salamanders. *Genome Biology and Evolution* 4:168–183.
- Uller, T., A.P. Moczek, R.A. Watson, P.M. Brakefield, and K.N. Laland. 2018. Developmental bias and evolution: a regulatory network perspective. *Genetics* 209:949–966.
- Uyeda, J.C., M.W. Pennell, E.T. Miller, R. Maia, and C.R. McClain. 2017. The evolution of energetic scaling across the vertebrate tree of life. *The American Naturalist* 190:185–199.
- Vaissi, S., P. Parto, and M. Sharifi. 2017. Anatomical and histological study of the liver and pancreas of two closely related mountain newts: *Neurergus microspilotus* and *N. kaiseri* (Amphibia: Caudata: Salamandridae). *Zoologia* 34:1–8.
- Vickerton, P., J. Jarvis, and N. Jeffery. 2013. Concentration-dependent specimen shrinkage in iodine-enhanced microCT. *Journal of Anatomy* 223:185–193.
- Villalobos, M., P. León, S.K. Sessions, and J. Kezer. 1988. Enucleated erythrocytes in plethodontid salamanders. *Herpetologica* 44:243–250.
- Vinogradov, A.E. 1999. Genome in toto. *Genome* 42:361–362.
- Wagner, A. 2011. Genotype networks shed light on evolutionary constraints. *Trends in Ecology and Evolution* 26:577–584.
- Wake D.B. 1966. Comparative osteology and evolution of the lungless salamanders, family Plethodontidae. *Southern California Academy of Sciences* 4:1–111.
- Wake, D.B. 1991. Homoplasy: the result of natural selection or evidence of design limitations? *Am. Nat.* 138:543–567.
- Womack, M.C., M.J. Metz, and K.L. Hoke. 2019. Larger genomes linked to slower development and loss of late-developing traits. *The American Naturalist* 194:854–864.

5. CONCLUSION

The evolution of large genome size imposes structural and physiological consequences that span biological levels of complexity (Fankhauser, 1945; Horner and Macgregor, 1983; Sessions and Larson, 1987; Hanken and Wake, 1993; Schmidt and Roth, 1993; Roth et al., 1994; Gregory, 2001, 2005; Roth and Walkowiak, 2015; Womack et al., 2019). Changes in cell size, driven by DNA content, have been proposed as the functional link between genome size and several complex traits, such as metabolism and development (Szarski, 1983; Horner and Macgregor, 1983; Sessions and Larson, 1987; Kozłowski et al., 2003). Specifically, cell size has been predicted to impact cellular processes that, in turn, have consequences on metabolism and development. Herein, I provided evidence that cell size does impact cell function. The transcriptomic analyses indicated that large cell size was associated with the upregulation of intracellular transport processes and the relative downregulation of cell cycle progression, protein biosynthesis and degradation (i.e., proteome turnover), cell-cell communication, and mitochondrial pathways. Larger cells were also found to upregulate chromatin structure and modification pathways likely connected to the increased DNA content. The transcriptomic analyses also showed there were cell-size dependent changes in physiology, including the downregulation of genes associated with cellular respiration and transmembrane ion transport. These results suggest that evolutionary changes in cell size are accompanied by changes in the metabolic state of the cell. Taken together, I have demonstrated that cell size does impact the physiology of the cell but not their metabolic cost.

Changes in development and morphology have been linked to increased genome size, but patterns of phenotypic change among the few examples are disparate (Fankhauser, 1945; Horner

and Macgregor, 1983; Sessions and Larson, 1987; Hanken and Wake, 1993; Schmidt and Roth, 1993; Roth et al., 1994; Roth and Walkowiak, 2015; Womack et al., 2019; Decena-Segarra et al., 2020). My comparative analysis of phenotypic change in the heart and liver associated with increased genome and cell size further highlights this broader pattern. In other words, genome and cell size does not appear to impact tissue and organ morphology in a universal manner. Instead, genome and cell size have organ-specific effects on morphology. It is likely that genome and cell size impose similar stressors or constraints on development, but only under certain circumstances do these traits impact the final morphology. I hypothesize that tissues and organs that undergo similar pathways during morphogenesis are likely to have similar patterns of morphological change in the final structure as genome and cell size become larger. Future research should focus on comparative ontogenetic studies of organs using histology and transcriptomics. By coupling morphological and transcriptomic data, it should be possible to identify the specific mechanisms that are disrupted by large genome and cell size. In addition, the functional implications of these genome and cell size-mediated changes should be assessed. Quantifying the functional impact of, for example, less musculature in the heart, is critical for a full understanding of the functional consequences of genome and cell size on the organism.

A remaining question pertains to why enormous genome sizes have evolved in association with low metabolic rates in lung fish and salamanders (Szarski, 1983). I found no evidence that genome and cell size are predictors of metabolic rate across 9 species and a 29.3–67.0 Gb range in genome size. I also found no support for the hypothesis that cell volume lowers the metabolic cost of tissues or that cell volume reduces the relative cost of maintaining ion gradients (Kozłowski et al., 2003). Further, the patterns of evolution seen in mitochondrial physiology do not suggest that cell size alters the metabolic demands of the cell. These results

are broadly concordant with recent studies that found genome size had no effect on the variation of basal metabolic rate in salamanders or all vertebrates (Uyeda et al., 2017; Gardner et al., 2020; Johnson et al., 2021). The association between low metabolic rate and large genome size continues to hold valuable insight into the evolution of these traits, and there is still strong evidence that small cell sizes are functionally correlated with high metabolic physiologies (Vinogradov, 1995, 1997; Gregory, 2002; Waltari and Edwards, 2002; Smith et al., 2013; Wright et al., 2014).

The evidence from birds and mammals indicate that cell size is an important metabolic trait, at least in taxa with high metabolisms. Small cell size is considered an adaptive trait for high metabolic physiologies (Vinogradov, 1995, 1997; Gregory, 2002; Waltari and Edwards, 2002; Smith et al., 2013; Wright et al., 2014). For example, small red blood cell size is an important adaptation to maintain high metabolic demands (Szarski, 1983; Gregory, 2002; Glazier, 2014). The increased SV ratio facilitates highly efficient diffusion to transfer nutrients and gases to metabolically demanding tissues, and the small cell size allows for highly vascularized tissues (Gregory, 2002, 2005). Because of this, we hypothesize that small cell size is an adaptive trait for high metabolic organisms and that is why there is a clear pattern within endotherms. In other words, high metabolic physiologies necessitate small cell sizes. We propose that the evolution of low metabolic rate in salamanders and lung fish permitted the evolution of enormous genome size. Once the constraint of metabolic demand was lifted, the functional requirements on the organ structures and biochemical pathways associated with metabolism were lessened, permitting a greater number of basically functionally equivalent phenotypes to evolve. Given this permissive (i.e., flat) adaptive landscape, molecular processes, such as TE dynamics, were unconstrained and freed to produce a variety of cell sizes, organ morphologies, and

metabolic networks that all met the lowered functional requirements sufficiently well. As a result, the diverse phenotypes we observe in these metabolic-related traits within salamanders are likely the result of nonadaptive evolution towards genome gigantism.

An important lesson from the evolution of large genome size is that not all correlated traits are adaptive, exemplified by the association between large genome size and low metabolic rate. While there is an apparent pattern of permissive evolution occurring across metabolic-related traits, genome and cell size is still bound by their effects on other phenotypes. For example, the effects on error-free and expeditious development during metamorphosis or the impact of extreme cell number reduction on visual acuity (Roth et al., 1994; Roth and Walkowiak, 2015; Mueller et al., 2021). A major goal for the field is to continue assessing the impact of genome and cell size on cell and organismal biology, informed by the fact that some traits will be structurally and/or functionally affected by genome size, while others are not. By identifying these overall patterns, we can begin to understand when selection is weighing in to shape TE and genome-level dynamics. A critical next step is to investigate the drivers of extremely low metabolic rate in vertebrates and to further test whether low metabolic rate lessens the constraint on genome size.

REFERENCES

- Decena-Segarra, L.P., L. Bizjak-Mali, A. Kladnik, S.K. Sessions, and S.M. Rovito. 2020. Miniaturization, genome size, and biological size in a diverse clade of salamanders. *The American Naturalist* 196:634–648.
- Fankhauser, G. 1945. The effects of changes in chromosome number on amphibian development. *The Quarterly Review of Biology* 20:20–78.
- Gregory, T.R. 2001. Coincidence, coevolution, or causation? DNA content, cell size, and the C-value enigma. *Biological Reviews of the Cambridge Philosophical Society* 76:65–101.
- Gregory, T.R. 2002. A bird's-eye view of the c-value enigma: genome size, cell size, and metabolic rate in class Aves. *Evolution* 56:121–130.
- Gregory, T.R. 2005. Genome size evolution in animals. In: Gregory T. R., editor. *The Evolution of the Genome*. New York: Elsevier.
- Glazier, D.S. 2014. Metabolic scaling in complex living systems. *Systems* 2:451–540.
- Hanken, J., and D.B. Wake. 1993. Miniaturization of body size: organismal consequences and evolutionary significance. *Annual Review of Ecology and Systematics* 24:501–519.
- Horner, H.A., and H.C. Macgregor. 1983. C value and cell volume: their significance in the evolution and development of amphibians. *Journal of Cell Science* 63:135–146.
- Kozłowski, J., Konarzewski, M., and Gawelczyk, A.T. 2003. Cell size as a link between noncoding DNA and metabolic rate scaling. *PNAS* 100:14080–14085.
- Mueller, R.L., C.E. Cressler, R.S. Schwarz, R.A. Chong, and M.A. Butler. 2021. Metamorphosis imposes variable constraints on genome expansion. *bioRxiv* 2021.05.05.442795; doi: <https://doi.org/10.1101/2021.05.05.442795>.
- Roth, G., J. Blanke, and D.B. Wake. 1994. Cell size predicts morphological complexity in the brains of frogs and salamanders. *Proceedings of the National Academy of Sciences* 91:4796–4800.
- Roth, G., and W. Walkowiak. 2015. The influence of genome and cell size on brain morphology in amphibians. *Cold Spring Harbor Perspectives in Biology* 7:a019075.
- Schmidt, A., and G. Roth. 1993. Patterns of cellular proliferation and migration in the developing tectum mesencephali of the frog *Rana temporaria* and the salamander *Pleurodeles waltl*. *Cell and Tissue Research* 272:273–287.
- Sessions, S.K., and A. Larson. 1987. Developmental correlates of genome size in plethodontid salamanders and their implications for genome evolution. *Evolution* 41:1239–1251.
- Szarski, H. 1983. Cell size and the concept of wasteful and frugal evolutionary strategies. *Journal of Theoretical Biology* 105:201–209.
- Vinogradov, A.E. 1995. Nucleotypic effect in homeotherms: Body-mass-corrected basal metabolic rate of mammals is related to genome size. *Evolution* 49: 1249–1259.
- Vinogradov, A.E. 1997. Nucleotypic effect in homeotherms: Body-mass-corrected basal metabolic rate of passerine birds is related to genome size. *Evolution* 51: 220–225.
- Waltari, E., and S.V. Edwards. 2002. Evolutionary dynamics of intron size, genome size, and physiological correlations in archosaurs. *The American Naturalist* 160:539–552.
- Womack, M.C., M.J. Metz, and K.L. Hoke. 2019. Larger genomes linked to slower development and loss of late-developing traits. *The American Naturalist* 194:854–864.

Wright, N.A., T.R. Gregory, and C.C. Witt. 2014. Metabolic 'engines' of flight drive genome size reduction in birds. *Proceedings of the Royal Society B: Biological Sciences* 281:20132780.

SUPPLEMENTAL INFORMATION 2.1

Locality and collection information

All permits were issued to M.W. Itgen and the animals were collected between May and August of 2018. *Plethodon idahoensis* was collected from Shoshone county, Idaho, under the wildlife collection permit #180226 issued by the Idaho Department of Fish and Game. *Plethodon cinereus* and *P. glutinosus* were collected from South Cherry Valley and Oneonta, Otsego County, New York, under the New York State Department of Environmental Conservation scientific collection permit #2303. *Plethodon vehiculum*, *P. vandykei*, and *P. dumni* were collected from Pacific County, Washington, under the scientific collection permit # ITGEN 17-309 issued by the Washington Department of Fish and Wildlife. *Plethodon metcalfi* was collected from Macon County, NC, and *P. montanus* and *P. cylindraceus* were collected from Avery County, NC, under the wildlife collection license # 18-SC01250 issued by the North Carolina Wildlife Resources Commission.